Improvements in the GC/MS Analysis of Polycyclic Aromatics in Fossil Fuels: Sampling, Separation, and Assessment

A dissertation submitted by

Patrick M. Antle

in partial fulfillment of the requirements for the degree of

Doctor of Philosophy
in
Chemistry

TUFTS UNIVERSITY

February 2015

Advisor: Dr. Albert Robbat Jr.

Contents

Executive Summary

The characterization of complex mixtures and accurate quantitation of their components is a challenging endeavor, requiring the application of a powerful analytical technique such as gas chromatography/mass spectrometry (GC/MS). The GC/MS analysis of polycyclic aromatic compounds (PAC) in fossil fuels is particularly difficult due to overlapping retention windows, common spectral ions, and sample matrices rife with interfering compounds. PAC are persistent and harmful, and the fossil fuels that they comprise are the predominant contaminant in thousands of hazardous waste sites worldwide. Accordingly, facilitation of their analysis can have a broad-reaching impact on human and environmental health.

This work describes several lines of research to this end. An *in situ* sample collection system that provides on-line continuous detection of environmental pollutants was developed; technology that can unambiguously profile organics in the subsurface from ground-level to bedrock. The effects of selected-ion data analysis methods on diagnostic ratios used in environmental forensics were examined, and it was found that methods employing fewer than three ions consistently overestimated alkylated homologue concentrations and led to biased and inaccurate diagnostics. The retention behavior of polycyclic aromatic sulfur heterocycles (PASH) on novel room temperature ionic liquid stationary phases was investigated; these columns can provide improved separation of both polars and nonpolars at higher temperatures than the columns typically utilized for the analysis of fossil fuels. Comprehensive two-dimensional gas chromatography-

quadrupole mass spectrometry (GC×GC/qMS) spectra were deconvolved, allowing for the first quantitative analysis of PAC in coal tar by this technique. And a simple and robust modeling technique for estimation of physical properties from GC×GC retention indices was developed. This method was embedded into a software program to produce a component map that provides, for the first time, the ability to assess the weathering of complex mixtures such as crude oil and coal tar by subsurface and sediment environments. In all, the work is relevant to all aspects of the analysis of complex samples: sample collection and preparation, chromatographic separation, data analysis, and utilization of these results in decision-making processes.

Acknowledgements

I first and foremost wish to thank Prof. Albert Robbat for his tireless guidance throughout my time at Tufts. While he obviously provided me with a great deal of knowledge regarding my research, I am just as grateful for the lessons that go beyond the realm of science; the need to make one's message cogent and persuasive and, above all, the importance of interpersonal skills. If I am a scientist of any repute, it is on account of him.

My committee members, both inside (Profs. Samuel Kounaves and Arthur Utz) and outside (Prof. Richard Gaines) the University, were kind and patient enough to listen to my ramblings about arson investigations and the like, all the while providing the feedback and motivation for self-improvement each step of the way. This, hopefully, has culminated in a document that provides at least a modicum of progress in my little corner of the big world of scientific research.

I next wish to thank the other members of the Robbat research group from throughout my time here, all of whom made the laboratory an enjoyable setting. In particular, I am appreciative of Dr. Christian Zeigler, who was a continuous sounding board and an intermittent gym buddy; Amanda Kowalsick, who was at my side for every hurdle we leapt over simultaneously; and Zinovy Katayenko, without whom the probe project would have literally never even begun. I was fortunate to have many close friends inside the department who I am proud to call colleagues, and a single individual in the Biology department also fits that bill.

The members of the research data management service (RDMS) team, in particular Dr. Lionel Zupan and (future Dr.) Andy Valenti, taught me a great deal about teamwork, leadership, and professionalism. My experience on the RDMS project was invaluable, and I hope that our work provides the University with the foundation of a data culture that will serve it for years to come.

Finally, I want to acknowledge several special people for their endless and prodigious love and support: my brother Matthew, who has always been my best friend, and my girlfriend Meredith, who is deserving of gratitude that could never be expressed via words written in a mere dissertation. And above all, I want to express my appreciation to my parents. If I am a person of any repute, it is on account of them.

List of Tables

List of Figures

List of Acronyms

1D – one-dimensional (or first dimension)

2D – two-dimensional (or second dimension)

BTEX – benzene, toluene, ethylbenzene, xylene

CIS – cooled injection system

C_n – alkylation with *n* carbons; e.g. C_1 = methyl, C_2 = dimethyl or ethyl, etc.

DBT – dibenzothiophene

ECD – electron capture detection

EPA – United States Environmental Protection Agency

FID – flame ionization detection

GC – gas chromatography

GC-GC – automated sequential gas chromatography ("heartcutting GC")

GC×GC – comprehensive two-dimensional gas chromatography

ID – inner diameter

K_{OW} – octanol-water partition coefficient

LFER – linear (or logarithmic) free energy relationship

LIF – laser-induced fluorescence spectroscopy

LOD – limit of detection

LOQ – limit of quantitation

LTPRI – linear temperature-programmed retention index

MDL – method detection limit

MPS – multipurpose sampling system

MFPPH – multiple fragmentation patterns per homolog

MGP – manufactured gas plant

MS – mass spectrometry

MVOC – microbial volatile organic compounds

MW – molecular weight

NIST – National Institute of Standards and Technology

PAC – polycyclic aromatic compounds

PAH – polycyclic aromatic hydrocarbons

PAH_{34} – the list of 18 parent and 16 alkylated PAH targeted by the EPA in their narcosis model

PASH – polycyclic aromatic sulfur heterocycles

PID – photoionization detection

qMS **–** quadrupole mass spectrometer

RA – relative abundance

RE – relative error

RF – response factor

RI – retention index

RIC – reconstructed ion current

RSD – relative standard deviation

RPD – relative percent difference

RT – retention time

SIE – selected ion extraction

SIM – selected ion monitoring

SVOC – semivolatile organic compounds

S_W – Aqueous solubility

TEDSS – Thermal Extraction/Desorption and Sensor System

TIC – total ion current

TOF – time of flight mass spectrometer

VOC – volatile organic compounds

VdW – van der Waals' interactions

V_P – Vapor Pressure

Chapter 1 Introduction and Background

1.1 Polycyclic Aromatic Compounds and their Presence in the Environment

Polycyclic aromatic compounds and their alkylated homologues are pervasive environmental pollutants and a risk to human health and environmental well-being. This class of compounds, defined as molecules with two or more fully-conjugated rings and $4n + 2\pi$ electrons per ring, include the polycyclic aromatic hydrocarbons (PAH) and substituted heterocycles, such as polycyclic aromatic sulfur heterocycles (PASH). Select PAH and PASH are toxic,[1,2,3] mutagenic,[4,5,6,7] and carcinogenic.[8,9,10,11,12] They are not only environmentally persistent,[13] but have been shown to bioaccumulate.[14,15,16,17,18] Due in no small part to this hazardous nature, PAH are among the most-studied pollutants, with their source, transport, plant and animal uptake, toxicity, and fate in the environment all of the utmost importance. In addition, PAH, PASH and their alkylated homologues serve as indicators of persistence and damage to the environment.[19,20,21] EPA toxicologists measure the concentration of 16 "parent" PAH and 18 alkylated naphthalene, fluorene, phenanthrene, pyrene, and chrysene homologues, known as the $\Sigma PAH_{34,}$ to estimate the toxic hazard of contaminated soils and sediments[22,23] and assess risks posed to human health.[24] PASH, however, have yet to be included in EPA toxicological assessments – despite sulfur being the principal heteroatom in tars and oils, sulfur-containing compounds such as PASH are an often-overlooked factor in assessing the impact of fossil fuel-based pollutants on the environment.

PAH and PASH exist as a result of fossil fuel combustion, natural oil seeps, asphalt and shingle runoff, petroleum recovery, storage and transport activities, and from past actions at manufactured gas plants (MGP). According to a recent publication,[25] tens of thousands of MGP sites worldwide require cleanup. For more than 100 years, the MGP industry produced coal tar as a waste product, and it continues to seep into the environment to this day. Its discharge is of primary importance, since coal tar moves in narrow seams long distances from its release point, with more mobile components traveling even longer distances. Coal tar is extremely complex, containing thousands of aliphatic, aromatic, asphaltenic, and polar compounds and resins, all of which span a wide range of physical and chemical properties, and this complexity makes coal tar one of the most difficult matrices in analytical chemistry. In addition, the substance's composition is not static, instead dynamic – changing in relation to the environment. How coal tar weathers in the environment is highly dependent on its surroundings,[26] with its composition differing from one location to the next, even within the same site.[27] Sample weathering determines the immediate and eventual impact on local ecosystems – at some sites, source material pollutants have seeped into sediment for decades, with weathering processes partitioning some components and transforming others.[28] Examples of these processes include evaporation, dissolution, emulsification, adsorption, and microbial degradation, [26] and the corresponding molecular properties – volatility, solubility, and resistance to environmental adsorption and degradation – vary dramatically from homologue to homologue, even from isomer to isomer within the same homologue.[29] This

variability makes it difficult to predict how PAH and PASH concentrations change in the environment. The challenge brought forth by this ever-changing analysis, however, is far outweighed by its necessity.

1.2 Improving the analysis of PAC: Field Analytics

The United States Environmental Protection Agency (EPA) Brownfields initiative, dedicated to the redevelopment of property affected by the presence of hazardous substances, has led to the remediation of nearly 40,000 acres of land for reuse since its inception in 1995.[30] Cleaning up and reinvesting in these properties has numerous environmental and economic benefits, but traditional site investigations often require exceedingly large outlays of time and effort at an extremely high cost. These procedures are too slow, expensive, and inefficient for a characterization and remediation process as expansive as the one currently required, which entails accurate monitoring of prospective contaminants throughout the entire ecosystem, as well as complete bioavailability and bioaccumulation assessments.

Rapid assessment of the state of contamination (and corresponding level of risk) at purported or existing hazardous waste sites is an essential first step in the remediation process. Based on this assessment, a decision is made as to whether further action, such as a full-scale site characterization, is necessary. Sampling and analysis programs are vital at each step in the process, from initial assessment to final remediation. However, traditional sampling programs, which rely on a predetermined number and location of samples to be collected and the type of

analyses to be conducted, do not provide an adaptive framework while in the field. Samples are sent off-site for analysis, which can lead to weeks-long turnaround. If data is insufficient (or inconclusive), precluding a remediation decision, subsequent lengthy and expensive field studies are required. In contrast, dynamic work plans rely on field-ready analytical instrumentation and methods for real-time information on site contamination and risk levels. Rather than specify predetermined sampling locations and methodologies, they simply specify levels of decision-making logic that allow for adaptation based on the analytical results produced in the field.[31]

Remediation decisions that are reliant upon site-specific data can reduce costs, lessen decision uncertainty, and expedite site closeout. In addition to these economic benefits, the rapid assessment of environmental contaminants at hazardous waste sites is of great importance when evaluating the risk to human health and the environment. In the late 1990s, environmental scientists and the EPA, recognizing the value of implementing a more dynamic approach to site cleanup, developed the Triad approach to hazardous waste site investigation and remediation.[32] The Triad incorporates systematic project planning, dynamic work plans, and real-time measurement technologies to both accelerate and improve the cleanup process. The dynamic workplans that play a major role in the Triad approach require analysis methods that produce rapid results, preferably in real time, so as to not delay decision-making. To this end, a number of analytical techniques have been applied to *in situ* detection of environmental pollutants.

The backbone of this line of research is advancement of an analytical probe into the subsurface via direct hydraulic push, allowing for either (a) instrumental signal or (b) sample itself to be transported to the surface. Specific to VOC (such as BTEX) and SVOC (such as PAH and PASH), strategy (a) has included LIF[33,34] and Raman and infrared[35,36] spectroscopy techniques. With regard to strategy (b), VOC and SVOC have been transferred to the surface for analysis by electron capture (ECD), flame ionization (FID), and photoionization (PID) detection,[37,38] as well as mass spectrometry.[39] However, an all-in-one solution for real-time speciation and quantitation of both VOC and SVOC in both soil and groundwater remains a challenge. To this end, twenty years of research at the Tufts University Center for Field Analytical Studies and Technology has focused on building analytical instruments and developing methods to overcome this challenge and produce high quality data in the field.[40,41,42,43]

1.3 Improving the analysis of PAC: Chromatography

Gas chromatography/mass spectrometry (GC/MS) is the technique most often used to identify and quantify PAH and PASH,[44,45,46] as it is the only analytical technique that can provide unambiguous identification of these compounds. However, the overlapping retention windows and common spectral ions (Figure 1-1),[47] in addition to the complexity of matrices such as coal tar, render the inter-related goals of target compound separation, identification, and quantification a distinct challenge to analytical chemists.

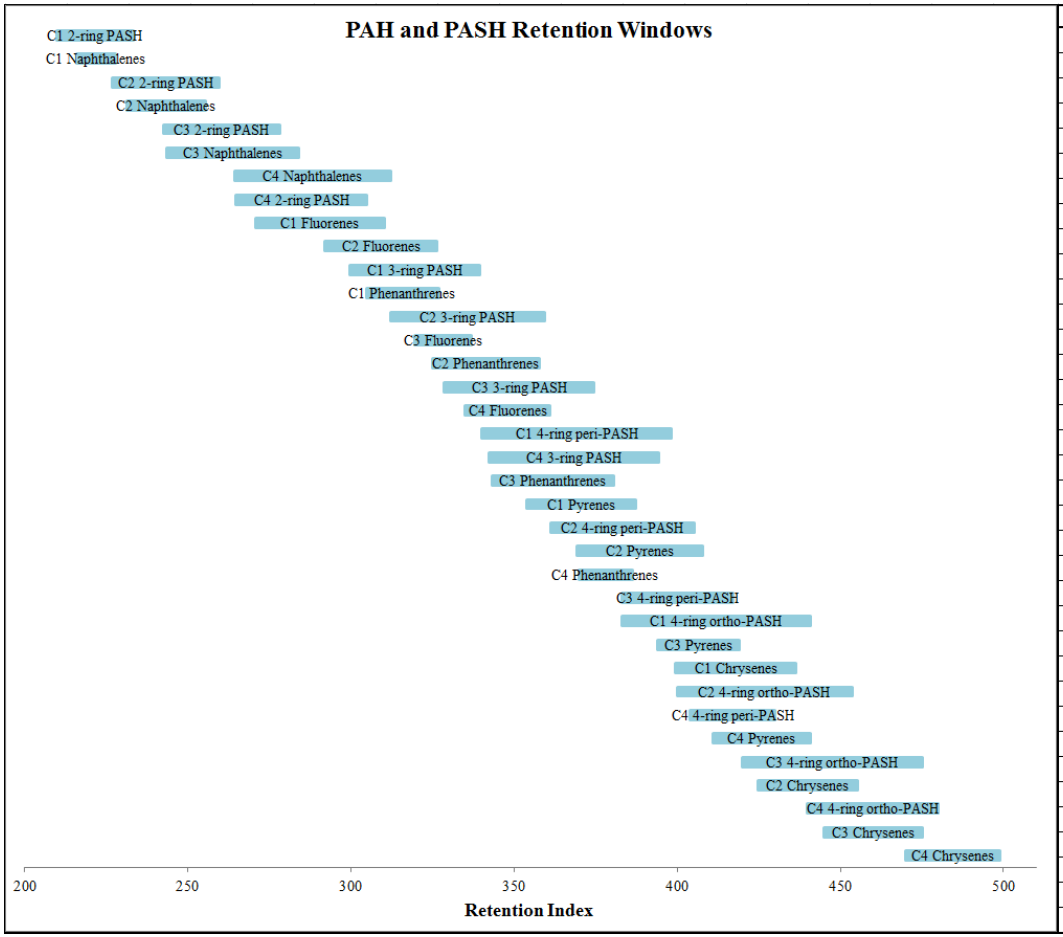

Homologue	Quant Ion	Interfering Homologues
C_1 2-ring PASH	148	C_2 2-ring PASH
C_1 Naphthalenes	142	C_2 Napthalenenes
C_2 2-ring PASH	162	C_3 2-ring PASH, C_4 2-ring PASH
C_2 Naphthalenes	156	C_3 Naphthalenes
C_3 2-ring PASH	176	C_4 2-ring PASH
C_3 Naphthalenes	170	C_4 Naphthalenes
C_4 Naphthalenes	184	C_0 3-ring PASH, C_2 3-ring PASH
C_4 2-ring PASH	190	C_1 Phenanthrenes
C_1 Fluorenes	180	C_2 Fluorenes
C_2 Fluorenes	194	C_3 Fluorenes, C_4 Fluorenes
C_1 3-ring PASH	198	C_2 3-ring PASH
C_1 Phenanthrenes	192	C_2 Phenanthrenes
C_2 3-ring PASH	212	C_3 3-ring PASH, C_0 4-ring *ortho* -PASH
C_3 Fluorenes	208	C_4 Fluorenes, C_2 3-ring PASH, C_3 3-ring PASH
C_2 Phenanthrenes	206	C_3 Phenanthrenes
C_3 3-ring PASH	226	C_4 3-ring PASH, C_0 Chrysene
C_4 Fluorenes	222	C_1 4-ring *peri* -PASH
C_1 4-ring *peri* -PASH	222	C_4 Fluorenes
C_4 3-ring PASH	240	C_1 Chrysenes, C_0 4-ring *ortho* -PASH
C_3 Phenanthrenes	220	C_4 Phenanthrenes, C_1 4-ring *ortho* -PASH
C_1 Pyrenes	216	C_2 Pyrenes
C_2 4-ring *peri* -PASH	236	
C_2 Pyrenes	230	C_3 Pyrenes
C_4 Phenanthrenes	234	C_2 4-ring *peri* -PASH, C_0 4-ring *ortho* -PASH
C_3 4-ring *peri* -PASH	250	C_0 5-ring PAH
C_1 4-ring *ortho* -PASH	248	C_3 4-ring *peri* -PASH
C_3 Pyrenes	244	C_4 Pyrenes, C_0 4-ring *ortho* -PASH
C_1 Chrysenes	242	
C_2 4-ring *ortho* -PASH	262	
C_4 4-ring *peri* -PASH	264	
C_4 Pyrenes	258	
C_3 4-ring *ortho* -PASH	276	C_0 6-ring PAH
C_2 Chrysenes	256	C_4 4-ring *peri* -PASH, C_0 5-ring PAH
C_4 4-ring *ortho* -PASH	290	
C_3 Chrysenes	270	
C_4 Chrysenes	284	C_0 5-ring PASH

Figure 1-1. Retention windows and quantitation ion interferences for alkylated PAH and PASH.

Researchers have looked to improve separation through advances in GC technology. In the last two decades, computerized temperature and flow control, wall-coated open tubular columns, and programmed temperature vaporizing inlets, among other improvements, have all been used to improve separation efficiency. More recently, researchers have looked to novel stationary phases such as room-temperature ionic liquids (IL), a class of non-molecular ionic solvents with low melting points (usually defined as < 100 °C).[48,49,50,51] Their "tunable" nature, negligible vapor pressure, and stability at high temperature when cross-linked make them well-suited for GC applications.

There are, however, limitations to the number of compounds that can be separated during a single-column analysis, no matter the column. Under Giddings' statistical model of overlap (SMO),[52,53] which uses Poisson statistics to model apparently random peak distribution, resolution of 95% of components of a complex multicomponent mixture requires a peak capacity 39 times greater than the number of components – an number unattainable by GC/MS. To make matters worse, in addition to these theoretical limitations, certain practical limitations also apply. Compounds with similar retention parameters produce crowding in certain parts of the chromatogram while leaving empty space in others.[54] This can be described by the concept of sample dimensionality, also introduced by Giddings.[55] Sample dimensionality is a measure of sample complexity, to be compared with the dimensionality of the system, and is visualized in Figure 1-2.[56] In this example, we see a "sample" that consists of

compounds that differ in size, shape, and color –a sample dimensionality of three. An attempt to separate these compounds by one of size, color, or shape will lead to interferences due to the other sample characteristics. In this case, the system dimensionality is one, and separation is far from satisfactory. As such, increasing system dimensionality, such as separation based on size and then separation by color (through an additional separation mechanism), can improve results.

This quest for improved separations by instrumental means (increased peak capacity and system dimensionality) has led to the development of multidimensional chromatographic methods and spectral deconvolution. The two most prevalent forms of multidimensional GC separations, which are defined as those separations in which each mechanism is orthogonal (uncorrelated), and separation gained in the first dimension must not be lost in subsequent steps,[57] are heart-cut GC (GC-GC), and comprehensive two-dimensional GC (GC×GC). GC-GC entails connecting two analytical columns of different phases and selectively transferring a portion of the effluent from one column into the other using a flow-control column switching device.[58] When a group of co-eluting components is transferred from one column to another with different separation characteristics, the hope is that the co-eluting compounds will be separated. For example, a typical GC-GC setup consists of a non-polar first column and a polar second column. In this way, two compounds with similar volatilities will elute at similar times on the first column, but upon transfer to the second column, they may separate based upon structural differences that lead to differing polarities.

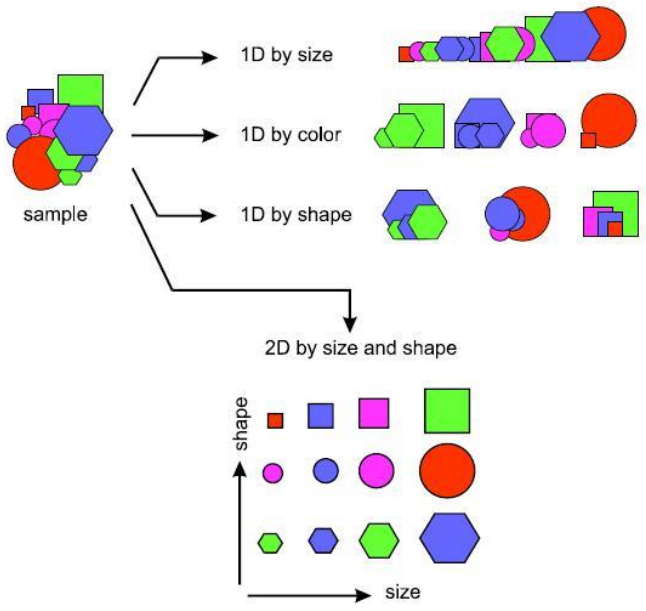

Figure 1-2. Visualization of sample dimensionality. If the components of the sample consist of *x* sample dimensions, a separation system with fewer than *x* dimensions will have difficulty separating all components

To use the concept of system dimensionality, this GC-GC experiment separates by both volatility and polarity – a system dimensionality of two.

GC×GC is seen as the limiting case of GC-GC when the width of the heart-cut approaches zero.[59] Ideally, extremely small sample portions are continuously, and with known frequency, transferred from the first column to a very short, narrow-bore second column at regularly-spaced intervals. A modulator rapidly transfers eluent from the 1st to the 2nd column through a valve system[60] or by cryogenically freezing and/or thermally desorbing each sample portion. If 2nd column runs finish before subsequent transfers occur, the outcome is an additional set of chromatograms produced on a 1-dimensional time-scale.[61] The resulting multidimensional chromatogram not only increases the separation space and visualization of sample components in complex mixtures,[62] but also offers

improved sensitivity,[63] as "space-compressed" 2nd dimension peaks are up to 50-times narrower than 1st dimension peaks.[64]

1.4 Improving the analysis of PAC: Data Analysis

To identify targeted or unknown compounds by MS, mass spectra from a sample are compared to those found in mass spectral libraries. However, success is dependent on these spectra being clean: free of interferences from other target compounds or matrix organics. To combat the issue of overlapping mass spectra, researchers have employed not only multidimensional separations, but also increasingly-complicated sample preparation procedures and lengthy chromatographic analysis times. Beyond the trade-offs required (increases in analyst burden and decreases in sensitivity), these approaches far from guarantee success. Our research group, instead, has focused on the "separation" of coeluting compounds through mathematics – that is, mass spectral deconvolution.[65] Mass spectral deconvolution is based upon the isolation and inter-comparison of individual ion signals from the full mass spectrum, followed by application of algorithmic filters for result confirmation or rejection. The deconvolution process is outlined below.

First, the analyst selects a number of component ions per compound based on MS fragmentation patterns. These ion signals are extracted from the full mass spectrum at each scan, normalized, and compared to the known abundances for the compound as found in a target compound library (such as the PAH and PASH fragmentation library discussed below). A number of equations, as will be

described in Chapter 5, are used to calculate the difference between the observed and library relative abundances (RA). By comparing these abundances against one another on a scan-to-scan basis, the equations can be used to eliminate the signal from a matrix-affected ion. With this information in hand, compounds can be identified based on relative abundance (RA) error, scan variance, and comaximization criteria.

Analysts who are charged with quantitation of target compounds in complex samples but do not employ mass spectral deconvolution often choose to operate the MS in selected ion monitoring (SIM) mode in order to increase measurement sensitivity of low concentration analytes.[66] SIM analysis is an acceptable alternative to full scan mass spectrometry when full-scan MS is incapable of detecting target compounds below the limits of quantitation needed to answer site-specific questions. However, because SIM methods typically monitor one or two ions per homologue, they can provide a lower degree of confidence due to the loss of spectral information.[67] Thus, analysts rely on pattern recognition of alkylated PAH and PASH ion chromatograms within specified retention windows, which can result in overestimated concentrations due to additive ion effects from the matrix.[68]

Motivated by the high rates of false positives and overestimated concentrations produced by GC/MS methods that rely on too few ions to confirm compound identity, [70,69] previous research focused on the analysis of the aromatic fraction of

fresh and weathered coal tar and crude oil samples by GC-GC/MS to obtain the retention windows and fragmentation patterns for C_1 to C_4 alkylated PAH and 119 parent and monoalklyated 2-, 3-, 4-, and 5-ring PASH.[68,70,71,72,73] The end result was an MS fragmentation library and corresponding data analysis method that employs 3- to 5-ions per compound and as many fragmentation patterns as needed (hence, multiple fragmentation patterns per homologue – MFPPH) to identify all homologue isomers and quantify alkylated PAH and PASH.[70,73] Development of this method has enabled the critical evaluation of SIM/SIE analyses, as the aforementioned concentration overestimations that can result from use of these techniques can have profound impacts on fate, transport, risk assessment, bioavailability, and weathering studies.

Chapter 2 A GC/MS Chemical Sensor System for VOC and SVOC Analysis in the Vadose Zone and Groundwater

2.1 Introduction

For more than twenty years, researchers at the Tufts University Center for Field Analytical Studies and Technology (FAST) have built analytical instruments and developed gas chromatography/mass spectrometry methods to produce high-quality data in the field. The two main thrusts of this research have been spectral deconvolution software for fast GC/MS analyses[65,74,75] and a GC/MS-based chemical sensing system to detect and identify volatile organic compounds (VOC) and semi-volatile organic compounds (SVOC) in real-time below grade without bringing sample to the surface.[76,77,78] The system consists of a heated sampling probe, high temperature transfer line (HTTL), cryotrap, and GC/MS. While *in situ* subsurface monitoring can be challenging, these direct measurements play a significant role in dynamic site investigations and are of the highest importance in the aftermath of environmental disasters. As such, research at FAST has focused on overcoming these challenges to produce the first technology that can completely and unambiguously profile the subsurface from ground-level to bedrock. These improvements include the following: (1) on-line GC/MS detection to minimize sample loss, (2) a photoionization detector to provide both continuous, real-time detection of organics and protection of the mass spectrometer by preventing detector overload, and (3) a Peltier cooler cryotrap to maximize collection of VOC.[39,79] However, given the unique requirements and

difficult conditions mandated by field work, the system is not without room for improvement.

First, VOC can be lost due to inconsistently low cryotrap temperatures, especially when the apparatus is sitting on a hot GC oven and outdoor temperatures approach 35 ºC.[79] The three-stage Peltier cooler design described in previous work could reach -30 ºC under these conditions and provided good data quality, but consistently lower temperatures would be preferred. Second, the system requires two sets of collection rods – one for the vadose zone and another for groundwater. For soil with a moisture content of < 15%, the current membrane-less sampling probe is heated to 400 ºC. At this temperature, soil temperatures reach > 300 ºC, more than sufficient for efficient desorption and extraction of soil-bound VOC and SVOC.[39] However, this sampling probe cannot be used for soils with moisture content > 15%, as water or steam can pass through the collection port and degrade the transfer line coating, leading to organic adsorption onto the HTTL walls. As such, a second sampling probe is needed for saturated soils and groundwater. A commercially-available membrane inlet probe (MIP) sufficiently blocks water and steam, but was temperature-limited to 140 ºC, which means that semivolatile organic compounds (SVOC) cannot be collected from soil.[79] Although the dual-probe method saves time and expense when compared to conventional sample collection systems, field personnel have indicated it would be preferable to have a single probe capable of collecting both VOC and SVOC at depth for both soil and groundwater. Third, VOC calibration of the sensor system

is performed in the laboratory prior to field work. While this has been shown to be effective, it prevents semi-quantitation of VOC in the field if QC samples fall out of range due to instrumental drift or if modification of system parameters is required.

This study reports improvements to the membrane inlet and cryotrap, as well as a novel on-line VOC calibration unit that addresses the above issues. The end result approaches the goal: a comprehensive *in situ* subsurface analysis system that allows for real-time detection, speciation, semi-quantitation, and mapping of all organics in the subsurface, referred to as the Thermal Extraction/Desorption and Sensor System (TEDSS).

2.2 Experimental

Instrumentation: Construction and operation of the TEDSS (Figure 2-1) has been extensively described in prior work;[39,79] a brief summary follows.

The collection port (Figure 2-2) consists of a newly-designed membrane of polytetrafluoroethylene (PTFE)-coated steel mesh inserted into a 33-cm steel pipe. A cartridge heater block (Watlow Heaters – St. Louis, MO) held in contact with the collection port allows for the thermal desorption of organic pollutants from soil or groundwater. Deactivated fused silica-lined stainless steel (Siltek, from Restek – Bellefonte, PA) inlet (from membrane inlet to 6-port valve) and outlet (from valve to inlet) tubes (OD = 1/16", ID = 0.040") are drill-fitted

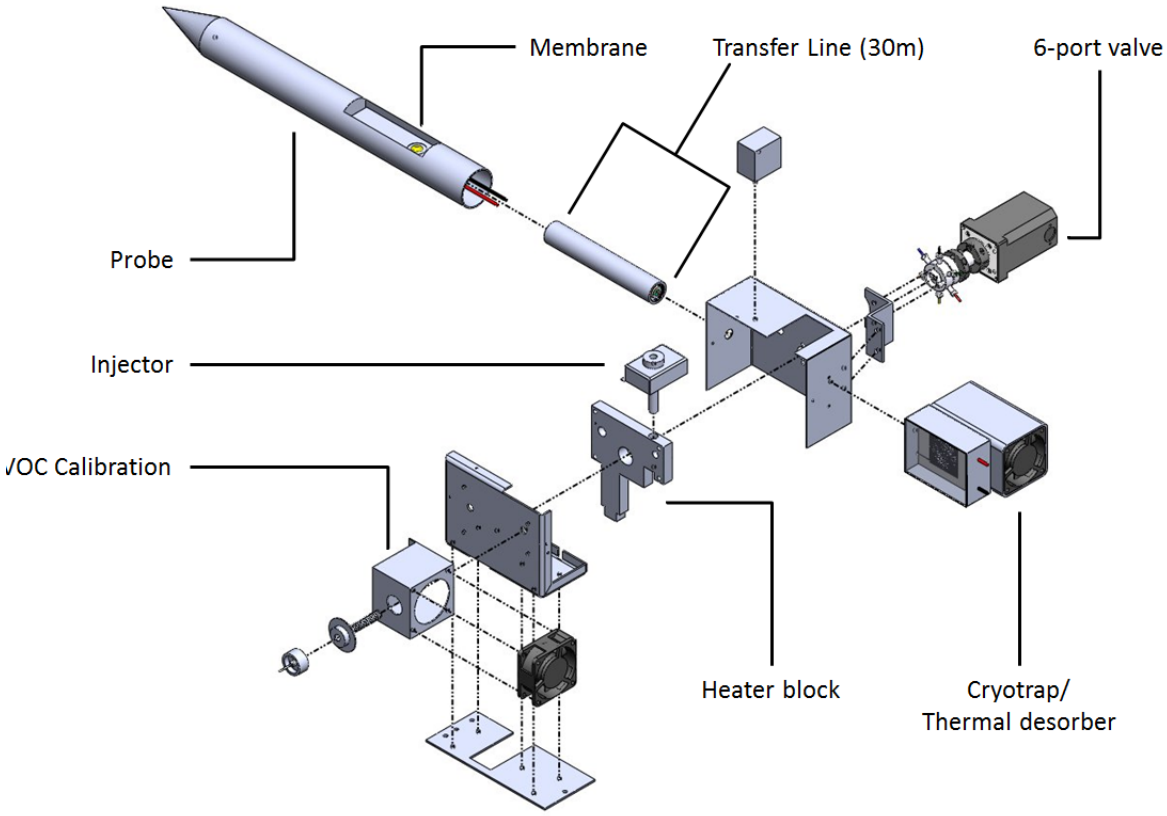

Figure 2-1. TEDSS schematic

through the pipe to allow for the passage of nitrogen gas and desorbed organic analytes through the membrane to the rest of the system. Optimal carrier gas flow was calculated using the method outlined in Gorshteyn *et al.*[80] The heated transfer line (Figure 2-3) consists of resistively-heated Siltek tubing (OD = 1/16", ID = 0.040") surrounded by layers of thermal insulation and electrical insulation (aluminum foil (McMaster-Carr – Robbinsville, NJ), fiberglass (Insulflex – Cobourg, Ontario, Canada), polyolefin (Newark Electronics – Chicago, IL) and ceramic layers), a Viton outlet line, and thermocouples (all from Omega Engineering – Stamford, CT). This entire bundle is wrapped in water-resistant heat-shrink tubing and tear-resistant fabric coating (both from Mouser – Mansfield, TX) and threaded into steel pipes when driven

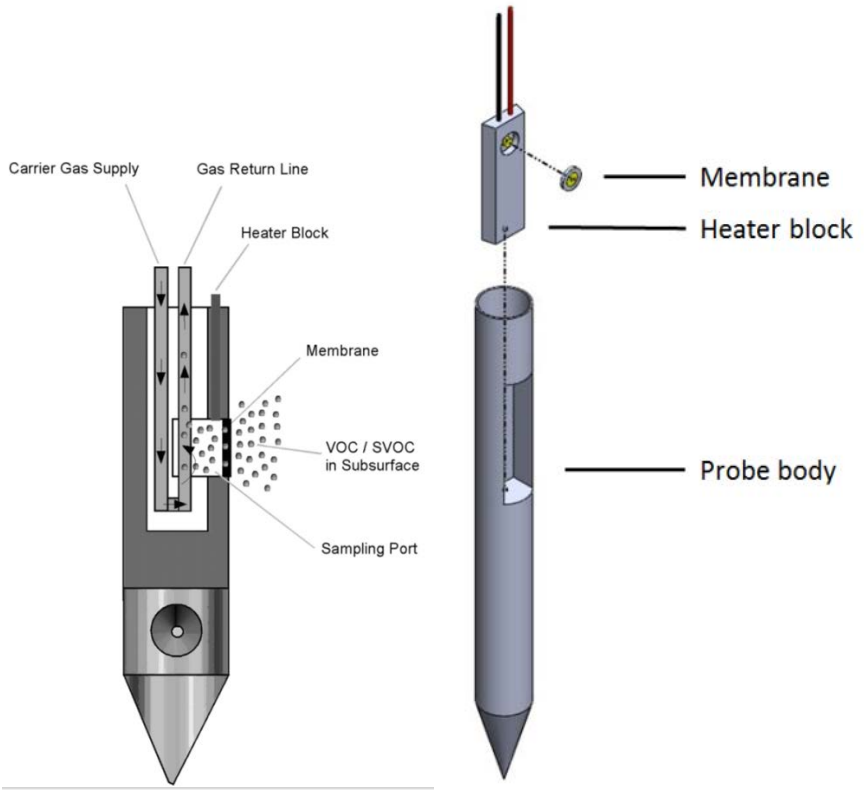

Figure 2-2. Two depictions of the TEDSS collection port and membrane inlet

into the subsurface. It is held at 280 ºC to prevent analyte condensation on the walls of the Siltek tubing. The transfer line is connected to a heater block-heated high-temperature 6-port valve (VICI Valco – Houston, TX) that is also connected to all other modules (VOC calibration unit, cryotrap, etc. – see Figure 2-4).

As the probe is advanced into the subsurface at 1 cm/s, the PID provides continuous on-line detection of environmental pollutants as they are transported to the surface from the probe through the transfer line. If the PID signal "spikes" (organics are detected), probe advancement is stopped and flow is switched (by rotating the six-port valve) from the PID to a cryotrap, where the sample is concentrated for 5-min.

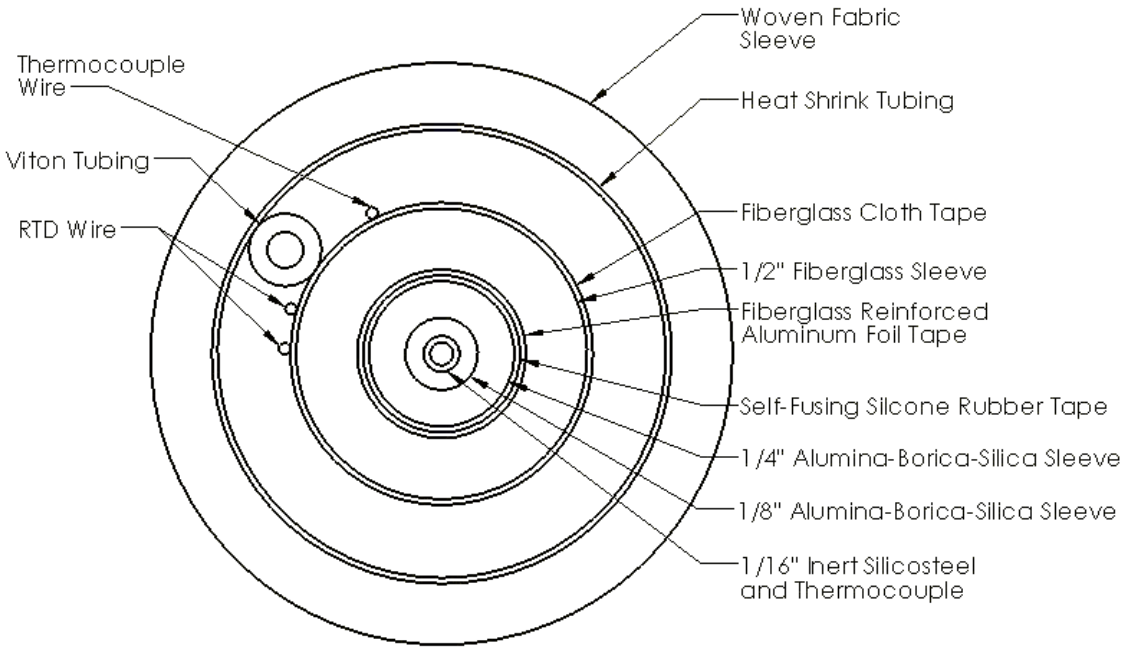

Figure 2-3. Cross-section of TEDSS high-temperature transfer line

The cryotrap (Figure 2-5) is consists of a three-stage thermoelectric module (Laird Technologies – London, UK) cemented in contact with a 12.5 cm coil of Siltek tubing (OD = 0.8 mm, ID = 0.53 mm) that also serves as a resistively-heated thermal desorber. Analytes are then thermally desorbed from the cryotrap and swept onto the GC column by helium, followed by analysis by GC/MS. Positive ID is made and the composition and concentration of the sample at known depth is recorded. Using mathematical algorithms developed at Tufts to deconvolve the characteristic narrow band MS signals, low concentrations of target analytes can be detected even in the presence of high levels of matrix interferences,[75,81] and chromatographic run-time can be reduced significantly.[74] The newly-designed VOC calibration unit is an additional thermal desorber customized for absorbent tubes. The GC/MS was an Agilent (Santa Clara, CA)

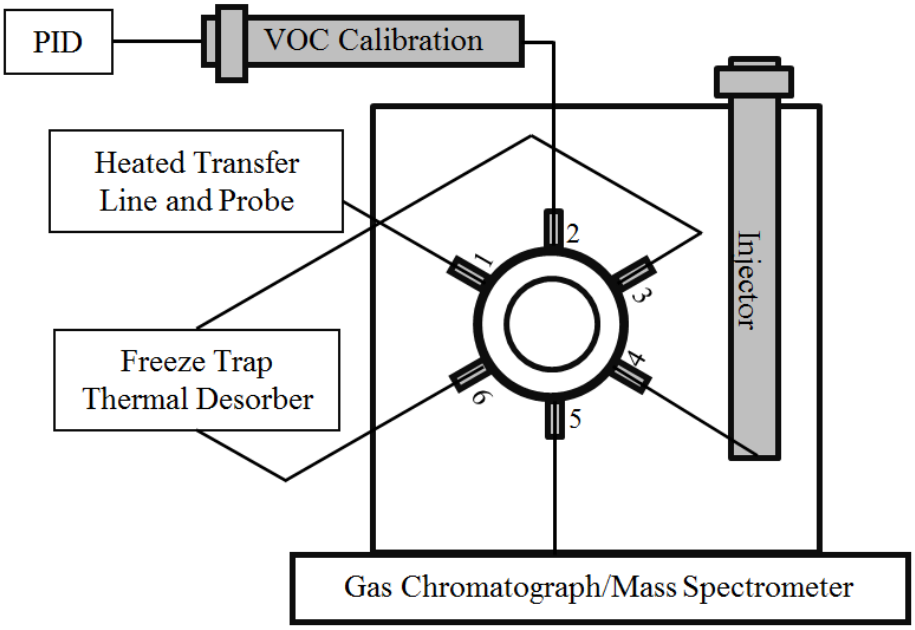

Figure 2-4. TEDSS 6-port valve

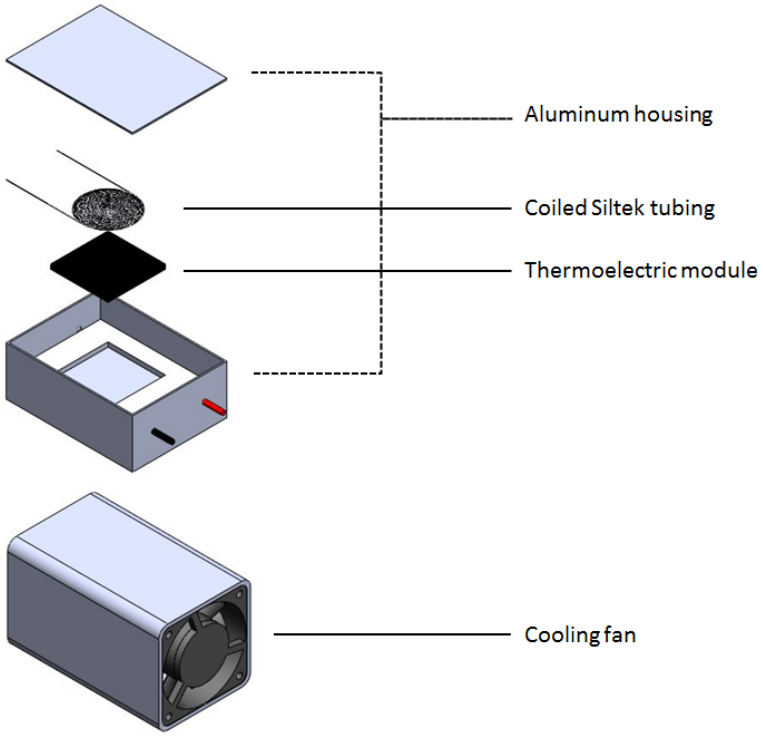

Figure 2-5. TEDSS cryotrap

7890/5975C modified for temperature and pressure control of Tufts-built modules via the instrument's auxiliary ports.

Membrane Materials and Testing: A variety of hydrophobic materials and stainless steel meshes were obtained for testing, see Table 2-1. Prospective membrane and support material viability was tested as follows.

a.) Ruggedness: Materials were impact- and scratch-tested. Scratch testing was performed by pulling sharpened rocks and razor blades across the material. Material integrity was then examined for physical damage under a microscope. This was repeated prior to each of tests (b) through (d).

b.) Thermal Resistance: Membrane materials that survived ruggedness testing were heated to failure in an oven. Samples that failed to reach 300 ºC were classified as "failed".

Table 2-1. Prospective membrane and support materials

Sample	Supplier	Ruggedness	Heat Tolerance	Water Blockage	Steam Blockage	Organic Passage
Membrane inlet mass spectrometry inlet	Bruker	Passed	Passed	Passed	Passed	Failed
PTFE process filter	Entegris	Passed	Failed	Passed	Failed	N/A
PTFE Dispersion (coated onto steel mesh)	Fuel Cell Earth	Passed	Passed	Passed	Passed	Passed
PTFE Laminate	W.L. Gore	Passed	Passed	Passed	Failed	N/A
PTFE-coated steel mesh	Fluoro Precision Coatings	Passed	Passed	Passed	Passed	Failed
PVDF process filter	Entegris	Passed	Failed	Passed	Failed	N/A
Woven PTFE Fabric	Stern & Stern	Passed	Passed	Passed	Failed	N/A

c.) Water Blockage: Materials were clamped between one 10 mL vial containing water and another containing calcium sulfate dessicant stones and cobalt chloride indicator (Drierite – Xenia, OH). The entire apparatus was heated to ~150 ºC, and each material's blockage of both steam and bubbles of liquid water was observed for 15 minutes. After this time period, the Drierite stones were examined and any color change was classified as a failure. Control experiments were performed with blank steel mesh, which allowed complete passage of steam and caused an immediate change in color of the indicator stones.

d.) Organic Passage: The same "sandwich" apparatus as used in part (c) was applied, with the water spiked with 10 ppb BTEX and a "Twister" SBSE (Gerstel – Mülheim an der Ruhr, Germany and Baltimore, MD) in place of the dessicant stones. In this way, any volatilized BTEX that passed through the membrane would be absorbed by the Twister, which was analyzed by GC/MS. Membrane builds that did not allow passage of BTEX were discarded.

Final Membrane Build: The membrane inlet used in the chemical sensor system is a 75 µm pore Dutch weave stainless steel mesh (Belleville Wire Cloth Co. – Cedar Grove, NJ) coated with PTFE TE3859 dispersion (Fuel Cell Earth Inc. – Stoneham, MA). Coating method (dip, spray, and brush), number of coats (1-3), curing temperatures (100-300 ºC) and durations (1-24 h per cure) were examined, and the resultant final membrane coating procedure is as follows. The stainless steel mesh is scoured with a wire brush to remove particulates and then sonicated in toluene for 30 minutes. Using a Pasteur pipette, drops of the PTFE dispersion

are placed on one side of the mesh and allowed to disperse until the mesh is completely covered. A small paintbrush is used to coat it evenly. After air drying for 15 minutes, it is placed into an oven and cured under argon: 30 min at 100 ºC, 30 min at 200 ºC, and then 60 min at 300 ºC. Once one side of the mesh coating is cured, the other side is spray-coated with the PTFE dispersion using a TCP G5500 low-pressure spray gun (TCP Global – San Diego, CA). The spray coated side is dried and cured using the same temperature program described previously. After repeating the spray/cure process two additional times on the spray-coated side, that side is scraped with a straight edge razor to remove excess material. Finally, the entire mesh is cured for an additional 24 h at 300 ºC.

Standards and Reagents: The 16 EPA-priority pollutant PAH standards, internal standards (1,4-dichlorobenzene-*d4*, naphthalene-*d8*, phenanthrene-*d10*, chrysene-*d12*, and perylene-*d12*) were purchased from Restek. BTEX (benzene, toluene, ethylbenzene, and *m*-, *o*-, and *p*-xylene) standards, internal standard toluene-*d8*, anhydrous sodium sulfate, neat dibenzothiophene (DBT), and the base/neutral surrogate mixture (2-fluorobiphenyl, nitrobenzene-*d5*, *p*-terphenyl-*d14*) were purchased from Sigma-Aldrich (St. Louis, MO). Airgas (Salem, NH) supplied the ultra-high purity helium and nitrogen.

GC/MS Analysis: To determine linear quantitation ranges, serially-diluted SVOC (PAH and DBT) and VOC (BTEX) standards were analyzed from 0.3 to 500 ng/µL and 10 to 100 pg/µL, respectively. VOC standards were analyzed by purge

and trap methods, both onto Tenax TA sample tubes (Gerstel) placed in the VOC calibration unit and direct purging onto the membrane probe. In each case, purging was performed for 5-min at ambient temperature, and thermal desorption performed at 200 °C for 2-min. For both VOC and SVOC analyses, the cryotrap was held at -40 °C. SVOC standards and samples were analyzed by both traditional sample injection (1 µL) into the GC/MS inlet and heated desorption through the membrane probe at 280 °C for 2-min followed by 2-min of desorption from the cryotrap at 270 °C. GC/MS conditions were as follows: DB-5MS Ultra Inert 30 m L × 0.25 mm ID × 0.25 µm film thickness (Agilent), 1.0 mL/min constant helium flow, temperature program of 40 °C (hold 1 min) to 325°C at 6 °C/min (hold 5 min), and full scan MS from 50-350 *m/z* at 5 Hz. PAH and DBT response factors (RF) were calculated for each concentration over the dynamic range as follows: $A_X C_{IS}/A_{IS} C_X$, where C_X is the analyte concentration and A_X its observed signal, with C_{IS} and A_{IS} the corresponding internal standard concentration and signal response. Alkylated PAH homologues were identified using the spectral patterns and retention windows outlined in the previously-published MFPPH data analysis method,[47,73] and quantified using each parent's average RF. Spectral deconvolution software from Ion Analytics (Andover, MA) was used to process GC/MS data.

2.3 Results and Discussion

This study details three modifications to the chemical sensor system that serve to improve system performance and flexibility. First, we addressed the cryotrap. It was proposed that a cryogenic trap, based on liquid CO_2 flowing past a Siltek coil,

would provide trap temperatures of nearly -60°C in lab conditions. While this was found to be the case, it also had a propensity for ice blockages and required excessive cryogen usage, both of which preclude it from effective utilization in field work. As such, we returned to thermoelectric-based designs. First, we replaced the three-stage Peltier cooler with a more powerful model: 18W maximum heating capacity versus 11W for the previous design. Next, we modified the volume of the trap itself. Prior cryotraps have been based on a flattened coil design spiraled five times. This trap design was chosen for maximum capacity, and is the maximum trap size that can be cemented in contact with the thermoelectric module. However, this trap capacity is unnecessary for analyses of even the most concentrated coal tar extracts, and only serves to augment the risk of sample carryover. By coiling the Siltek tubing only twice, the cryotrap thermal mass is decreased by 58%. This lower thermal mass, along with increased coil pitch to prevent “hot spots”, led to decreased trap temperatures, as low as -50 °C under lab conditions.

Next, we addressed the need for a VOC calibration unit. The addition of a thermal desorber to the system, while seemingly a simple task, was not without challenges, as it required a complete overhaul of the plumbing of the six-port valve and system carrier gas lines. The system plumbing is shown in Figure 2-6 – gas flows can be traced along the color-coded lines, green for nitrogen and orange for helium. In valve position A, organics are collected from the subsurface

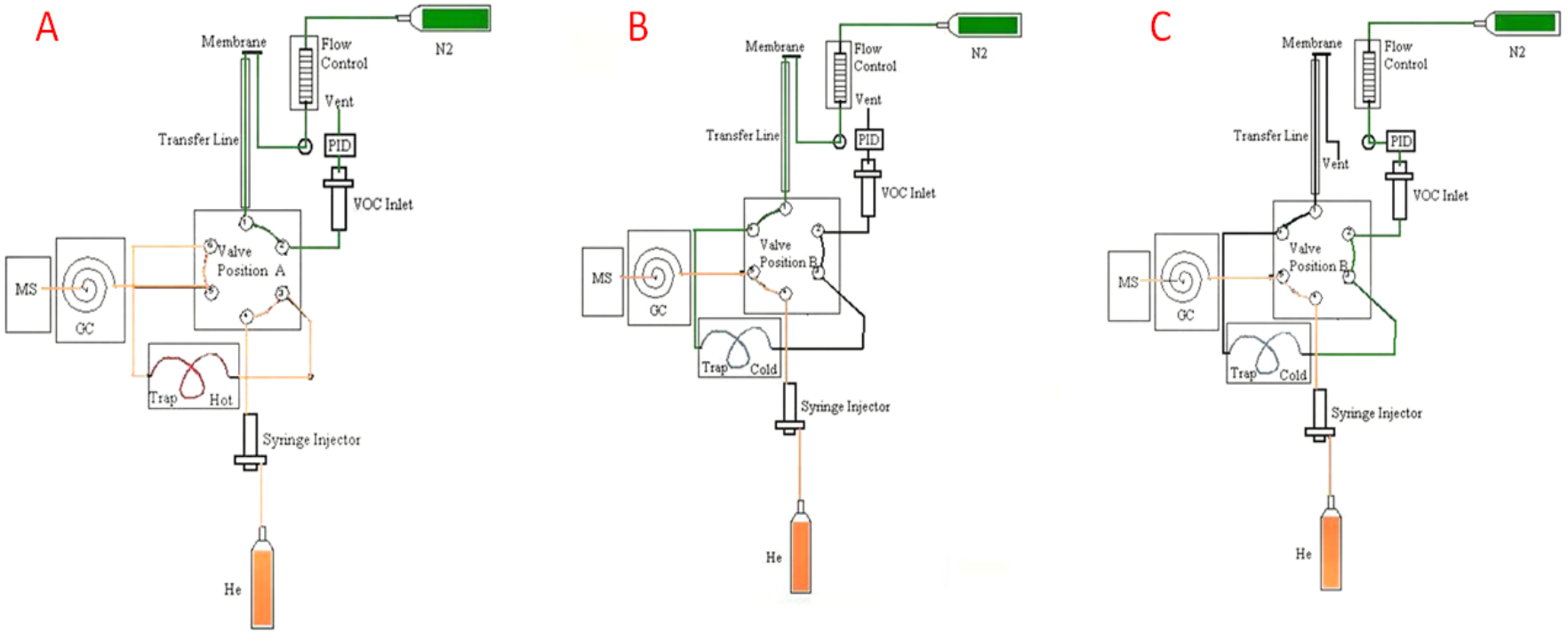

Figure 2-6. TEDSS gas flow schematic

through the membrane and transported through the heated transfer line by nitrogen, see Figure 2-6A.

The valve is switched to position B and the sample is collected in the cryotrap, see Figure 2-6B. After collection, the valve is switched to position A (Figure 2-6A), the cryotrap is resistively heated, and sample is desorbed and swept onto the column by helium gas flow. Figure 2-6C shows calibration of the GC/MS prior to analysis using the abovementioned injectors to provide quantitative estimates of VOC and SVOC concentrations. While SVOC calibration is performed using conventional syringe injections, the VOC calibration unit allows for both off-line and on-line calibration via purge-and-trap. In off-line calibration, compounds are purged from an aqueous medium onto an adsorbent packed tube. These tubes are placed in the VOC thermal desorber, which is then heated to 200 ºC to desorb compounds onto the freeze trap (valve position B). The valve is switched back to position A (Figure 2-6A), and helium sweeps the heated VOC standards onto the column for analysis. During on-line calibration, VOC are purged directly through the heated thermal desorber into the freeze trap, followed by normal GC/MS analysis. Either method can be performed in the field.

Finally, we addressed the membrane inlet. An ideal membrane material would provide the following: (1) the ruggedness needed to survive contact with rocks and debris during the subsurface push, (2) passage of organics and blockage of

water and steam, in order to protect the transfer line coating, and (3) resistance to temperatures upwards of 300 ºC, to allow for thermal extraction of SVOC from soil within 1 mm of the membrane.[39] After investigating the ruggedness, thermal resistance, water blockage, and organic passage of a number of commercially-available membrane probes, we determined that none could offer these properties and, as such, worked to develop an in-house solution – a hydrophobic material protected by steel mesh. The only membrane material to pass all tests and meet all criteria (robustness, temperature resistance, hydrophobicity and organic passage) was the PTFE dispersion when applied to Dutch weave meshes with mesh counts of 40 × 200, 24 × 110, or 30 × 150. These meshes have pore sizes of 60, 75, and 100 µm, respectively – pore sizes above and below this range led to passage of water and poor coating integrity, respectively. The coating procedure was then optimized, with the four tests described above repeated for each iteration.

With these three improvements in hand, the entire system was tested. VOC calibrations were performed using (1) purge-and-trap onto absorbent tubes and (2) direct passage through the membrane inlet onto the cryotrap. While the BTEX calibrations provided an acceptable LOQ (10 ng/mL) and linearity (r^2 = 0.99) over the calibration range, the same cannot be said for SVOC calibrations by passage through the membrane inlet onto the cryotrap; PAH, especially the 6-ring PAH (indeno[1,2,3-*c,d*]pyrene, dibenz[*a,h*]anthracene, and benzo[*g,h,i*]perylene), could not be detected at acceptably low concentrations (3-ring PAH MDL = 7

µg/mL, 5 and 6-ring PAH MDL = 250 µg/mL). This was due to the lower-than-optimal maximum temperature of the thermal desorber (270 ºC) and multiple "cold spots" in the plumbing leading from the cryotrap to the GC/MS. At press time, we have developed a more thermally-robust cryotrap/thermal desorber for complete volatilization of these high-MW components that has delivered promising results (detection of 3-ring PAH at 0.6 ng/µL and 6-ring PAH at 2 ng/µL) during preliminary tests.

This study has outlined improvements to an *in situ* subsurface analysis system that allows for rapid analysis and real-time speciation of even the most complex samples. It is, then, well-suited to tracking petroleum and coal tar plumes in the subsurface, the results of which can be combined with geological and hydrogeological data to develop timely and accurate site conceptual models. When examined in conjunction with our previous research, the improved membrane inlet, cryotrap, and calibration readiness of the system add up to first technology that can completely and unambiguously profile the subsurface and groundwater from ground-level to bedrock. If the improved cryotrap/thermal desorber provides acceptable performance in laboratory testing, the system will tested during simulated field experiments and at a hazardous waste site.

Chapter 3 **A More Accurate Analysis of Alkylated PAH and PASH and its Implications in Environmental Forensics**

3.1 Introduction

For more than thirty years, investigators have used diagnostic ratios, based on individual and homologue-specific PAH and PASH concentrations, to support site investigation and cleanup projects and litigation.[82] For example, forensic scientists use diagnostic ratios to identify and differentiate one source material from another and to estimate the amount of weathering that has occurred.[46] These assessments rely on the principle that each source has a unique chemical composition with a recognizable PAH/PASH distribution pattern, and that changes in concentration over time, due to physical, chemical, and biological processes, can affect ecosystem toxicity and, thus, cleanup strategy.[83] PAH/PASH ratios that are constant over time are useful in delineating source identity, and those that change substantially provide an estimate of how much the source material has weathered. In 1999, Wang and coworkers published an authoritative review in which they state that alkylated PAH homologues are the "backbone of chemical characterization and identification of oil spill assessments".[46] Forensic scientists and toxicologists rely on accurate methods of PAH and PASH analysis, as errors in peak assignments produce inaccurate concentration estimates, which, in turn, lead to incorrect diagnostics and costly site remediation activities.

The scientific community, state and federal agencies, and the private sector rely heavily on SIM data to draw conclusions on the impact of PAH and PASH in the environment. For example, a search of the primary literature reveals nearly 75%

of all research published over the last 20 years employed SIM detection and that methods such as those published by the American Society for Testing and Materials[84] and National Oceanic and Atmospheric Administration[85] prescribe one-ion detection. Recently, we analyzed several coal tar and crude oil samples and showed that, due to incorrect peak assignments, SIM/1-ion analyses overestimate alkylated PAH and PASH concentrations and produce an unacceptable number of false positives compared to full scan data analysis.[47,73] We also found that if one fragmentation pattern per homologue is used to quantify C_2 to C_4 alkylated PAH, concentrations are underestimated compared to using three-to-five ions per isomer pattern and multiple fragmentation patterns per homologue.[69]

The objective of this study is to examine the effects of PAH and PASH concentration differences produced by one- and two-ion detection or selected ion extraction methods versus analysis by MFPPH ions on the diagnostic ratios used in environmental forensics. This study is the first comprehensive SIM/SIE vs. MFPPH assessment of the impact on the diagnostic ratios commonly used by forensic chemists.

3.2 Experimental

Standards and reagents: The 16 EPA-priority pollutant PAH standards, internal standards (1,4-dichlorobenzene-d_4, naphthalene-d_8, phenanthrene-d_{10}, chrysene-d_{12}, and perylene-d_{12}), and activated copper were purchased from Restek (Bellefonte, PA). Anhydrous sodium sulfate, neat dibenzothiophene, and the

base/neutral surrogate mixture (2-fluorobiphenyl, nitrobenzene-d_5, p-terphenyl-d_{14}) were purchased from Sigma-Aldrich (St. Louis, MO). Airgas (Salem, NH) supplied the ultra-high purity helium and nitrogen.

Samples: ONTA (Toronto, Ontario, Canada) supplied the Merey and Orinoco crude oils. Zhendi Wang from Environment Canada (Ottawa, Ontario, Canada) provided the weathered Arabian crude oil sample. We obtained unweathered coal tar from MGP sites in North Carolina and Illinois. Coal tar contaminated soils were obtained from the same site in Illinois and from a site in Wisconsin, and contaminated sediment from the Hudson River in New York. Environmental engineering companies collected these samples and shipped them overnight on ice to the university, where they were stored at 3 °C until analyzed.

Sample preparation: We followed the prescribed extraction procedure for soil and sediment samples as described in EPA methods 3550C and 3660B. Briefly, borosilicate glass vials (Fisher Scientific, Pittsburgh, PA) containing 15 g of soil or sediment spiked with base/neutral surrogate spike mix and 8 mL of 50% toluene/50% dichloromethane (v/v) were sonicated for 10 minutes (Branson 2210, Danbury, CT). After removing the extract and adding fresh solvent each time, the sonication procedure was repeated 7-times to ensure maximum extraction efficiency. For soils, the filtered extract was concentrated under a steam of nitrogen. For sediments, addition of activated copper and anhydrous sodium sulfate to the filtered extract removed elemental sulfur and water prior to

concentration under a stream of nitrogen. A known quantity of the internal standard mixture was added to each extract before it was analyzed.

Instrumentation: An Agilent Technologies (Santa Clara, CA) 6890/5973 GC/MS with a Gerstel (Mülheim an der Ruhr, Germany) MPS2 autosampler and CIS6 PTV inlet and a Shimadzu (Columbia, MD) GC2010/QP2010+ GC/MS, each with an RTX-5MS 30 m x 0.25 mm ID x 0.25 μm column from Restek, were used in this study. Instrument operating conditions were as follows: for the Shimadzu GC, 1 μL splitless sample injection, 1 mL/min constant helium flow, 60 °C (1 min) to 330 °C at 5 °C/min temperature program, with MS conditions of 50-350 *m/z* scan range at 8.3 Hz; and for the Agilent GC, 1 μL splitless injection, 268 kPa constant pressure helium flow, 60 °C (1 min) to 330 °C at 5 °C/min temperature program, and MS of 50-400 *m/z* scan range at 5 Hz.

Data analysis: Known concentrations of the 16 EPA-priority PAH and DBT standards were serially diluted and analyzed to obtain the method detection limit and average response factor over the concentration range. The linear calibration range was based on a minimum of eight points over the concentration range of 0.2-25 μg/mL for the 2- and 3-ring PAH and 0.4-25 μg/mL for the larger PAH. Calculation of the RF at each concentration was $A_X C_{IS}/A_{IS} C_X$, where C_X is the concentration of PAH injected, A_X the observed signal for said injection, and C_{IS} and A_{IS} are the corresponding internal standard concentration and signal response. The same average RF was used for both SIM and MFPPH analyses. We found the

average RF over the calibration-range for parent PAH was less than 15%, with these values used to calculate concentrations of the corresponding alkylated homologues.

All samples were analyzed by full-scan mass spectrometry, followed by extraction of 1-, 2- and MFPPH ion signals from the same data file. For SIM/1-ion, the molecular ion, and for SIM/2-ion, the molecular and most abundant confirming ions were used for C_1 to C_4 alkylated naphthalene, fluorene, phenanthrene, pyrene, chrysene, and dibenzothiophene. Those peaks that contained these ions found within the retention windows were integrated. For MFPPH, we used the recently published PAH and PASH spectral patterns and retention windows.[47,68,73] Spectral deconvolution algorithms and software developed by Ion Analytics (Andover, MA) and the following three-fold compound identification criteria were employed during data analysis.[68] First, detection of each homologue's spectral patterns, *i.e.*, ions and relative abundances, must comaximize and be ≤ 20% at each scan across the peak. This criterion ensures that the spectra are invariant across the peak. Second, the Q-value must be ≥ 90. The Q-value is a measure of the deviation between the expected and observed ion ratios for each ion across the peak and ranges between 1 and 100. The higher the Q-value, the higher the certainty that sample and library spectra match one another. Finally, the Q-ratio, the peak area ratio of the base and confirmation ions, must be ≤ 20% of the library relative abundance for each spectral pattern to confirm compound identity. Only the molecular ion signal

from those scans that meet all three criteria are extracted from the peak are used to quantify the homologues.

3.3 Results and Discussion

Figure 1-1 shows the overlap in PAH and PASH retention windows from which analysts must recognize homologue-specific peak patterns. Also shown are those homologues whose fragmentation ions interfere with the quantification ion of a specific homologue if a single ion is used to detect the homologue (SIM/1-ion) or is extracted from full scan data (SIE/1-ion). For purposes of constructing the figure, only fragment ions whose relative abundance is greater than 15% of the homologue's molecular ion are considered. Note that both PAH and PASH interfere with one another. Signal from non-target matrix compounds can also add to the total homologue peak area when reliance on pattern recognition is employed.

Figures 3-1 and 3-2 illustrate an example of wrongly assigned peak patterns caused by the detection of too few ions to unambiguously identify target compounds and its effect on homologue concentrations. Figure 3-1 shows the ion current chromatogram at *m/z* 234, which is the molecular ion for C_4-phenanthrene. A total of four compounds elute within the retention window for this homologue. Detection by SIM or extraction of this ion from full scan GC/MS data would result in these peaks being identified as C_4-phenanthrenes. Examination of this homologue's fragmentation ions, however, reveals that these

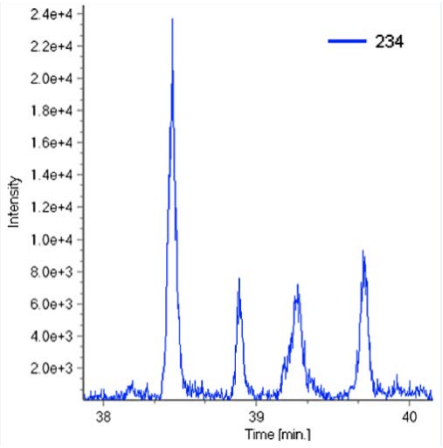

Figure 3-1. *m/z* 234 ion trace from a coal tar contaminated soil, SOIL

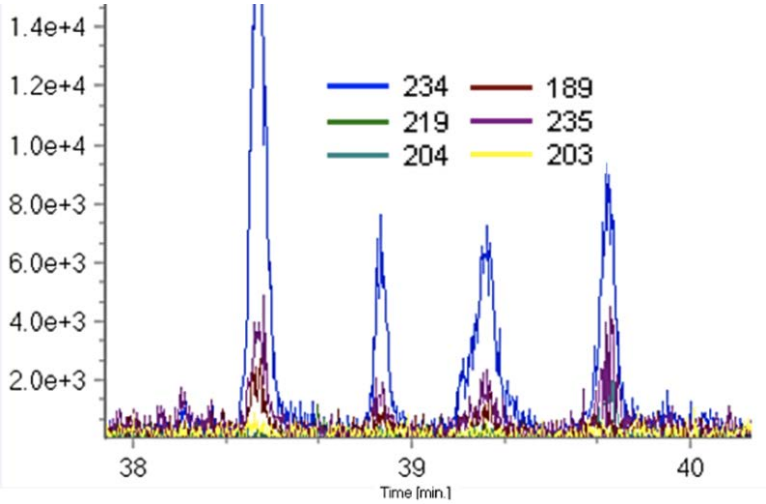

Figure 3-2. C_4-phenanthrene fragmentation ions and their relative abundances; *m/z* 234 (100%); 219 (75); 204 (31%); 203 (23%); 235 (20%) for the 2,4,5,7- and 3,4,5,6-tetramethyl isomers (pattern A) and *m/z* 234 (100%); 219 (60%); 235 (21%); 204 (17%); 189 (13%) for the 2,7,9,10-tetramethyl isomer (pattern B). Also shown are the reconstructed ion chromatograms from the sample in Figure 3-1

peaks are the result of matrix interferences. Figure 3-2 shows the fragmentation ion traces (*m/z* 235, 234, 219, 204, 203, and 189) for the 2,4,5,7- and 3,4,5,6-tetramethylphenanthrenes and the 2,7,9,10-tetramethylphenanthrene isomers, see figure caption for fragmentation pattern relative abundances. Although the reconstructed ion current chromatograms maximize at the peak apexes for some ions, not all fragmentation ions are present; i.e. *m/z* 219, whose relative abundance is 60% and should be evident in the chromatograms. Moreover, the

signals of the confirming ions based on their relative abundances should have been well-above instrument noise and do not match those relative abundances listed in the figure caption for these isomers. For example, the *m/z* 235 ion should have relative abundances similar to that of *m/z* 203 in pattern A and *m/z* 204 in pattern B, but does not. As a result, the peaks in Figure 3-1 are rejected as C_4-phenanthrene compounds when the identification criterion described in the experimental section is employed. In this example, relying solely on the molecular ion to measure C_4-phenanthrene produces a concentration of 220 μg/g. In contrast, MFPPH yields no measurable concentration. According to the EPA equilibrium partitioning sediment benchmark model, 220 μg/mL of C_4-phenanthrene corresponds to 0.34 toxic units for a sample that contains 1% total organic carbon.[23] Since a toxic unit of 1 is the threshold for ascribing potential soil/sediment toxicity, the C_4-phenanthrene homologue concentration would have added one-third of the toxic equivalent to a site contaminated with crude oil or coal tar when, in fact, the homologue should not have contributed to site toxicity at all. This finding is problematic, since more than 50% of the publications we reviewed relied on one-ion SIM detection, and is consistent with concerns expressed by others.[86,87] Although inclusion of *m/z* 219 (the most abundant confirming ion) would proscribe inclusion of these peak signals in the C_4-phenanthrene concentration estimate, the addition of a single qualifying ion will not always produce the correct concentration for all homologues. For example, when examining C_2-fluorene in the same sample, both SIM/1-ion at *m/z* 179 and SIM/2-ion at *m/z* 179 and 194 identify several peaks revealed to be false positives

by MFPPH when other confirmation ions are included. Moreover, if the confirming ion (as opposed to the molecular ion) is the base ion, as is the case for some isomers of C_3-phenanthrene, concentrations will be underestimated depending on which relative abundance is selected to determine compound identity; see, for example, the trimethyl and methyl-ethyl PAH isomers.[70] Some analysts ignore ion ratios and assume that if the two ions comaximize as in the example above, the peak is from a target compound. Still other methods rely on pattern recognition of homologue peaks, which places a significant burden on the analyst to determine which peaks should and should not be included. Such discretion can lead to unpredictable results from one analyst to the next.[73]

To examine the effects of this overestimation on environmental forensic diagnostic ratios, we analyzed coal tar and crude oil samples and extracted 1-, 2-, and MFPPH ion signals (as a surrogate for SIM analysis) from the same GC/MS data file. Our purpose is to illustrate the differences in the forensic data when too few ions are employed; it is not aimed at comparing the differences in measurement sensitivity between full scan and SIM detection. Such an analysis would introduce an additional error source, whereas using the same data file isolates the differences between the two data analysis methods. Tables 3-1 and 3-2 list our findings, which show that the standard SIM analysis biased the diagnostic ratios in every sample. Use of SIM/SIE with too few ions consistently overestimated alkylated homologue concentrations, leading to both positive and negative biases which ranged from a few percent to thousands of percent.

Table 3-1. SIM/1-ion vs. MFPPH diagnostic ratio percent bias

Ratio	Application	Coal Tar								Crude Oil			Min	Max
		CTIL	SOIL	CTNC	SDNY1	SDNY2	SOWI1	SOWI2	SOWI3	ME	OR	AR		
1.) ΣC / ΣD	Biodegradation[88]	-18	-6	30	-170	-228	-56	-90	-17	FP	34	FP	-228	34
2.) [ΣN+Σ(C0-C3)DBT + (1/2*Σ(C0-C1)P) + Σ(C2-C4)P] / ΣPAH	Biodegradation[89]	1	0	-8	-1	-2	-15	-7	-10	95	-21	-16	-21	95
3.) Pyrogenic Index	Pyrogenic v. Petrogenic Source[90]	-39	-26	-35	-32	-39	-30	-26	-25	-63	-58	-45	-63	-25
4.) C2D/C2P // C3D/C3P	Source Allocation[91]	-556	-2719	-20	-1969	-2954	-539	-25	-75	15	8	37	-2954	37
5.) ΣP / ΣD	Source Allocation[83]	-53	-27	7	-479	-237	-38	-118	-41	-36	-14	9	-479	9
6.) P / ΣP	Source Allocation[89]	-41	-22	-35	37	-10	-21	-17	-11	-36	-28	-45	-45	37
7.) C1C / C	Source Allocation[89]	40	14	26	5	12	18	4	26	FP	FP	FP	4	40
8.) C2C / C	Source Allocation [89]	54	83	64	76	14	3	FP	6	FP	FP	FP	3	83
9.) C3C / C	Source Allocation[89]	ND	ND	FP	FP	9	FP	FP	FP	ND	ND	ND	9	9
10.) C1D / C1Pyr	Source Allocation[87]	15	0	3	67	1	-8	-8	-3	46	16	23	-8	67
11.) Σ(C2-C4)N / ΣPAH	Source Allocation and Weathering[92]	14	32	7	6	44	40	1	6	95	-15	-21	-21	95
12.) C1P / ΣP	Source Allocation and Weathering[93]	-30	-16	-31	-93	-10	-7	-8	-6	-14	-16	-40	-93	-6
13.) C1D / ΣD	Source Allocation and Weathering[92]	-69	-46	-19	-265	-267	-59	-155	-55	16	-12	1	-267	16
14.) ΣN / ΣP	Weathering[89]	-21	-5	-21	1	21	-13	-11	9	9	3	-20	-21	21
15.) ΣC / ΣP	Weathering[94]	23	16	25	53	4	-14	13	17	FP	43	FP	-14	53
16.) C2N / C1P	Weathering[87]	1	2	-6	7	68	-10	0	18	-19	0	15	-19	68
17.) ΣN / ΣC	Weathering[95]	-56	-25	-63	-15	19	6	-28	-9	FP	-68	FP	-68	19
18.) ΣP / ΣC	Weathering[96]	-29	-20	-34	-114	-3	23	-15	-20	FP	-74	FP	-114	23
19.) ΣD / ΣC	Weathering[95]	15	5	-44	63	69	44	47	14	FP	-53	FP	-53	69
20.) ΣF / ΣC	Weathering[95]	12	29	17	41	83	59	33	17	FP	11	FP	11	83
21.) C / ΣC	Weathering[97]	-83	-46	-82	-36	-13	-7	-34	-33	FP	ND	FP	-83	-7
22.) C1C / ΣC	Weathering[94]	-11	-25	-35	-30	0	-10	-29	1	FP	15	FP	-35	15
23.) C2C / ΣC	Weathering[94]	17	75	-35	67	2	-4	FP	-25	FP	-89	FP	-89	75
24.) C3C / ΣC	Weathering[94]	ND	ND	FP	FP	-3	FP	FP	FP	ND	ND	ND	-3	-3
25.) Σ(N+F+P+D) / Σ(P+D)	Weathering[95]	-11	2	-4	17	17	9	-21	9	-1	10	1	-21	17
Min		-556	-2719	-82	-82	-1969	-539	-155	-75	-63	-89	-45		
Max		54	83	64	64	76	59	47	26	95	43	37		

Table 3-2. SIM/2-ion vs. MFPPH diagnostic ratio percent bias

Ratio	Application	Coal Tar								Crude Oil			Min	Max
		CTIL	SOIL	CTNC	SDNY1	SDNY2	SOWI1	SOWI2	SOWI3	ME	OR	AR		
1.) ΣC / ΣD	Biodegradation	14	-13	34	-64	-168	-16	-90	5	FP	34	FP	-168	34
2.) [ΣN+Σ(C0-C3)DBT + (1/2*Σ(C0-C1)P) + Σ(C2-C4)P] / ΣPAH	Biodegradation	-15	0	36	22	-2	-13	-7	22	-9	-21	-16	-21	36
3.) Pyrogenic Index	Pyrogenic v. Petrogenic Source	-38	-10	-28	-48	-35	-28	-24	-24	-63	-56	-44	-63	-10
4.) C2D/C2P // C3D/C3P	Source Allocation	75	72	16	-879	-2288	-14	-25	-74	15	8	37	-2288	75
5.) ΣP / ΣD	Source Allocation	-12	-17	14	-92	-185	-3	-118	-20	-36	-14	9	-185	14
6.) P / ΣP	Source Allocation	-41	-11	-35	-16	-7	-17	-17	-5	-36	-27	-44	-44	-5
7.) C1C / C	Source Allocation	40	14	26	5	12	2	4	26	FP	FP	FP	2	40
8.) C2C / C	Source Allocation	54	0	61	76	14	0	FP	6	FP	FP	FP	0	76
9.) C3C / C	Source Allocation	ND	ND	FP	FP	9	FP	FP	FP	ND	ND	ND	9	9
10.) C1D / C1Pyr	Source Allocation	15	0	0	-5	1	-8	-8	-3	46	16	23	-8	46
11.) Σ(C2-C4)N / ΣPAH	Source Allocation and Weathering	0	9	7	19	45	-12	-3	8	-7	-19	-14	-19	45
12.) C1P / ΣP	Source Allocation and Weathering	-30	-5	-31	-11	-6	-3	-8	-1	-14	-15	-45	-45	-1
13.) C1D / ΣD	Source Allocation and Weathering	-23	-23	-14	-123	-201	-16	-155	-26	16	-12	1	-201	16
14.) ΣN / ΣP	Weathering	-21	-7	-29	-4	24	-10	-14	14	9	0	-19	-29	24
15.) ΣC / ΣP	Weathering	23	4	23	14	4	-12	13	21	FP	43	FP	-12	43
16.) C2N / C1P	Weathering	1	2	-3	-5	68	-10	0	18	-19	0	16	-19	68
17.) ΣN / ΣC	Weathering	-56	-11	-69	-21	19	1	-31	-9	FP	-75	FP	-75	19
18.) ΣP / ΣC	Weathering	-29	-4	-31	-17	-6	11	-15	-27	FP	-74	FP	-74	11
19.) ΣD / ΣC	Weathering	-16	11	-51	39	63	13	47	-5	FP	-53	FP	-53	63
20.) ΣF / ΣC	Weathering	9	28	7	41	83	54	30	17	FP	11	FP	7	83
21.) C / ΣC	Weathering	-83	-16	-77	-36	-13	-5	-34	-33	FP	ND	FP	-83	-5
22.) C1C / ΣC	Weathering	-11	1	-32	-30	0	-3	-29	1	FP	15	FP	-32	15
23.) C2C / ΣC	Weathering	17	-16	31	67	2	-5	FP	-25	FP	-89	FP	-89	67
24.) C3C / ΣC	Weathering	ND	ND	FP	FP	-3	FP	FP	FP	ND	ND	ND	-3	-3
25.) Σ(N+F+P+D) / Σ(P+D)	Weathering	-6	-1	-8	8	19	10	-24	53	-1	10	-1	-24	53
Min		-83	-23	-77	-879	-2288	-28	-155	-74	-63	-89	-45		
Max		75	72	61	76	83	54	47	53	46	43	37		

Notes for Tables 3-1 and 3-2:

1. Bias calculated as follows: $\frac{Ratio_{SIM} - Ratio_{MFPPH}}{Ratio_{MFPPH}} \times 100$
2. CT = Coal tar, SO = Coal tar-contaminated soil, SD = Coal tar-contaminated sediment
3. IL = Illinois, NC = North Carolina, NY = New York, WI = Wisconsin
4. ME = Merey, AR = Arabian, OR = Orinoco
5. C = Chrysene, D = Dibenzothiophene, N = Naphthalene, P = Phenanthrene, Pyr = Pyrene
6. ND = Not detected by either method
7. FP = Signal acquired by SIM, but ion traces fail to comaximize or meet MFPPH relative abundance criteria
8. Pyrogenic Index = the relative ratio of the sum of the other EPA priority three- to six-ring PAH divided by the sum of the alkylated naphthalene, phenanthrene, dibenzothiophene, fluorene, and chrysene homologues.
9. Σ = Sum of homologues, i.e. Σ(C) = all C_1-, C_2, C_3, and C_4 Chrysene homologues

These biases are dependent on whether the homologue is in the numerator or denominator of the diagnostic. Examples of incorrect peak assignments for the alkylated 3-ring PASH used in C_1D / ΣD (ratio #13) in sample SOWI2 are provided in Figures 3-3 to 3-5. The figures display ion chromatograms *m/z* 198 (C_1), 212 (C_2), and 226 (C_3) for correctly assigned peaks (green star) and those that failed to meet the criteria for compound identity (red X). The non-homologue peaks contribute to the overestimation of the C_2 and C_3 3-ring PASH, and, in turn, increase the concentrations in the denominator of the ratio.

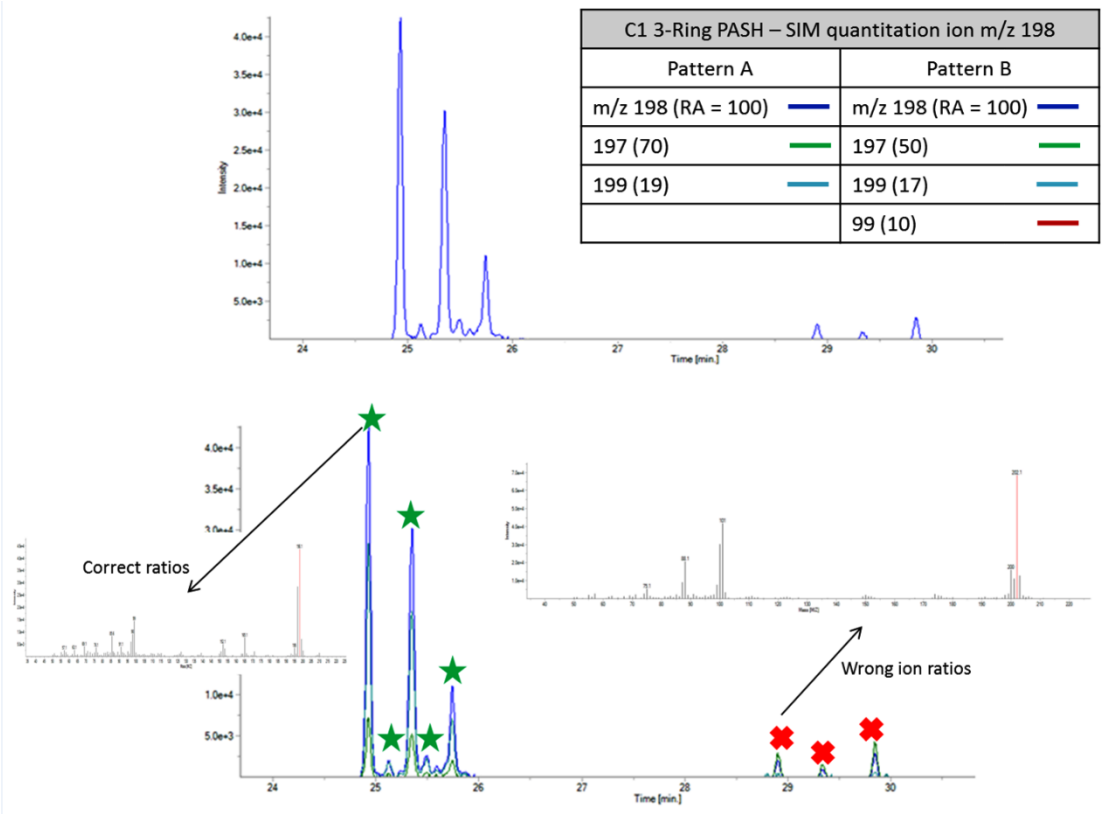

Figure 3-3. SIM (*m/z* 198) and MFPPH ion traces, fragmentation patterns, and mass spectra for C1 3-ring PASH. Peaks with green stars correspond to homologue isomers, while those with red X's did not meet MFPPH peak identity criteria

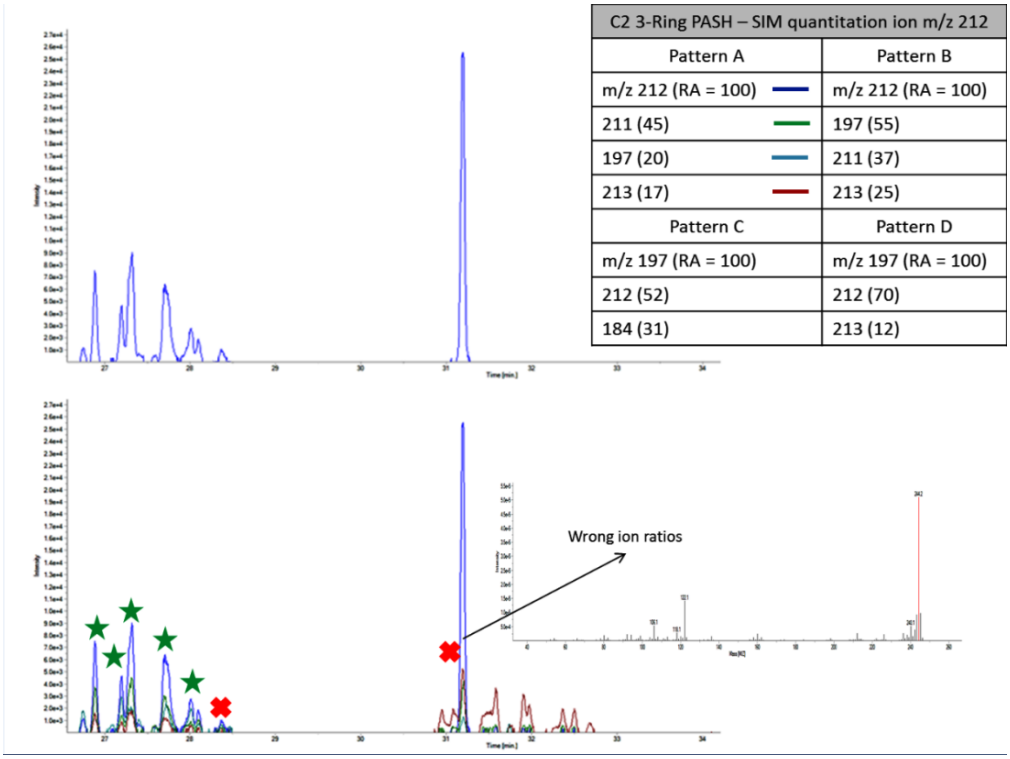

C2 3-Ring PASH – SIM quantitation ion m/z 212	
Pattern A	Pattern B
m/z 212 (RA = 100)	m/z 212 (RA = 100)
211 (45)	197 (55)
197 (20)	211 (37)
213 (17)	213 (25)
Pattern C	Pattern D
m/z 197 (RA = 100)	m/z 197 (RA = 100)
212 (52)	212 (70)
184 (31)	213 (12)

Figure 3-4. SIM (*m/z* 212) and MFPPH ion traces, fragmentation patterns, and mass spectra for C_3 3-ring PASH. Peaks with green stars correspond to homologue isomers, while those with red X's did not meet MFPPH peak identity criteria

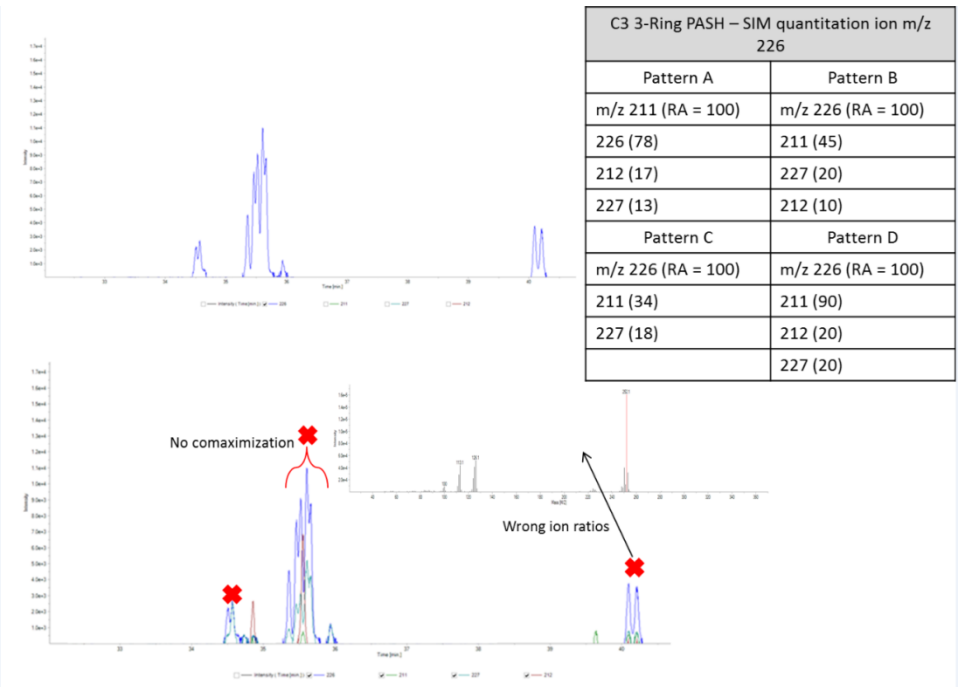

C3 3-Ring PASH – SIM quantitation ion m/z 226	
Pattern A	Pattern B
m/z 211 (RA = 100)	m/z 226 (RA = 100)
226 (78)	211 (45)
212 (17)	227 (20)
227 (13)	212 (10)
Pattern C	Pattern D
m/z 226 (RA = 100)	m/z 226 (RA = 100)
211 (34)	211 (90)
227 (18)	212 (20)
	227 (20)

Figure 3-5. SIM (*m/z* 226) and MFPPH ion traces, fragmentation patterns, and mass spectra for C_2 3-ring PASH. Peaks with green stars correspond to homologue isomers, while those with red X's did not meet MFPPH peak identity criteria

Nearly 50% of the diagnostic ratios were affected by overestimated homologue concentrations or false positives. In general, higher-order (C_3 and C_4) alkylated PAH and PASH homologues were more affected than the lower order (C_1 and C_2) homologues. These results are consistent with Figure 1-2. Diagnostic ratio differences were more prevalent in the weathered (sediment) samples than non-weathered (oil) samples, but many false positives were seen in the crude oil results. Nonetheless, no systematic error was observed in the diagnostic ratio differences; thus, we suspect that measurement bias is matrix-dependent. Since errors are indiscriminate, no simple correction factor is able to relate SIM to MFPPH results.

Table 3-2 lists the diagnostic ratio biases obtained from the SIM/2-ion and MFPPH measured concentrations. Although in some cases the addition of a confirming ion to establish compound identity dramatically improved results, see, for example, the alkylated phenanthrene to dibenzothiophene ratio ($\Sigma P / \Sigma D$, ratio #5), which dropped from -479% to -92% for sediment SDNY1, nearly three-quarters of the differences in diagnostic ratios are similar, if not identical, to those of SIM/1-ion analyses. Notably, false positives did not decrease when only one confirming ion was added to identify target compounds. As expected, the more complex the matrix, the higher the likelihood that too few ions will lead to concentration overestimation and false positives. Based on the analysis of eleven coal tar and crude oil samples, not a single diagnostic ratio was unaffected; see minima and maxima in the tables. These altered diagnostic ratios can have

significant repercussions on site investigations, as seen in the following examples. Since C_1-phenanthrene weathers more slowly than C_2-naphthalene, the C_2-naphthalene/C_1-phenanthrene ratio (ratio #16) is indicative of the extent of weathering between locations caused by site-specific environmental factors. Selection of this ratio as an indicator of weathering was made, in part, because the molecular ions for these homologues were believed to be less affected by matrix interferences.[87] However, differences in the homologue concentration by SIM compared to MFPPH produced increases in the ratio as high as 68%. The ratio of the naphthalene homologue concentrations divided by the phenanthrene homologue concentrations ($\Sigma N / \Sigma P$, ratio #14) is also used to determine the extent of weathering, as the former can be influenced by the local environment faster than the latter. Six SIM/1-ion samples and five SIM/2-ion samples produced larger increases in ΣN compared to ΣP concentrations than the corresponding MFPPH results. This finding would lead to positively biased ratios and incorrect conclusions that the samples are less weathered than they actually are. For the remaining samples, the naphthalene to phenanthrene ratio decreased, suggesting the samples are more weathered than they actually are. The former could lead to unnecessary cleanup, the latter to a declaration the site is clean when it is not.

Investigators use double ratio plots to determine weathering and to differentiate source materials.[46,66,94,98] An example of a double ratio plot used to assess source allocation is (C2D/C2P)/(C3D/C3P). Since the degradation rates of these

homologues are similar, this diagnostic ratio should be relatively constant over time. Of all diagnostics examined in this study, double ratio plots were the most affected by SIM overestimation. Figure 3-6 shows the double ratio plot for the samples. For three samples (Orinoco, Merey, SOWI2), the SIM and MFPPH data are located closely to one another. For example, the Orinoco plot points are located within the triangle in the figure. In contrast, the other seven samples have much different SIM and MFPPH plot coordinates, see rectangle for illustration. These two coal tar contaminated sediments, although collected from the same site, have widely different *x*-axis coordinates when calculated by SIM and MFPPH.

The result is consistent with the finding that the two data analysis methods produce greatly different C_3 homologue concentrations. The MFPPH double ratio

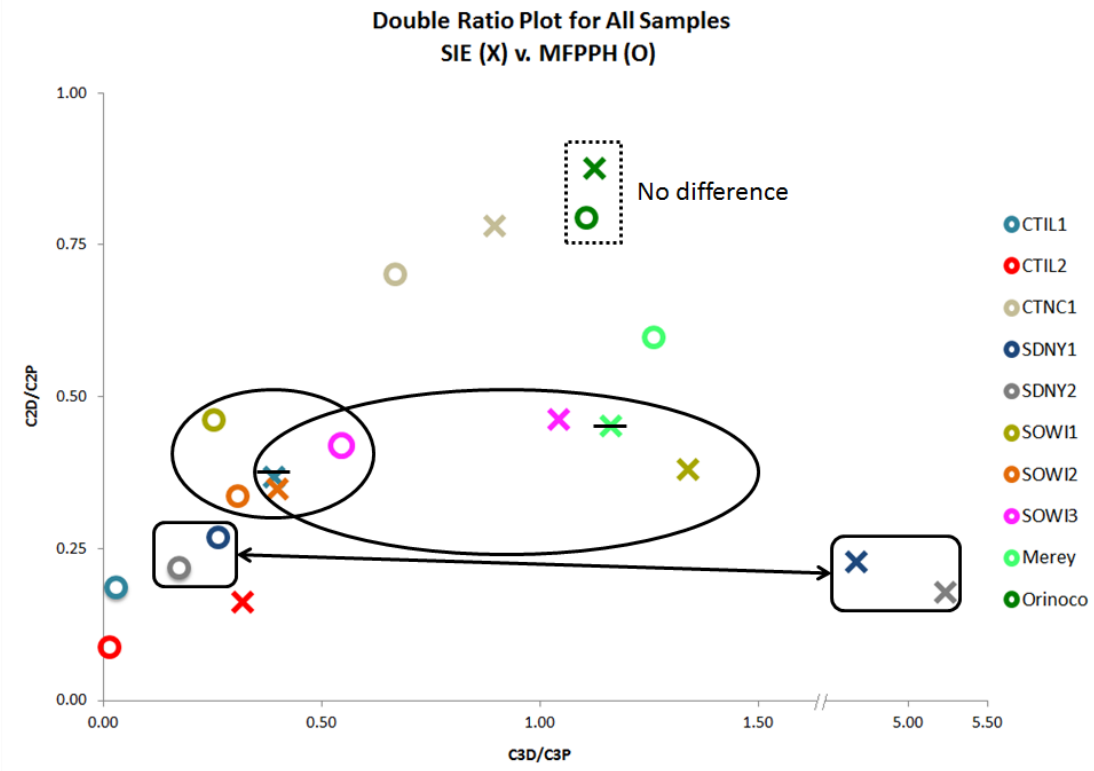

Figure 3-6. C2D/C2P//C3D/C3P double ratio plot of samples analyzed by SIM and MFPPH

plot points for the coal tar contaminated soils from the same site in Wisconsin cluster together as they should, see oval in figure. In contrast, the SIM data are spread throughout the plot.

Relative distribution histograms are also used to "fingerprint" oil spills and elucidate source types.[66] Investigators draw conclusions based on the distribution of concentrations amongst parent and alkylated homologues. For example, when homologue concentrations are $C_1 > C_2 > C_3 > C_4$, the source is pyrogenic. In contrast, a bell-shaped distribution is indicative of a petrogenic source. Figure 3-7 depicts the PAH distribution for a coal tar contaminated sediment, SDNY2.

The top histogram, data calculated by MFPPH, exhibits a downward slope, indicating homologue distributions characteristic of a pyrogenic tar. The bottom histogram, produced by SIM, exhibits a change in the "fingerprint" due to overestimated homologue concentrations. An example of this overestimation is seen in Figure 3-8, which shows the SIM ion traces for the C_1-C_4 3-ring PASH for the same sample. As seen in the figure, the C_3 and C_4 homologues (as depicted by their 1-ion traces) are more abundant than the C_1 and C_2 homologues, and as such, more concentrated. However, many of these SIM peaks are due to matrix interferences, and as such, are eliminated by MFPPH analysis (see peaks marked by red X's), leading to lower concentrations and corresponding profile features that indicate a coal tar sample. The SIM alkylated fluorene profile appears bell-shaped and the 2-ring and 3-ring PASH C_3 and C_4 homologue concentrations are

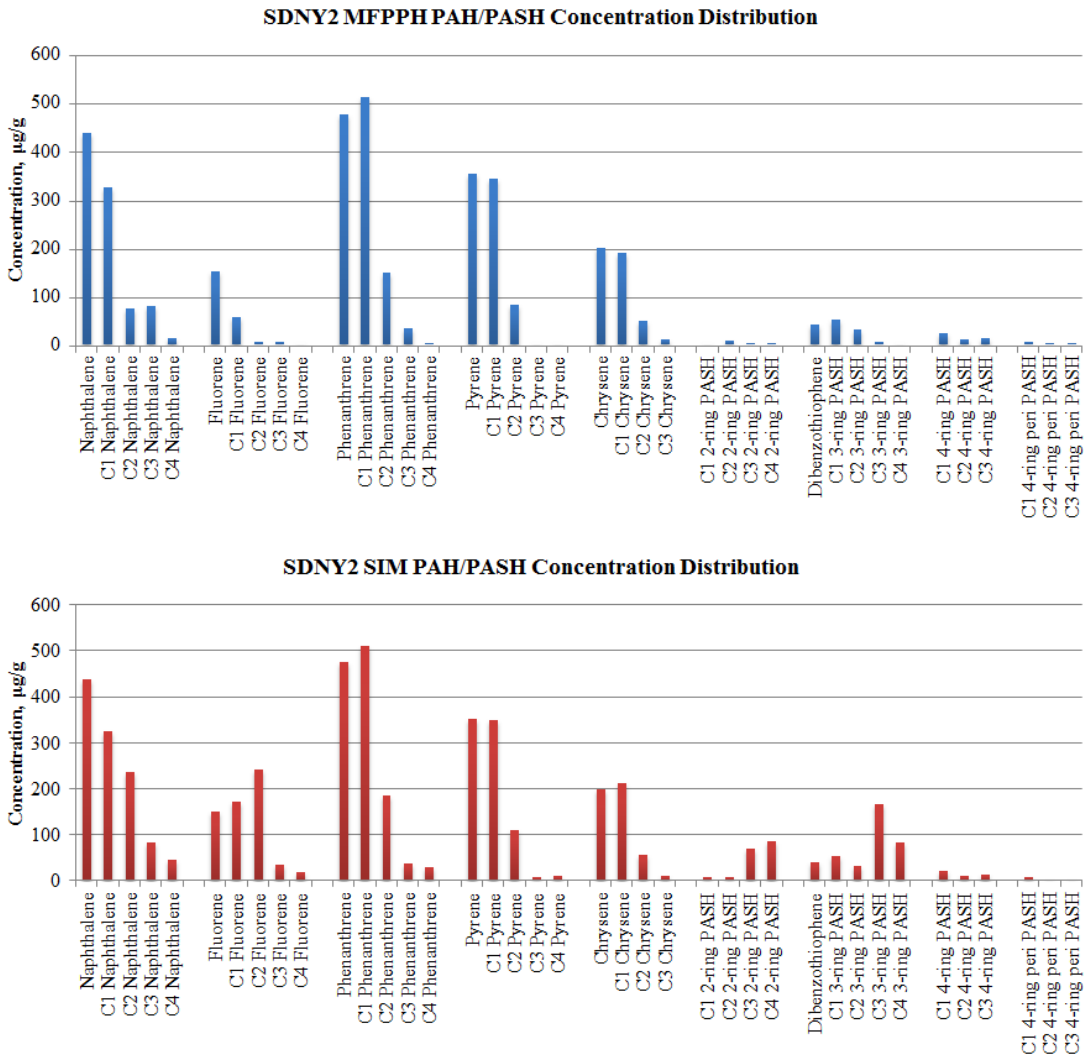

Figure 3-7. SIM and MFPPH relative distribution histograms of a coal tar contaminated sediment, SDNY2

higher than those found by MFPPH, so interpretation could suggest the presence of a mixed plume.

The results of this study support our contention that analyses of alkylated PAH and PASH homologues should require the same identification criteria, i.e., multiple ions and their relative abundances, as is widely-accepted for PAH analysis. Employing too few ions eliminates the two-dimensional information

content inherent in GC/MS data. Full scan or SIM analysis using the MFPPH ions and abundances (SIM/MFPPH) eliminates the need to recognize chromatographic patterns of the many isomers comprising each homologue, which can dramatically change from one sample to the next due to matrix effects. The aim of this work is not to critique SIM analysis, only the use of too-few ions to provide unambiguous identification of target analytes. The use of too-few ions leads to inaccurate concentration estimates, incorrect diagnostic ratios and falsely-considered assessments, and meaningful forensic studies should employ MFPPH analysis independent of MS detection mode.

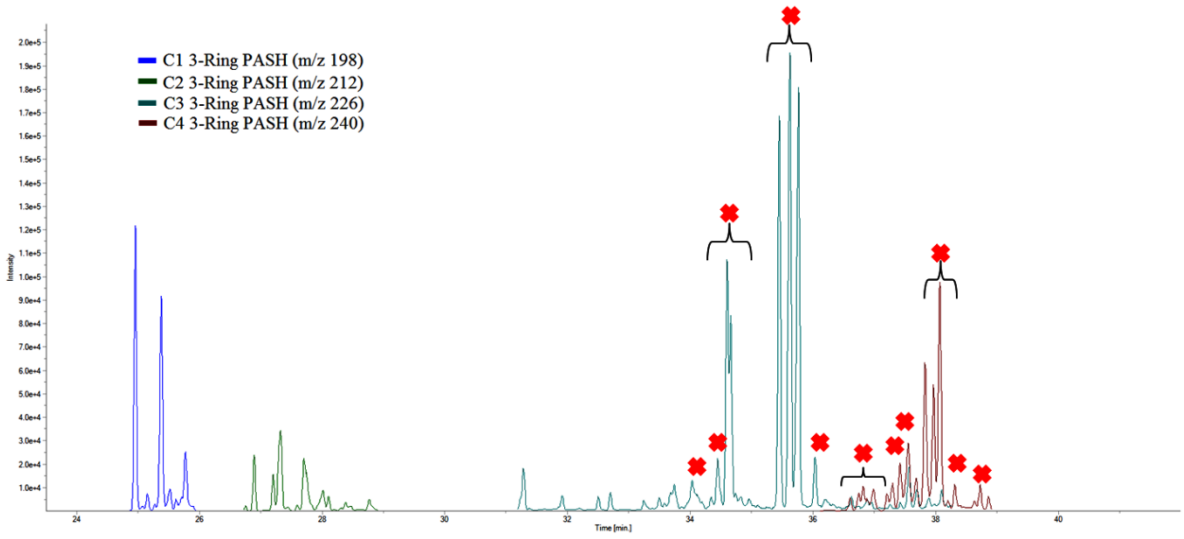

Figure 3-8. C_1-C_4 3-ring PASH SIM traces for sample SDNY2. Peaks marked with a red X were eliminated by MFPPH, since their ions and relative abundances failed to meet the compound identity criteria for this homologue

Chapter 4 **Retention Behavior of Alkylated Polycyclic Aromatic Sulfur Heterocycles on Immobilized Ionic Liquid Stationary Phases**

4.1 Introduction

Despite sulfur being the principal heteroatom in coal, crude oil, tar and their by-products, sulfur-containing compounds[99,100] are an often-overlooked factor[101] in assessing the impact of fossil fuel pollutants on the environment.[102] For example, sulfur compounds can poison catalysts, cause acid rain, and travel long distances as particulate matter.[103,104] An understanding of the behavior of polycyclic aromatic sulfur heterocycles (PASH), including thiophenes, benzothiophenes (2-ring), dibenzothiophenes (3-ring), and other 4- and 5-ring parent compounds and their alkylated homologues, is necessary. Since some PASH homologues have 20 or more isomers due to the asymmetry imposed by the sulfur atom, separation[105] and determination of their retention characteristics[68,106,107] is a challenge.[108] To facilitate their analysis, researchers have developed improved sample preparation procedures[109,110] and methods based on capillary electrophoresis[111] and liquid chromatography coupled to Fourier transform ion cyclotron resonance mass spectrometry (MS)[112] and atomic emission[103] detection. The technique of choice, however, remains gas chromatography/mass spectrometry (GC/MS).[73,113] Because of the complexity of fossil fuels, a comprehensive analysis of PASH in these substances requires multiple separation mechanisms[114] on stationary phases that are stable at high temperatures.

Alkylated polycyclic aromatic hydrocarbons (PAH) and PASH have overlapping retention windows and common mass spectral ions,[47] making their selective identification critically important for both one-dimensional and two-dimensional analyses. Toward this end, we reported the retention behavior of 119 PASH on 5%-diphenyl/95%-dimethyl polysiloxane (DB-5), 50%-diphenyl/50%-dimethyl polysiloxane (DB-17), and 35%-trifluoropropyl/65%-dimethyl polysiloxane (DB-200) columns.[68] We used these moderate- to non-polar columns to determine the best column pair for analyzing fresh and weathered crude oil and coal tar samples by automated sequential two-dimensional gas chromatography/mass spectrometry (GC-GC/MS). From these analyses, we obtained the information needed to elucidate the C_1 to C_4 2- to 5-ring PASH fragmentation mechanisms. Although these columns provided sufficient separation to obtain the fragmentation library, none of the column pairs we investigated provided the selectivity needed to fully separate all isomers within a given homologue. On the other hand, columns that provide stationary phase orthogonality during multidimensional separations lack the temperature stability necessary for analysis of 4- and 5-ring PASH.

Room temperature ionic liquids (IL), a class of non-molecular ionic solvents with low melting points (usually defined as < 100 °C),[115] have recently found application as stationary phases in gas chromatography.[116,117,118] In some cases, ionic liquid stationary phases exhibit “dual nature” characteristics – that is, they allow separation of nonpolar molecules like nonpolar (polydimethylsiloxane, PDMS) stationary phases do, while at the same time have a high affinity for

dipolar molecules and hydrogen-bond acids like cyanopropyl-siloxane and wax (polyethylene glycol, PEG) columns.[116] Table 4-1 also lists the relative polarities of some commercially-available IL columns along with several GC columns commonly used to analyze PAH and PASH.[119] The IL columns are all more polar than PEG columns, but with higher operating temperatures. Furthermore, SLB-IL111 is classified as more polar than the 1,2,3-tris[2-cyanoethoxy]propane (TCEP) phase, but with a maximum operating temperature nearly double that of TCEP. It is not surprising, then, that IL stationary phases, including the commercially-available columns examined in this study, have been evaluated as a prospective solution to a number of chromatographic challenges in environmental,[120,121] food and flavor research.[122]

Recently, IL columns have been used to analyze nonpolar compounds in kerosene[123] and heavy petroleum distillates.[124] The ability of immobilized ionic liquid stationary phases to separate polar and non-polar organics at higher temperatures than typical polar stationary phases makes them ideal "polar column" candidates for GC-GC and GC×GC analysis of PASH.[125] In this study, we examine the retention behavior of PASH on IL stationary phases to investigate if these columns can improve the separation of polar and non-polar compounds in complex samples such as coal tar. We report the first systematic retention behavior study of PASH, by both ring number and degree of alkylation, on IL stationary phases and their utility for the analysis of PASH in coal tar by GC/MS and GC×GC/MS.

Our retention behavior study of alkylated PASH follows prior investigations that have examined the retention characteristics of homologous families of alkyl phosphates[126,127] and fatty acids[128,129,130] on IL columns. Knowledge of retention behavior can provide the foundation to optimize GC methods, study structure-retention relationships,[131] and assign compound identity to unknowns in complex samples.[132] In addition, retention properties can be used in conjunction with molecular descriptors to predict the retention behavior of unknowns when standards are not available.[133,134,135] Finally, free-energy relationships between chromatographic retention and thermodynamic and physical properties are well-established and allow for estimation of these properties and assessment of environmental weathering; see Chapter 6.

Table 4-1. Properties of ionic liquid (IL) and non-IL GC columns

Stationary Phase	**Trade Name**	**Relative Polarity[119]**	**Maximum Operating Temperature (°C)**
5%-Phenyl / 95%-dimethyl polysiloxane	DB-5	5	360
50%-Diphenyl / 50%-dimethyl polysiloxane	DB-17	17	360
14%-Cyanopropyl-phenyl / 86%-dimethyl polysiloxane	DB-1701	19	360
35%-Trifluoropropyl / 65%-dimethyl polysiloxane	DB-200	~35	320
Polyethylene glycol (PEG)	Wax	52	250
1,2,3-Tris[2-cyanoethoxy]propane	TCEP	97	145
1,12-Di(tripropylphosphonium)dodecane bis(trifluoromethylsulfonyl)imide	SLB-IL60	60	300
1,12-Di(tripropylphosphonium)dodecane bis(trifluoromethylsulfonyl)imide trifluoromethylsulfonate	SLB-IL61	61	290
Tri(tripropylphosphoniumhexanamido)triethylamine bis(trifluoromethylsulfonyl)imide	SLB-IL76	76	270
1,5-Di(2,3-dimethylimidazolium)pentane bis(trifluoromethylsulfonyl)imide	SLB-IL111	111	270

4.2 Experimental

PASH: Two- to five-ring aromatic thiophenes were synthesized by Andersson[131] and Lee,[136] and obtained directly from Andersson or the U.S. National Institute of Standards and Technology (NIST, Gaithersburg, MD). Dibenzothiophene-*d8*, 2-ethyldibenzothiophene, and 1-methyldibenzothiophene were obtained from Cambridge Isotopes Laboratory (Cambridge, MA, USA), Chiron Laboratory (Trondheim, Norway), and ASTEC GmbH (Münster, Germany), respectively. Compound names and abbreviations are found in Table 4-2. Those PASH we did not analyze in our previous study are italicized in Table 4-2, with their structures shown in Figure 4-1.

Traditional IUPAC naming conventions were followed,[137] along with compound-specific nomenclature previously described.[68] To summarize, *ortho*-fused refers to PASH in which two connected rings have only two atoms in common (*n* common faces and 2*n* common atoms), and *ortho*- and *peri*-fused refer to PASH with two atoms in common with each of two or more rings of a contiguous series of rings (*n* common faces and fewer than 2*n* common atoms).[138] The latter is termed "*peri*-condensed" to differentiate it from *ortho*-fused compounds.[139] We use the term "linear" to refer to compounds that are ortho-fused on, at most, two sides of a given ring and "non-linear" to refer to compounds that contain an *ortho*-fused ring on more than two sides.

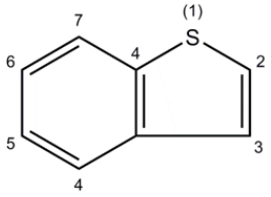

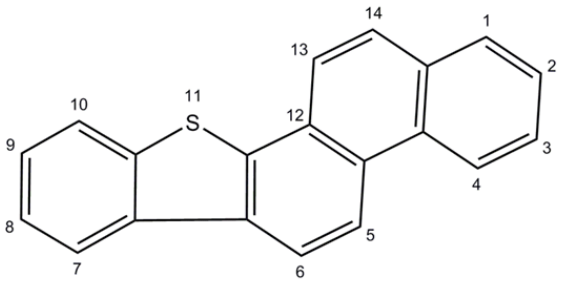

Alkyl benzothiophenes:
2,3-dimethyl
2,6-dimethyl
3,5-dimethyl
4,6-dimethyl
2,3,4-trimethyl
2,3,5-trimethyl
2,3,6-trimethyl
2,3,7-trimethyl
2,3,4,7-tetramethyl

Benzo[b]phenanthro[2,1-d]thiophene

Figure 4-1. PASH and alkyl PASH analyzed in the ionic liquid column retention work that were not analyzed in *Zeigler et al*.[68]

Other Standards and Samples: Neat naphthalene, phenanthrene, chrysene, benzo[*a*]pyrene, and benzo[*g,h,i*]perylene were purchased from Restek (Bellefonte, PA). A coal tar-contaminated soil was obtained from a hazardous waste site in Wisconsin, extracted using the sonication method described in Chapter 3 and spiked with internal standards 1,4-dichlorobenzene-d_4, naphthalene-d_8, phenanthrene-d_{10}, chrysene-d_{12}, and perylene-d_{12}, all purchased from Restek.

GC/MS Analysis: A Shimadzu (Columbia, MD) GC2010/QP2010+ GC/MS was used in this study. Instrument operating conditions were as follows: 1 μL sample injection with 3:1 split, 1.2 mL/min constant helium flow, and temperature

program of 75 °C (hold 1 min) to column maximum at 8 °C/min, and hold at column max until final bracket elution. The MS was scanned from 50-350 *m/z* at 8.3 Hz.

GC/MS Columns: While many ionic liquid columns are commercially available, we studied only those provided by Supelco (Bellefonte, PA) whose phases were stable at 250 °C and higher. These temperature-stable stationary phases are predominantly bulkily-substituted phosphonium- or imidazolium-based dicationic liquids[140] and included the SLB-IL60, SLB-IL61, SLB-IL76, and SLB-IL111 phases, all 30 m × 0.25 mm × 0.2 µm columns, see Table 4-1 for properties.

GC×GC/MS Analysis of Coal Tar: GC×GC/MS analyses were performed using an Agilent Technologies (Santa Clara, CA) 6890/5975C GC/MS with Gerstel (Mülheim an der Ruhr, Germany) MPS2 autosampler and CIS6 injector. The GC×GC/MS temperature program was 75 °C (1 min) to 300 °C at 8 °C/min. Previous work reported the experimental parameters used to attain the prescribed modulation period and scan density.[75] The 1st dimension column was a Restek 30 m × 0.25 mm × 0.25 µm RXI-5MS, and the 2nd dimension column a Supelco 1.1 m × 0.1 mm × 0.08 µm SLB-IL60 or Restek 1 m × 0.18 mm × 0.36 µm RXI-17MS. Columns were connected using a Restek press-fit connector. The GC×GC cryogenic and thermal modulation hardware was obtained from Zoex Corporation (Houston, TX). Ion Analytics (Andover, MA) spectral deconvolution software was used to identify PASH homologues prior to GC×GC image creation.

GC Image (Lincoln, NE) supplied the software to create the GC×GC chromatograms.

Calculation of Index Values: PASH were analyzed in triplicate on each IL column, with their retention indices calculated as follows:

$$RI_x = RI_B + \left[\left(\frac{t_x - t_B}{t_{(B+1)} - t_B}\right) \times 100\right] \quad (4\text{-}1)$$

where *t*'s refer to the retention time of the target compound, *x*, and bracketing compounds, *B* and (*B+1*), and RI_B is the linear temperature-programmed retention index of the earliest-eluting bracket compound. The retention indices for the bracketing compounds are as follows: naphthalene (200), phenanthrene (300), chrysene (400), benzo[*a*]pyrene (450), and benzo[*g*,*h*,*i*]perylene (500).[141,142] Due to the difficulty of calculating 2nd dimension RI from GC×GC data,[143] RI values were calculated from 1D GC/MS results only.

4.3 Results and Discussion

We compared the retention behavior of PASH on ionic liquid columns and several non-polar and moderately-polar columns typically used to analyze coal tar samples. Figure 4-2 shows the retention times of the bracketing compounds on each IL column investigated in this study, as well as the siloxane-based columns from prior work.[68] The figure shows the last two bracketing compounds either have very long retention times or do not elute from columns that have low maximum operating temperatures.

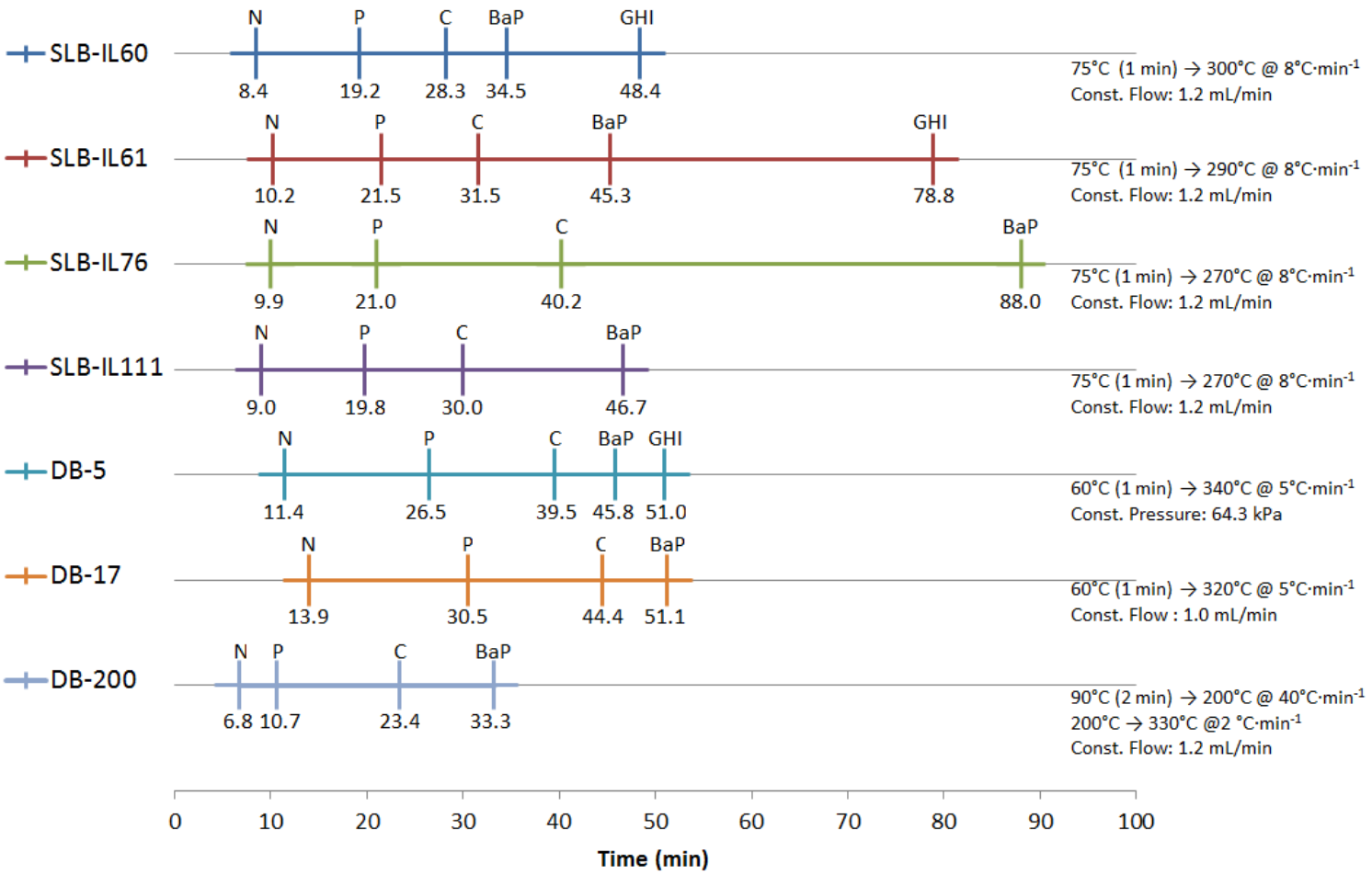

Figure 4-2. Bracket compound retention times as a function of temperature and carrier gas program parameters

Although the RI for the same compound changed from column-to-column, we obtained excellent precision on each column ($\overline{SD}$ was 0.18 RI units, n = 3 for all compounds). To investigate prospective improvements in separation, we calculated the number of coeluting compounds on each column. Assuming an average peak width of 6 s, see Figure 4-2, and resolution of 1.0, only 32% of the 119 PASH coeluted on the SLB-IL111 column. This is slightly better than the performance of the other IL columns, which ranged from 35% to 38% coelution. Even the least-effective IL columns yielded comparable performance to the most-effective siloxane columns, which produced 38% to 56% coelution. After regressing the ionic liquid retention indices against one another, the 0.993 Pearson correlation coefficient obtained indicates high correlation among the columns. When the IL columns are regressed against the siloxane columns, the average retention index correlation is 0.976. If only the 5-ring PASH, the most polarizable compounds in this study, are considered, the correlation coefficient is 0.545. In summary, the IL columns strongly correlate with one another, moderately correlate with siloxane-based columns, and poorly correlate with these columns for 5-ring PASH. Examination of the retention indices obtained for PASH and alkyl PASH in Table 4-2 (this study) compared to those in Table 4-3 (prior study) reveals that the majority of the polarizable PASH have distinctly different retention characteristics on the ionic liquid stationary phases. Retention indices on the IL columns are less than or essentially the same as those measured on the siloxane columns for all PASH – those compounds with retention changed by more than 10 index units are italicized in the table.

Table 4-2. PASH, abbreviations, and calculated retention indices on ionic liquid columns

		SLB-IL59		SLB-IL61		SLB-IL76		SLB-IL111	
Compound Name	Compound Abbreviation	Index[a]	SD	Index	SD	Index	SD	Index	SD
2-ring PASH									
C_2 Benzothiophenes									
2,3-dimethylbenzothiophene[b]	2,3-MeBT	230.00	0.01	229.15	0.01	226.64	0.03	219.45	0.42
2,6-dimethylbenzothiophene	2,6-MeBT	227.09	0.03	226.32	0.03	223.89	0.04	218.94	0.15
3,5-dimethylbenzothiophene	3,5-MeBT	229.55	0.06	228.82	0.05	226.74	0.04	220.79	0.36
4,6-dimethylbenzothiophene	4,6-MeBT	228.13	0.05	227.59	0.01	225.39	0.03	221.16	0.17
C_3 Benzothiophenes									
2,3,4-trimethylbenzothiophene	2,3,4-MeBT	250.78	0.08	249.17	0.01	246.10	0.05	238.36	0.28
2,3,5-trimethylbenzothiophene	2,3,5-MeBT	242.86	0.04	241.19	0.03	237.62	0.04	230.18	0.25
2,3,6-trimethylbenzothiophene	2,3,6-MeBT	242.52	0.11	240.78	0.03	237.29	0.02	229.24	0.32
2,3,7-trimethylbenzothiophene	2,3,7-MeBT	237.72	0.02	235.93	0.05	232.05	0.04	225.73	0.21
C_4 Benzothiophenes									
2,3,4,7-tetramethylbenzothiophene	2,3,4,7-MeBT	256.89	0.04	254.60	0.11	250.07	0.01	244.55	0.07
3-ring PASH									
Dibenzothiophenes									
Dibenzothiophene-D8	DBT-d8	290.66	0.02	291.07	0.06	290.52	0.08	287.84	0.09
C_1 Dibenzothiophenes									
1-methyldibenzothiophene	1-MeDBT	302.14	0.03	301.80	0.15	299.93	0.05	294.47	0.04
2-methyldibenzothiophene	2-MeDBT	302.78	0.04	301.90	0.09	300.22	0.04	296.36	0.08
3-methyldibenzothiophene	3-MeDBT	302.54	0.06	301.82	0.13	300.03	0.02	295.69	0.04
4-methyldibenzothiophene	4-MeDBT	297.38	0.19	297.10	0.12	295.05	0.08	290.44	0.04
C_2 Dibenzothiophenes									
2-ethyldibenzothiophene	2-EtDBT	308.84	0.05	307.06	0.11	302.47	0.05	298.03	0.02
4-ethyldibenzothiophene	4-EtDBT	303.22	0.03	302.01	0.12	298.95	0.06	292.52	0.10
C_3 Dibenzothiophenes									
1,3,7-trimethyldibenzothiophene	1,3,7-TriMeDBT	328.17	0.02	323.30	0.08	310.31	0.07	311.03	0.16
1,4,7-trimethyldibenzothiophene	1,4,7-TriMeDBT	323.26	0.06	319.12	0.05	307.64	0.03	305.96	0.11
2,4,6-trimethyldibenzothiophene	2,4,6-TriMeDBT	318.69	0.06	314.64	0.04	305.32	0.02	303.62	0.08
2,4,7-trimethyldibenzothiophene	2,4,7-TriMeDBT	324.29	0.09	319.61	0.05	308.05	0.01	308.05	0.04
2,4,8-trimethyldibenzothiophene	2,4,8-TriMeDBT	324.04	0.08	319.40	0.05	308.10	0.01	309.26	0.04
3,4,7-trimethyldibenzothiophene	3,4,7-TriMeDBT	331.95	0.09	326.97	0.09	312.17	0.02	315.98	0.19
Naphthothiophenes									
naphtho[2,1-b]thiophene	N21T	299.40	0.08	299.93	0.31	299.91	0.01	300.90	0.20

Table 4-2 (Continued)

naphtho[2,3-b]thiophene	N23T	303.84	0.13	304.48	0.06	302.89	0.90	305.13	0.11
C_1 Naphthothiophenes									
2-methylnaphtho[1,2-b]thiophene	2-meN12T	306.30	0.07	304.80	0.32	301.34	0.01	298.61	0.02
5-methylnaphtho[1,2-b]thiophene	5-meN12T	309.25	0.06	308.24	0.32			303.62	0.01
6-methylnaphtho[1,2-b]thiophene	6-meN12T	310.03	0.07	308.71	0.01	303.65	0.02	303.31	0.07
7-methylnaphtho[1,2-b]thiophene	7-meN12T	307.83	0.07	306.73	0.38	302.52	0.01	301.18	0.09
8-methylnaphtho[1,2-b]thiophene	8-meN21T	306.75	0.08	305.04	0.00	301.68	0.01	300.87	0.17
9-methylnaphtho[1,2-b]thiophene	9-meN12T	307.79	0.07	306.71	0.33	302.51	0.02	301.56	0.09
4-methylnaphtho[2,1-b]thiophene	4-meN21T	309.38	0.03	308.45	0.01	303.76	0.02	305.24	0.03
5-methylnaphtho[2,1-b]thiophene	5-meN21T	314.14	0.02	313.05	0.05	306.36	0.01	311.08	0.05
6-methylnaphtho[2,1-b]thiophene	6-meN21T	315.48	0.05	313.80	0.08	306.76	0.03	310.69	0.06
7-methylnaphtho[2,1-b]thiophene	7-meN21T	314.88	0.15	313.05	0.08	306.35	0.01	315.30	0.49
8-methylnaphtho[2,1-b]thiophene	8-meN21T	312.20	0.00	311.10	0.07	305.36	0.02	308.33	0.03
9-methylnaphtho[2,1-b]thiophene	9-MeN21T	314.37	0.00	311.54	0.10	305.55	0.03	308.48	0.06
4-ring PASH									
linear, *ortho*-fused									
phenanthro[1,2-b]thiophene	P12bT	394.63	0.03	393.07	0.07	387.28	0.05	389.24	0.08
phenanthro[2,1-b]thiophene	P21bT	400.75	0.05	401.07	0.06	401.04	0.05	400.70	0.08
phenanthro[2,3-b]thiophene	P23bT	401.97	0.05	402.37	0.08	402.38	0.08	402.61	0.09
phenanthro[3,2-b]thiophene	P32bT	400.12	0.04	400.82	0.08	401.01	0.07	401.40	0.05
phenanthro[3,4-b]thiophene	P34bT	393.92	0.00	392.15	0.09	386.45	0.17	387.11	0.24
phenanthro[4,3-b]thiophene	P43bT	397.52	0.24	394.87	0.06			390.56	0.12
anthra[1,2-b]thiophene	A12bT	395.73	0.69	392.19	0.10	386.16	0.10	392.84	0.38
anthra[2,1-b]thiophene	A21bT	398.80	0.03	400.04	0.13	400.07	0.03	400.53	0.08
benzo[b]naphtho[2,1-d]thiophene-d10	BN12T-d10	382.04	0.02	377.44	0.88	361.89	0.10	369.01	0.35
benzo[b]naphtho[1,2-d]thiophene	BN12T	385.23	0.09	380.19	0.12	368.05	0.09	388.39	0.19
benzo[b]naphtho[2,1-d]thiophene	BN21T	381.53	0.03	376.97	0.91	360.82	0.08	368.30	0.47
benzo[b]naphtho[2,3-d]thiophene	BN23T	388.53	0.04	385.66	0.08	375.49	0.06	381.11	0.52
non-linear, *ortho*-fused									
phenanthro[9,10-b]thiophene	P9,10bT	394.33	0.06	392.31	0.06	385.89	0.01	388.02	0.05
peri-condensed									
phenaleno[6,7-bc]thiophene	Phelo67BCT	355	0.26	351.29	0.06	332.14	0	350.54	0.24
C_1 4-ring PASH (linear, *ortho*-fused)									
3-methylphenanthro[2,1-b]thiophene	3-MeP21bT	408.60	0.06	406.72	0.01	405.86	0.03	404.40	0.07
10-methylphenanthro[2,1-b]thiophene	10-MeA21bT	412.20	0.18	409.50	0.06	408.08	0.03	405.56	0.17
1-methylanthra[2,1-b]thiophene	1-MeA21bT	401.62	0.03	402.59	0.07	401.92	0.01	400.82	0.07

Table 4-2 (Continued)

1-methylbenzo[b]naphtho[1,2-d]thiophene	1-MeBN12T	395.70	0.03	392.76	0.11	385.60	0.12	382.76	0.43
2-methylbenzo[b]naphtho[1,2-d]thiophene	2-MeBN12T	391.88	0.09	387.49	0.11	377.67	0.12	377.75	0.29
3-methylbenzo[b]naphtho[1,2-d]thiophene	3-MeBN12T	396.03	0.03	394.06	0.98	385.65	0.09	384.04	0.36
4-methylbenzo[b]naphtho[1,2-d]thiophene	4-MeBN12T	398.40	0.03	397.53	0.80	390.82	0.08	388.29	0.34
5-methylbenzo[b]naphtho[1,2-d]thiophene	5-MeBN12T	398.34	0.09	396.70	0.07	391.86	0.14	388.39	0.19
6-methylbenzo[b]naphtho[1,2-d]thiophene	6-MeBN12T	393.43	0.04	390.25	0.93	379.36	0.07	380.68	0.17
8-methylbenzo[b]naphtho[1,2-d]thiophene	8-MeBN12T	392.78	0.05	389.40	0.90	377.78	0.06	379.14	0.28
9-methylbenzo[b]naphtho[1,2-d]thiophene	9-MeBN12T	396.42	0.09	393.49	0.11	386.55	0.15	383.31	0.27
10-methylbenzo[b]naphtho[1,2-d]thiophene	10-MeBN12T	392.92	0.08	388.80	0.10	379.77	0.07	378.78	0.22
1-methylbenzo[b]naphtho[2,1-d]thiophene	1-MeBN21T	397.14	0.03	394.92	0.11	387.09	0.07	386.06	0.58
2-methylbenzo[b]naphtho[2,1-d]thiophene	2-MeBN21T	391.54	0.09	386.67	0.05	374.97	0.08	373.52	0.74
3-methylbenzo[b]naphtho[2,1-d]thiophene	3-MeBN21T	393.52	0.03	389.21	0.05	378.28	0.01	376.97	0.87
4-methylbenzo[b]naphtho[2,1-d]thiophene	4-MeBN21T	395.44	0.01	392.19	0.08	382.63	0.13	380.34	0.70
5-methylbenzo[b]naphtho[2,1-d]thiophene	5-MeBN21T	394.86	0.03	392.71	0.94	382.90	0.13	381.65	0.36
6-methylbenzo[b]naphtho[2,1-d]thiophene	6-MeBN21T	393.25	1.18	390.09	0.10	379.41	0.05	378.25	0.81
7-methylbenzo[b]naphtho[2,1-d]thiophene	7-MeBN21T	393.78	0.01	389.85	0.08	378.87	0.08	377.41	0.77
8-methylbenzo[b]naphtho[2,1-d]thiophene	8-MeBN21T	392.76	0.01	389.54	0.93	377.68	0.10	377.11	0.45
9-methylbenzo[b]naphtho[2,1-d]thiophene	9-MeBN21T	393.28	0.04	389.10	0.06	378.15	0.06	375.96	0.75
10-methylbenzo[b]naphtho[2,1-d]thiophene	10-MeBN21T	388.31	0.04	382.70	0.07	368.46	0.07	371.49	0.52
1-methylbenzo[b]naphtho[2,3-d]thiophene	1-MeBN23T	395.86	0.07	394.03	0.21	386.80	0.01	384.32	0.32
2-methylbenzo[b]naphtho[2,3-d]thiophene	2-MeBN23T	400.40	0.15	400.11	0.04	397.12	0.03	393.21	0.25
3-methylbenzo[b]naphtho[2,3-d]thiophene	3-MeBN23T	399.97	0.09	399.66	0.10	395.59	0.01	391.55	0.45
4-methylbenzo[b]naphtho[2,3-d]thiophene	4-MeBN23T	394.52	0.10	392.18	0.21	383.59	0.03	389.49	0.56
6-methylbenzo[b]naphtho[2,3-d]thiophene	6-MeBN23T	397.30	0.02	395.89	0.03	389.53	0.02	400.46	0.13
7-methylbenzo[b]naphtho[2,3-d]thiophene	7-MeBN23T	398.28	0.03	396.89	0.07	390.93	0.02	400.74	0.07
8-methylbenzo[b]naphtho[2,3-d]thiophene	8-MeBN23T	399.57	0.02	399.15	0.03	395.17	0.01	400.50	0.20
9-methylbenzo[b]naphtho[2,3-d]thiophene	9-MeBN23T	399.77	0.05	398.96	0.06	394.97	0.06	401.52	0.31
10-methylbenzo[b]naphtho[2,3-d]thiophene	10-MeBN23T	396.01	0.02	394.23	0.12				
11-methylbenzo[b]naphtho[2,3-d]thiophene	11-MeBN23T	402.43	0.05	401.73	0.03	400.57	0.01	392.81	0.04
C_1 4-ring PASH (non-linear, *ortho*-fused)									
3-methylphenanthro[9,10-b]thiophene	3-MeP9,10bT	406.02	0.40	402.66	0.05	401.68	0.02	403.19	0.22
C_1 4-ring PASH (*peri*-condensed)									
1-methylphenanthro[4,5-bcd]thiophene	1-MeP45T	358.40	0.08	353.59	0.02	332.28	0.04	346.42	0.17
2-methylphenanthro[4,5-bcd]thiophene	2-MeP45T	356.14	0.07	351.45	0.03			343.33	0.09
5-ring PASH									
linear, *ortho*-fused									

Table 4-2 (Continued)

Benzo[b]phenanthro[2,1-d]thiophene	BP21T	466.90	0.21	466.39	0.02			473.41	1.6
peri-condensed									
benzo[2,3]phenanthro[4,5-bcd]thiophene	B23P45T	428.34	0.37	424.32	0.13	421.09	0.11	413.20	0.18
chryseno[4,5-bcd]thiophene	C45T	435.16	0.52	431.82	0.09	429.40	0.71	440.07	0.42
triphenyleno[4,5-bcd]thiophene	Triphelo45T	434.51	0.29	431.47	0.02	429.03	0.09	428.25	0.05
C_1 5-ring PASH (*peri*-condensed)									
1-methylbenzo[2,3]phenanthro[4,5-bcd]thiophene	1-MeB23P45T	433.26	0.30	428.53	0.02	424.62	0.04	424.02	0.38
3-methylbenzo[2,3]phenanthro[4,5-bcd]thiophene	3-MeB23P45T	442.85	0.33	438.63	0.08			431.49	0.36
7-methylbenzo[2,3]phenanthro[4,5-bcd]thiophene	7-MeB23P45T	440.39	0.32	436.20	0.09			426.96	0.14
9-methylbenzo[2,3]phenanthro[4,5-bcd]thiophene	9-MeB23P45T	441.11	1.18	433.92	0.17			443.41	1.47

[a] RI calculation: $RI_x = RI_B + \left[\left(\frac{t_x - t_B}{t_{(B+1)} - t_B}\right) \times 100\right]$, where the *t*'s refer to the retention time of target compound, *x*, and bracketing compounds, *B* and (*B+1*), and RI_B is the linear temperature-programmed retention index of the earlier-eluting bracket compound.

[b] Italicized compounds were not analyzed in our prior study.

Table 4-3. Comparison of PASH retention behavior between polydimethylsiloxane (PDMS) and ionic liquid columns

	SLB-IL60			SLB-IL61			SLB-IL76			SLB-IL111		
Compound Abbreviation	vs. DB5[a]	vs. DB17	vs. DB200	vs. DB5	vs. DB17	vs. DB200	vs. DB5	vs. DB17	vs. DB200	vs. DB5	vs. DB17	vs. DB200
3-ring PASH												
Dibenzothiophenes												
DBT-d8	4.8	4.9	5.5	4.4	4.5	5.1	5.0	5.1	5.7	7.7	7.7	8.4
C_1 Dibenzothiophenes												
1-MeDBT	*17.3*[b]	*15.3*		*17.6*	*15.7*		*19.5*	*17.5*		*24.9*	*23.0*	
2-MeDBT	*12.5*	8.4	5.2	*13.4*	9.2	6.0	*15.1*	*10.9*	7.7	*18.9*	*14.8*	*11.6*
3-MeDBT	*24.6*			*25.3*			*27.1*			*31.4*		
4-MeDBT	14.8	11.2		15.1	11.4		*17.2*	*13.5*		*21.8*	*18.1*	
C_2 Dibenzothiophenes												
2-EtDBT	*22.2*	*14.2*	*10.9*	*23.9*	*16.0*	*12.7*	*28.5*	*20.6*	*17.3*	*33.0*	*25.0*	*21.7*
4-EtDBT	*23.9*	*17.3*	*12.4*	*25.1*	*18.6*	*13.6*	*28.2*	*21.6*	*16.7*	*34.6*	*28.0*	*23.1*
C_3 Dibenzothiophenes												
1,3,7-TriMeDBT	*27.3*	*19.0*	*14.8*	*32.2*	*23.9*	*19.7*	*45.2*	*36.9*	*32.6*	*44.5*	*36.2*	*31.9*
1,4,7-TriMeDBT	*30.4*	*21.1*	*15.0*	*34.5*	*25.2*	*19.2*	*46.0*	*36.7*	*30.7*	*47.7*	*38.4*	*32.3*
2,4,6-TriMeDBT	*27.1*	*16.5*	*13.9*	*31.1*	*20.5*	*17.9*	*40.4*	*29.9*	*27.2*	*42.1*	*31.6*	*28.9*
2,4,7-TriMeDBT	*24.7*	*14.2*	*12.0*	*29.4*	*18.8*	*16.6*	*41.0*	*30.4*	*28.2*	*41.0*	*30.4*	*28.2*
2,4,8-TriMeDBT	*24.5*	*13.1*	*12.4*	*29.1*	*17.7*	*17.1*	*40.4*	*29.0*	*28.4*	*39.2*	*27.8*	*27.2*
3,4,7-TriMeDBT	*23.9*	*15.1*	*11.6*	*28.9*	*20.0*	*16.6*	*43.7*	*34.8*	*31.4*	*39.9*	*31.0*	*27.6*
Naphthothiophenes												
N21T	0.6	3.1	-0.9	0.1	2.6	-1.4	0.1	2.6	-1.4	-0.9	1.6	-2.4
N23T	0.7	3.6		0.1	3.0		1.7	4.6		-0.6	2.4	
C_1 Naphthothiophenes												
2-MeN12T	7.4	4.6		8.9	6.1		*12.4*	9.6		*15.1*	*12.3*	
5-MeN12T	9.2	8.0		*10.2*	9.0				0.0	*14.8*	*13.6*	
6-MeN12T	9.3	8.1	0.2	*10.6*	9.4	1.5	*15.7*	*14.5*	6.6	*16.0*	*14.8*	6.9
7-MeN12T	7.5	5.1	0.6	8.6	6.2	1.7	*12.8*	*10.4*	5.9	*14.1*	*11.7*	7.3
8-MeN12T	7.9	5.5	1.1	9.6	7.2	2.8	*13.0*	*10.6*	6.2	*13.8*	*11.4*	7.0
2-MeN21T	0.5	-1.7	7.8									
4-MeN21T	8.4	7.0	-0.4	9.3	7.9	0.6	*14.0*	*12.6*	5.3	*12.5*	*11.1*	3.8
5-MeN21T	8.6	8.6	-1.9	9.7	9.7	-0.8	*16.4*	*16.4*	5.9	*11.7*	*11.7*	1.2
6-MeN21T	8.2	8.0	-2.8	9.9	9.7	-1.1	*16.9*	*16.7*	5.9	*13.0*	*12.8*	2.0
7-MeN21T	4.9	3.4	-4.2	6.7	5.3	-2.3	*13.4*	*11.9*	4.4	4.4	3.0	-4.6
8-MeN21T	7.0	4.8	-1.7	8.1	5.9	-0.6	*13.8*	*11.6*	5.2	*10.9*	8.7	2.2
9-MeN21T	*11.0*	*12.0*	-1.0	*13.9*	*14.8*	1.9	*19.9*	*20.8*	7.9	*16.9*	*17.9*	4.9
4-ring PASH												
linear, *ortho*-fused												

Table 4-3 (Continued)

P12bT	1.7	2.8	-3.5	3.2	4.4	-1.9	9.0	*10.2*	3.9	7.1	8.2	1.9
P21bT	0.0	2.5	-3.2	-0.3	2.1	-3.6	-0.3	2.2	-3.5	0.1	2.5	-3.2
P23bT	0.1	2.0	-2.0	-0.3	1.6	-2.4	-0.3	1.6	-2.4	-0.5	1.3	-2.7
P32bT	1.5	3.2	-1.0	0.8	2.5	-1.7	0.6	2.3	-1.8	0.2	1.9	-2.2
P34bT	2.8	4.9	-3.6	4.5	6.7	-1.9	*10.2*	*12.4*	3.8	9.6	*11.7*	3.2
P43bT	-2.2	-0.6	-7.4	0.5	2.0	-4.8				4.8	6.3	-0.5
A12bT	-0.4	-0.4		3.2	3.1		9.2	9.1		2.5	2.4	
A21bT	0.5	1.3	-2.5	-0.8	0.0	-3.7	-0.8	0.0	-3.8	-1.3	-0.5	-4.2
N21T	0.6	3.1	-0.9	0.1	2.6	-1.4	0.1	2.6	-1.4	-0.9	1.6	-2.4
BN12T-d10	6.8	5.4		*11.4*	*10.0*		*27.0*	*25.6*		*19.8*	*18.5*	
BN12T	7.7	7.2		*12.7*	*12.3*		*24.9*	*24.4*		4.5	4.1	
BN23T	7.2	6.5		*10.1*	9.4		*20.3*	*19.5*		*14.6*	*13.9*	
non-linear, *ortho*-fused												
P9,10bT	0.8	1.8	-5	2.8	3.8	-3	9.2	*10.2*	3.5	7.1	8.1	1.3
peri-condensed												
Phelo67BCT	0.2	3.6	-18.2	3.5	7.3	-14.5	*22.7*	*26.4*	4.7	4.3	8	-13.7
C_1 4-ring PASH (linear, *ortho*-fused)												
3-MeP21bT	*12.1*	*11.5*	*9.5*	*14.0*	*13.4*	*11.4*	*14.8*	*14.2*	*12.2*	*16.3*	*15.7*	*13.7*
1-MeA21bT	*14.4*	*12.0*	*12.9*	*13.4*	*11.0*	*11.9*	*14.1*	*11.7*	*12.6*	*15.2*	*12.8*	*13.7*
1-MeBN12T	*24.2*	*23.0*		*30.0*	*28.7*		*48.3*	*47.1*		*43.8*	*42.5*	
2-MeBN12T	*14.3*	8.6	*13.5*	*18.7*	*13.0*	*17.9*	*28.5*	*22.8*	*27.7*	*28.4*	*22.7*	*27.6*
3-MeBN12T	*13.5*	8.8	*11.7*	*15.5*	*10.8*	*13.7*	*23.9*	*19.2*	*22.1*	*25.5*	*20.8*	*23.7*
4-MeBN12T	*15.1*	*11.8*		*15.9*	*12.7*		*22.7*	*19.4*		*25.2*	*21.9*	
5-MeBN12T	*14.7*	*11.6*	*11.9*	*16.3*	*13.2*	*13.5*	*21.2*	*18.1*	*18.4*	*24.6*	*21.5*	*21.8*
6-MeBN12T	*14.5*	*10.1*	*11.6*	*17.7*	*13.3*	*14.8*	*28.6*	*24.2*	*25.6*	*27.3*	*22.9*	*24.3*
8-MeBN12T	*14.8*	*10.9*	*12.3*	*18.1*	*14.2*	*15.7*	*29.8*	*25.9*	*27.3*	*28.4*	*24.5*	*26.0*
9-MeBN12T	*13.4*	9.2	*11.8*	*16.3*	*12.1*	*14.8*	*23.3*	*19.0*	*21.7*	*26.5*	*22.3*	*24.9*
10-MeBN12T	*14.1*	8.7	*13.2*	*18.2*	*12.8*	*17.4*	*27.2*	*21.9*	*26.4*	*28.2*	*22.8*	*27.4*
1-MeBN21T	*15.8*	*13.4*		*18.0*	*15.6*		*25.9*	*23.5*		*26.9*	*24.5*	
2-MeBN21T	*14.1*	8.5	*13.5*	*18.9*	*13.4*	*18.4*	*30.6*	*25.1*	*30.1*	*32.1*	*26.5*	*31.5*
3-MeBN21T	*12.7*	7.9	*12.4*	*17.0*	*12.3*	*16.7*	*27.9*	*23.2*	*27.7*	*29.2*	*24.5*	*29.0*
4-MeBN21T	*14.7*	*10.4*	*13.3*	*17.9*	*13.7*	*16.5*	*27.5*	*23.2*	*26.1*	*29.8*	*25.5*	*28.4*
5-MeBN21T	*14.1*	9.4	*12.3*	*16.2*	*11.5*	*14.5*	*26.0*	*21.3*	*24.3*	*27.3*	*22.6*	*25.5*
6-MeBN21T	*17.1*	*13.4*		*20.2*	*16.6*		*30.9*	*27.3*		*32.1*	*28.4*	
7-MeBN21T	*16.8*	*13.1*	*14.1*	*20.7*	*17.0*	*18.0*	*31.7*	*28.0*	*29.0*	*33.2*	*29.4*	*30.5*
8-MeBN21T	*13.2*	8.1	*13.0*	*16.4*	*11.3*	*16.2*	*28.3*	*23.2*	*28.0*	*28.8*	*23.7*	*28.6*
9-MeBN21T	*13.2*	8.7	*12.9*	*17.4*	*12.9*	*17.0*	*28.3*	*23.8*	*28.0*	*30.5*	*26.0*	*30.2*
10-MeBN21T	*14.9*	*10.1*	*13.5*	*20.5*	*15.7*	*19.1*	*34.7*	*30.0*	*33.4*	*31.7*	*26.9*	*30.3*
1-MeBN23T	*17.8*	*13.9*	*15.7*	*19.6*	*15.7*	*17.6*	*26.8*	*23.0*	*24.8*	*29.3*	*25.4*	*27.3*
2-MeBN23T	5.7	0.4		6.0	0.7		9.0	3.6		*12.9*	7.6	

Table 4-3 (Continued)

3-MeBN23T	*12.9*	8.9	*12.4*	*13.2*	9.2	*12.8*	*17.3*	*13.2*	*16.8*	*21.3*	*17.3*	*20.9*
4-MeBN23T		*10.7*			*13.1*			*21.7*			*15.8*	
6-MeBN23T	*14.8*	*11.9*		*16.3*	*13.3*		*22.6*	*19.6*		*11.7*	8.7	
7-MeBN23T	*16.4*	*12.1*		*17.8*	*13.5*		*23.8*	*19.5*		*14.0*	9.6	
8-MeBN23T	*12.8*	8.1		*13.2*	8.5		*17.2*	*12.5*		*11.9*	7.1	
9-MeBN23T	*12.7*	7.6	*11.6*	*13.5*	8.4	*12.4*	*17.5*	*12.4*	*16.4*	*10.9*	5.8	9.8
10-MeBN23T	*17.0*		*14.7*	*18.8*		16.4						
11-MeBN23T	*18.3*	*17.1*		*19.0*	*17.8*		*20.1*	*18.9*		*27.9*	*26.7*	
C_1 4-ring PASH (nonlinear, *ortho*-fused)												
3-MeP9,10bT	9.8	7.7	6.8	*13.2*	*11.0*	*10.2*	*14.1*	*12.0*	*11.2*	*12.6*	*10.5*	9.7
C_1 4-ring PASH (*peri*-condensed)												
1-MeP45T	*12.8*	*11.5*	-2.4	*17.6*	*16.3*	2.4	*38.9*	*37.6*	*23.7*	*24.8*	*23.5*	9.6
2-MeP45T	*11.9*	*10.0*		*16.6*	*14.7*				0.0	*24.7*	*22.8*	
5-ring PASH												
peri-condensed												
B23P45T			7.8			*11.9*			*15.1*			*23.0*
C45T	*11.9*	*12.2*	7.2	*15.3*	*15.6*	*10.6*	*17.7*	*18.0*	*13.0*	7.0	7.3	2.3
Triphelo45T	*40.9*		5.5	*44.0*		8.5	*46.4*		*11.0*	*47.2*		*11.8*
C_1 5-ring PASH (*peri*-condensed)												
1-MeB23P45T	*19.4*	*13.6*	*17.1*	*24.1*	*18.3*	*21.8*	*28.1*	*22.3*	*25.7*	*28.6*	*22.8*	*26.3*
3-MeB23P45T	*18.3*	*12.6*	*15.6*	*22.5*	*16.8*	*19.8*				*29.6*	*23.9*	*27.0*
7-MeB23P45T	*20.0*	*13.6*	*17.1*	*24.1*	*17.8*	*21.3*				*33.4*	*27.0*	*30.5*
9-MeB23P45T	*15.5*	9.3	*14.1*	*22.7*	*16.4*	*21.2*				*13.2*	7.0	*11.8*

[a] Differences in retention index were calculated as $RI_{Siloxane} - RI_{IL.}$
[b] Retention changes >10 index units are italicized.

Beyond this general trend, PASH retention behavior can be cast in terms of polarizability and polarity. The former is generally dependent on molecular geometry – for molecules with the same number of rings, linear PASH (e.g., anthracene analogs) are more polarizable than condensed PASH (e.g., pyrene analogs).[144] The latter is generally influenced by the location of the sulfur atom. For PASH of the same size, polarity (and retention behavior) should differ if the

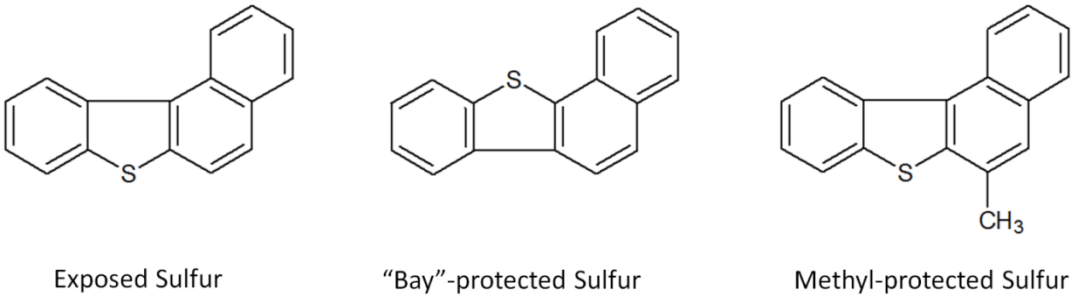

Figure 4-3. 4-ring PASH benzo[*b*]naphtho[1,2-*d*]thiophene, benzo[*b*]naphtho[2,1-*d*]thiophene, and 6-methylbenzo[*b*]naphtho[1,2-*d*]thiophene illustrate exposed, "bay-", and methyl-protected sulfur heteroatoms, respectively

sulfur atom is "protected" in a bay region or by an alkyl-group on an adjacent carbon, see Figure 4-3. As expected, these molecular features lead to distinct trends in retention behavior.

Examining polarizability first, linear PASH indices are higher than those of non-linear PASH, with condensed compounds having the lowest retention index of all. For example, benzo[*b*]phenanthro[2,1-*d*]thiophene, the most linear of the 5-ring PASH examined in this study, has the highest RI, while the *peri*-condensed methylphenanthro[4,5-*b,c,d*]thiophenes have retention indices approximately 40 units lower than the *ortho*-fused C_1 4-ring PASH. Next examining polarity, those compounds that have the same ring number with a bay region-protected S have lower retention indices than those with an exposed S. This trend is evident in the 3-, 4-, and 5-ring PASH and their C_1, C_2, and C_3 homologues. For example, 2,4,6-trimethyldibenzothiophene and benzo[2,3]phenanthro[4,5-*b,c,d*]thiophene are the only C_3 DBT and 5-ring PASH we investigated with bay region-protected

sulfur atoms; these compounds have the lowest RI among their respective groups. This trend, however, is not as prevalent when the sulfur atom is protected by an alkyl group, as this leads to non-negligible differences in retention for only the 2- and 3-ring PASH. Increased retention of PASH with exposed sulfur atoms suggests strong H-bonding characteristics in the IL phases studied. This result is consistent with other ionic liquid stationary phases, which were found to have Abraham α and β parameters far greater than siloxane-based columns.[145]

Ionic liquid stationary phases can improve the separation of target compounds used in environmental forensic studies. Often in these studies, ratios of target compound concentrations are used to determine the source and the extent of fossil fuel weathering in the environment;[90] for example, the ratios of 1-, 2-, 3-, and 4-methyldibenzothiophene to one another vary with petroleum source.[146] However, the 2- and 3-MeDBT isomers coelute on non-polar stationary phases,[147] requiring the analyst to combine the concentrations of these two isomers. In contrast, the SLB-IL111 column produced baseline separation of these isomers, providing a more accurate estimate of the concentration and corresponding diagnostic. In addition, the environmentally-important[102] isomer pair 1,3,7- and 3,4,7-TriMeDBT coeluted on the siloxane-based columns but were baseline separated on the IL columns; the same can be said for naphthothiophene pairs 6- and 8-MeBN12T, 2- and 9-MeBN12T, 4- and 7-MeBN21T.

The SLB-IL76 and SLB-IL111 stationary phases lead to the largest retention changes, while SLB-IL60 and SLB-IL61 produce retention values closer to those of the non-polar columns. This finding is expected due to the relative polarity of each column, and for the majority of compounds examined, the magnitude of retention changes can be correlated with the polarity rating of the column. As the effects of stationary phase polarity on selectivity become more pronounced as elution temperature is increased, the larger compounds (with higher boiling points) are expected to be increasingly separated on the more-polar columns, and this was found to be the case. The magnitude of the dibenzothiophene retention change increases with additional alkylation, as the $\overline{RI}_{IL}$ of the C_0, C_1, C_2, and C_3 DBT differ from $\overline{RI}_{siloxane}$ by 6, 16, 21, and 28 RI units, respectively. This change in retention corresponds to the ionic columns' ability to separate these compounds; as size increases, so too do changes in retention behavior versus non-polar columns. The same trend is evident amongst 4-ring PASH, and nearly every 5-ring PASH displays significant decreases in retention index compared to the siloxane-based columns. While none of the PASH examined can be classified as truly polar, the IL columns offer distinct differences in retention behavior for these compounds.

Ionic liquids are capable of an extremely broad range of physical-chemical solvation interactions, which results in phases having unique selectivity compared to traditional siloxane-based stationary phases.[118] This is evident when one compares retention indices from the IL columns to those of the other stationary

phases, and is likely the cause of drastic shifts in retention for many compounds. For example, the C_1 naphthothiophenes elute before the C_2 DBT on the siloxane columns, but this order is reversed on the IL columns. Elution order reversals occurred for roughly one-third of the PASH groups examined in this study. Additionally, several compounds have retention indices that decrease with increasing column polarity for SLB-IL60, 61, and 76, but are highest on the most polar IL column, SLB-IL111. This stationary phase is more polar than the others – in fact, it is currently the most polar commercially-produced column. Its structure differs from the other IL columns, as its cation is imidazolium-based, compared to tripropylphosphonium-based for the other three columns. It is likely, then, that this extreme polarity and dissimilar stationary phase structure explain the retention behavior differences.

The combination of unique selectivity and retention behavior provided by IL columns has led to their use in high-temperature two-dimensional separations where, typically, non-polar and moderately-polar column combinations are employed.[124] For the analysis of a PASH fraction,[148] it is expected that, based on coelution percentages, the SLB-IL111 column would provide the best separation of PASH. However, analyses of unweathered coal tars, crude oils, and other complex matrixes with many low-volatility compounds, often require 1st and 2nd dimension column temperatures that exceed 300 °C. As such, larger PASH such as 2-methylnaphtho[2,1-*b*]thiophene and 10-methylbenzo[*b*]naphtho[2,3-*d*]thiophene and other low volatility coal tar components such as polycyclic

aromatic hydrocarbons (PAH) will not elute from the SLB-IL111 column at its maximum operating temperature, see Figure 4-2. Due to these temperature restrictions, only SLB-IL60, the most temperature-stable of the ionic columns, was used for GC×GC/MS analysis of coal tar samples. Selected GC×GC/MS chromatograms of PAH standards analyzed using DB-5/DB-17 and DB-5/SLB-IL60 column pairs are shown in Figures 4-5A and 4-5B, respectively. The figure highlights the dual nature of the ionic liquid phase, as the same general separation pattern is observed between the two chromatograms. While PAH with 3 rings or fewer are separated similarly on both columns, close inspection reveals that the larger, more polarizable PAH (MW > 202) are separated to a greater degree on the ionic liquid phase. For example, examining the 2nd dimension resolution, see table inset, the isomer pairs fluoranthene (peak number 7) and pyrene (8), benzo(a)anthracene (9) and chrysene (10), and benzo(b and k)fluoranthene (11 and 12) all exhibit increased resolution on the SLB-IL60 column. While separation on DB-17 leads to 2nd dimension coelution, the IL stationary phase provides distinctly visible spacing between peaks. Coal tar analysis also provides evidence that, for some compounds, use of the IL column leads to increases in separation. This improved separation occurs on the IL column for several homologous series of PAH, including the alkyl phenanthrene/anthracenes and chrysenes, as well as for several PASH. These results are in agreement with previous findings that ionic liquid columns provide increased separation space and resolution in 2-dimensional GC applications.[124] An examination of PASH structure versus 2D separation is illustrated in Figures 4-5 and 4-6.

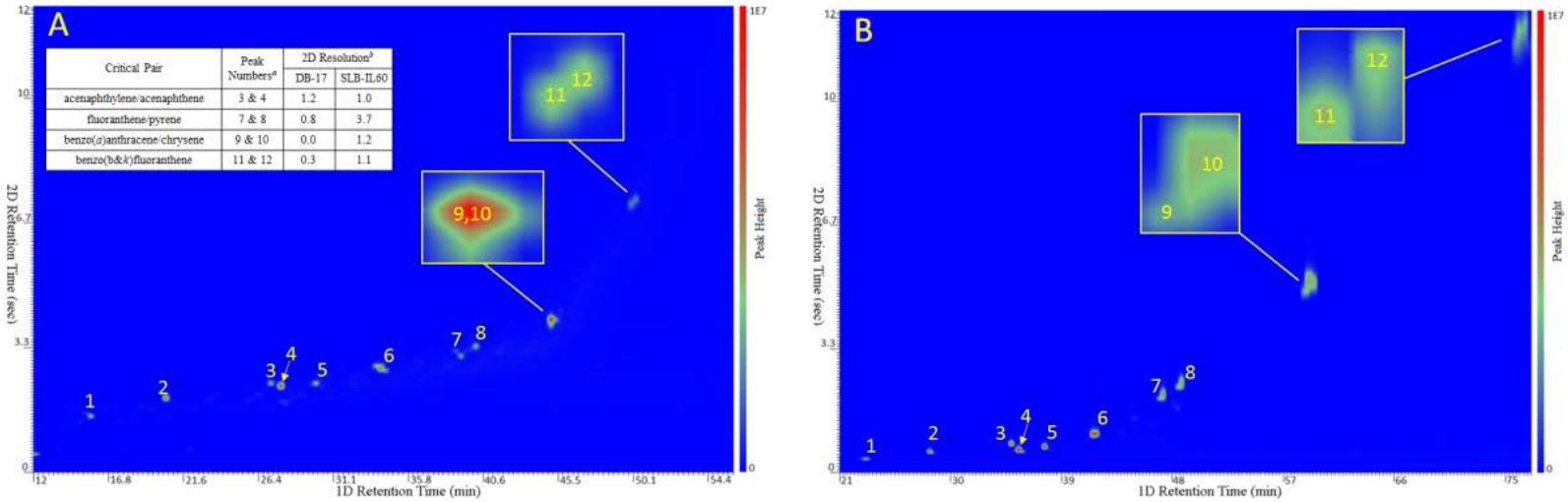

Critical Pair	Peak Numbers[a]	2D Resolution[b]	
		DB-17	SLB-IL60
acenaphthylene/acenaphthene	3 & 4	1.2	1.0
fluoranthene/pyrene	7 & 8	0.8	3.7
benzo(*a*)anthracene/chrysene	9 & 10	0.0	1.2
benzo(b&*k*)fluoranthene	11 & 12	0.3	1.1

Figure 4-4. GC×GC/MS analysis of PAH standards using DB-5/DB-17 (A) and DB-5/SLB-IL60 (B).

Notes:
a.) Peaks: 1,4-dichlorobenzene-*d4* (1); naphthalene (2); acenaphthylene (3); acenaphthene (4); fluorene (5); phenanthrene/anthracene (6); fluoranthene (7); pyrene (8); benzo(*a*)anthracene (9); chrysene (10); benzo(*b*)fluoranthene (11); benzo(*k*)fluoranthene (12)

b.) Resolution calculated between compounds in 2nd-dimension: $R_S = \frac{\left(RT_{2D,(x-1)} - RT_{2D,x}\right)}{\left(0.5W_x + 0.5W_{(x-1)}\right)}$ where RT_{2D} and W refer to the 2nd dimension retention times and peak widths of compounds *x* and (*x-1*), (*x-1*) eluting before *x* in the 2nd dimension.

Illustrated in the figures are reconstructed ion current chromatograms of PASH homologues from the analysis of an unfractionated coal tar contaminated soil on DB-5/DB-17 and DB-5/SLB-IL60. As described above, the linear polyaromatics are generally more polarizable than condensed compounds with the same number of rings. This is confirmed by our findings, namely, the *ortho*-PASH separate more than the *peri*-PASH on the IL column. For example, Figures 4-5A and 4-5B make clear similar separation of the *peri*-condensed homologues occurs on DB-17 or SLB-IL60. However, Figures 4-6A and 4-6B show the C_1 to C_3 4-ring *ortho*-fused PASH overlap on DB-5/DB-17, but are separated into distinct 2^{nd} dimension bands on DB-5/SLB-IL60. While ionic liquids have long been considered "promising" stationary phases, the time has come where they should be routinely used for the analysis of complex samples such as tars and oils.

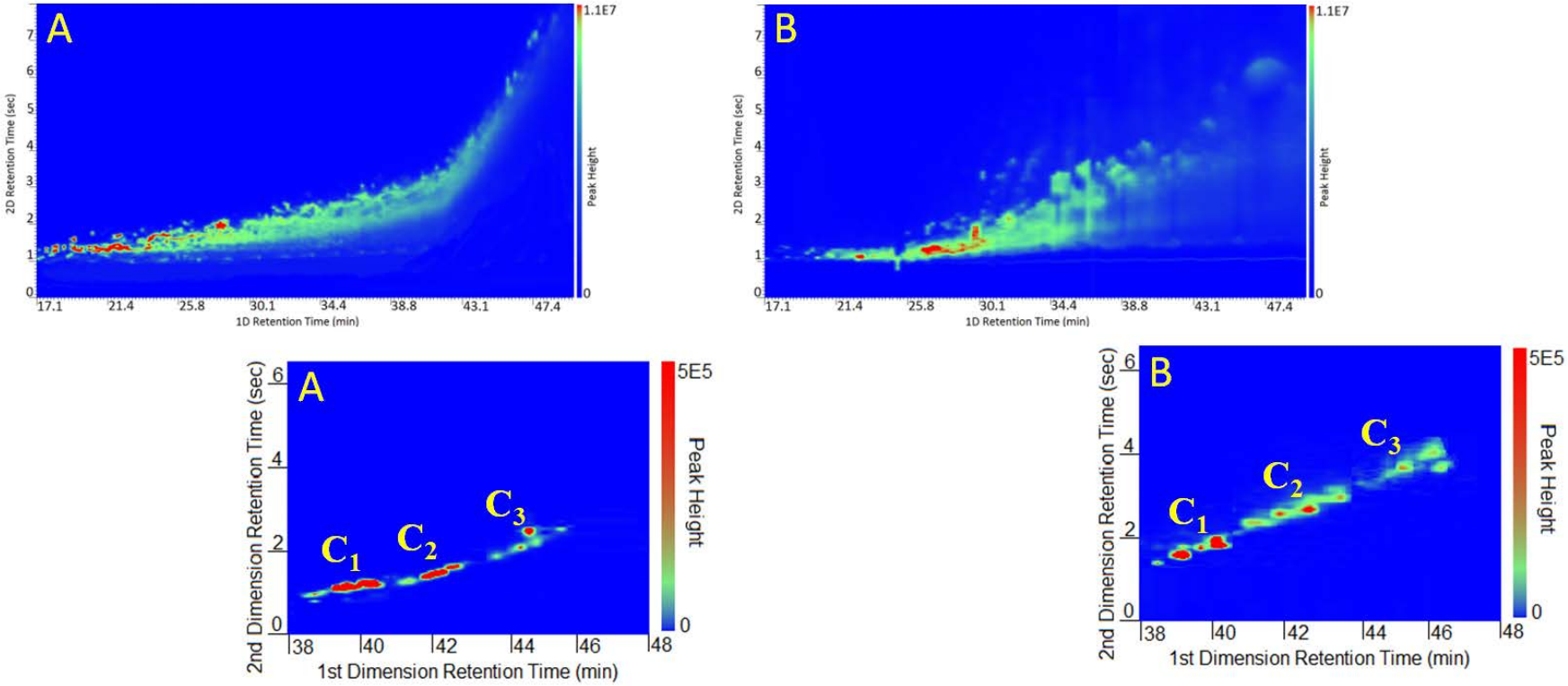

Figure 4-5. GC×GC/MS analysis of C_1-C_3 4-ring *peri*-condensed PASH in coal tar using DB-5/DB-17 (A) and DB-5/ SLB-IL60 (B). Note the difference in *y*-axis scale between full chromatogram (10^7) and expanded view (10^5).

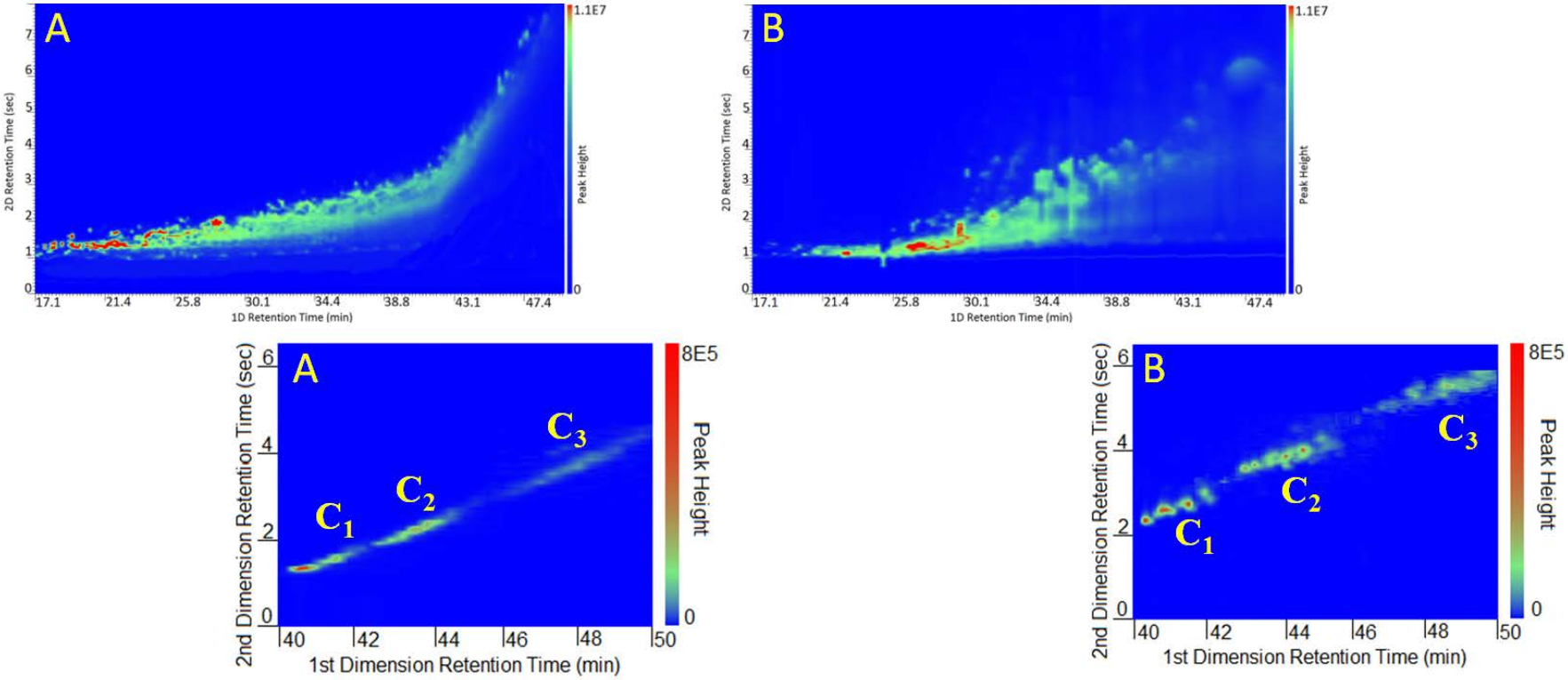

Figure 4-6. GC×GC/MS analysis of C_1-C_3 4-ring *ortho*-fused PASH in coal tar using DB-5/DB-17 (A) and DB-5/SLB-IL60 (B). Note the difference in *y*-axis scale between full chromatogram (10^7) and expanded view (10^5).

Chapter 5 New Spectral Deconvolution Algorithms for the Analysis of Polycyclic Aromatic Hydrocarbons and Sulfur Heterocycles by Comprehensive Two-Dimensional Gas Chromatography/Mass Spectrometery

5.1 Introduction

Because automated sequential GC-GC/MS provides clean spectra of sample components in complex mixtures, it is ideal for building libraries. However, it is difficult to obtain quantitative data from this technique, since a single compound can elute in more than one heart-cut and each heart-cut requires its own sample injection. Moreover, the amount transferred between columns is dependent on the modulation phase in relation to component position at time of sample transfer. Generally, separations on both columns must finish before subsequent injections occur, which results in impractically long analysis times for routine analytical work. This study is an evaluation of the data quality produced by new spectral deconvolution algorithms specifically developed for 2-dimensional GC×GC/MS. GC×GC is seen as the limiting case of GC-GC when the width of the heart-cut approaches zero,[149] offering multiple dimensions of separation on a far shorter time-scale than GC-GC.[150]

Notwithstanding statistical overlap theory,[151] research has shown increases in separation capacity produced by GC×GC require compromise.[152] For example, suboptimal column conditions[152] and non-orthogonal stationary phases[153] impact peak capacity improvements.[154] Also, employing conventional mass spectrometry identification criteria requires reconciling the narrowness of the 2nd dimension

band width with achieving sufficient invariant peak scans to correctly identify sample components. This can be problematic when low resolution mass filters, such as quadrupoles, are employed. Additionally, the modulation ratio (the number of sample portions transferred per 1st dimension peak)[155,156] and modulation phase (the sampling start time with respect to peak shape)[157] can alter detector signal, leading to quantitative errors.[63] When the effects of separation time on 2nd dimension peak widths are ignored, longer modulation periods allow for increases in 2nd column separation of coeluting compounds, but the correspondingly low modulation ratios lead to decreases in signal precision. In contrast, higher modulation ratios lead to increases in quantitative accuracy, but the correspondingly shorter modulation times limit the 2nd dimension analysis time, which decreases separation capacity. Calculations show that by modifying separation and measurement attributes to obtain at least three modulations per 1st dimension peak, quality data is achievable.[152,156] Nonetheless, when isomers elute near enough to one another, their narrow, modulated peaks overlap such that spectral patterns of one compound are not discernible from others without spectral deconvolution.

While different mathematical and statistical models have been used in an attempt to deconvolve coeluting compounds in GC×GC/MS, these studies have used TOF mass filters and as such, have had the advantage of increased data density (mass spectra) across the peak compared to scanning quadrupole mass spectrometers.[158,159,160] For this reason, the use of a fast qMS with GC×GC is far

less common. Only recently have researchers used this technique for quantitative analyses, including a semi-quantitative study of coal tar-contaminated sediment.[161] However, neither this investigation nor other GC×GC/TOF fingerprint[162] or classification[163] studies of coal tar have capitalized on the wealth of mass spectral information available in the data. Despite significant differences in the number of data points produced by qMS and TOF analyzers, quadrupole filters have advanced to produce sufficient peak scans so that low concentration analytes can be unambiguously identified when employing conventional mass spectrometry data analysis criteria. To test this hypothesis, a new spectral deconvolution algorithm was developed for GC×GC/qMS.

5.2 Experimental

Standards and Reagents: Airgas (Salem, NH) supplied the ultra-high purity helium and nitrogen used in this study. The 16 EPA priority pollutant PAH, dibenzothiophene (DBT), and internal standards 1,4-dichlorobenzene-d_4, naphthalene-d_8, phenanthrene-d_{10}, chrysene-d_{12}, and perylene-d_{12} were purchased from Restek (Bellefonte, PA). A base/neutral surrogate spike mix (2-fluorobiphenyl, nitrobenzene-d_5, p-terphenyl-d_{14}) was purchased from Supelco (Bellefonte, PA) and chromatography-grade toluene and dichloromethane from Sigma-Aldrich (St. Louis, MO). PAH and dibenzothiophene (DBT) standards ranging from 0.001 to 25 μg/mL were prepared by serial dilution in dichloromethane.

Samples and Sample Preparation Procedure: A coal tar contaminated soil and bitumen tar sand were obtained from a utility in New York and from the Athabasca tar sand reservoir in Canada, respectively. For the coal tar soil, the ultrasonic-based extraction method described in previous chapters was employed. For the Athabasca tar sand, a 30 g sample was extracted in 30 mL of toluene using a CEM (Matthews, NC) Mars 6 microwave extraction unit. Activated copper and anhydrous sodium sulfate were used to eliminate elemental sulfur and water from the extracts, which were concentrated under a stream of nitrogen prior to the addition of internal standards. Calibration standards and samples were spiked with 1 μg/mL of the internal standard mixture.

Instrumentation: GC×GC/MS analyses were performed using an Agilent Technologies (Santa Clara, CA) 6890/5975C GC/MS with Gerstel (Mülheim an der Ruhr, Germany) MPS2 autosampler and CIS6 injector. Columns were connected using a Restek press-fit connector. The GC×GC cryogenic and thermal modulation hardware was obtained from Zoex Corporation (Houston, TX). GC Image (Lincoln, NE) supplied the software to create the three-dimensional chromatograms. Corresponding GC/MS analyses were performed using a Shimadzu (Columbia, MD) GC2010/QP2010+ instrument.

GC×GC/MS and GC/MS Analysis: The GC×GC/MS and GC/MS operating conditions are listed in Table 5-1. To establish measurement sensitivity, 1 μL of a

Table 5-1. GC/MS and GC×GC/MS instrument parameters

GC Parameters	**GC×GC/MS Method**	**GC/MS Method**
Injection Mode	Splitless	Splitless
Injection Volume	1 µL	1 µL
Inlet Program	-20°C, 12°C/min, 320°C (5 min)	300°C
Carrier Gas	Constant Flow, 1 mL/min He	Constant Flow, 1.5 mL/min He
Column 1	30 m x 0.25 mm ID x 1.0 µm DB-5MS Ultra Inert	30 m x 0.25 mm ID x 0.25 µm DB-5
Column 2	1 m x 0.18 mm ID x 0.36 µm RXI-17SilMS	N/A
Transfer Line Temperature	300°C	290°C
Modulation Time	8 sec	N/A
Hot Jet Temperature	310°C	N/A
Cryogen Flow	15 L/min	N/A
Temperature Program	60°C (1 min), 6.5°C/min, 325°C (20 min)	60°C (1 min), 5°C/min, 340°C (0 min), -20°C/min, 300°C (5 min)
Run Time	61.77 min	64 min
MS Parameters	**GC×GC/MS Method**	**GC/MS Method**
Solvent Delay	17 min	8 min
Mass Range	50-350 *m/z*	50-450 *m/z*
Scan Rate	19.79 scans/s	8.3 scans/s
Quadrupole Temperature	150°C	150°C
Ion Source Temperature	230°C	230°C

serially diluted PAH and DBT standard was analyzed from 1 pg/µL to 25 ng/µL. The linear ranges and quantitation limits were determined, and the statistical limit of detection was calculated using the student's *t*-test from the analysis of nine standards whose concentration was approximately one-half the LOQ. PAH and DBT response factors were calculated for each concentration over the dynamic range as follows: $A_X C_{IS}/A_{IS} C_X$, where C_X is the analyte concentration and A_X its observed signal, with C_{IS} and A_{IS} the corresponding internal standard concentration and signal response. As discussed in our previous work,[69] a complete and accurate method would employ response factors for all fragmentation patterns, but due to a lack of existing standards, this is not possible. As such, in this study, alkylated PAH homologues were quantified using each parent's average RF. Additionally, alkyl PASH concentrations were calculated using the DBT response factor due to insufficient quantities of 4-ring parent PASH standards. These response factors only affect absolute concentrations, not the relative concentrations when comparing findings between MFPPH and single-ion analyses or between GC×GC/qMS and GC/qMS analyses, since the same alkylated PAH response factors were used independent of detection method. Spectral deconvolution of GC/MS data was described in earlier work (Ion Analytics, Andover, MA).[153] For this study, new spectral deconvolution algorithms were developed to process GC×GC/MS data.

The expressions below outline the identification process. A background signal for each PAH and PASH qualifier ion (in this case the MFPPH ions) is subtracted

from the peak signal. The reduced (relative to the base ion, $i = 1$) ion intensity, $I_i(t)$, at scan (t) is defined as follows:

$$I_i(t) = \frac{A_i(t)}{R_i A_1} \tag{5-1}$$

where $A_i(t)$ is the i-th qualifier ion intensity at scan (t) and R_i is the expected relative ion abundance ratio, which can be found in MS libraries such as NIST and Wiley or by analyzing standards. All qualifier ions are normalized to the base ion (for the base ion, $I_1 \equiv 1$). The spectral match, ΔI, is calculated by:

$$\Delta I = \frac{\sum_{i=1}^{N-1} \sum_{j=i+1}^{N} Abs(I_i - I_j)}{\sum_{i=1}^{N-1} i} \tag{5-2}$$

where ΔI is the average relative reduced intensity deviation of each of the N qualifier ions. For each compound, the number of qualifier ions is selected by the analyst. In addition to the base ion, there should be at least two qualifier ions per compound. For this study, we used three ions for each parent compound and five ions per alkylated homologue fragmentation pattern.[73] The closer ΔI is to zero, the better the match. In addition to this compound identity criterion, and to avoid inclusion of scans with skewed ion ratios, the scan-to-scan variance (SSV), ΔE, is calculated:

$$\Delta E = \Delta I \cdot \log(A_1) \tag{5-3}$$

The target compound is considered present when the extracted ion ratios at scan (t) yield $\Delta E \leq \Delta E_{max}$, where the maximum allowable SSV is ΔE_{max}. Peak scans that fail this criterion are not included in the total peak area used to estimate analyte concentration in the sample. Another compound acceptance condition is:

$$\Delta I \leq K + \frac{\Delta_0}{A_1} \tag{5-4}$$

where K is an acceptable percent relative difference selected by the analyst and Δ_0 is the additive error attributable to background (matrix) signal or instrument noise. This criterion measures both the ΔI at each scan and its variance from one scan to the next. If the intensity of a qualifier ion is higher than expected due to additive ion signal, the software compares all ion ratios against one another (computing a relative error for each peak scan) and will eliminate the signal from the matrix-affected ion if all other ions are in agreement (meaning ΔI is lower than the threshold value).

Target compound identity occurs when the ΔE or ΔI criterion is ≤ 7 in at least four consecutive peak scans. In addition, three other compound identity criteria must be met. First, the qualifier ratio deviation of the target ion must be $\leq u_i$ (the uncertainty value for the *i*-th confirming ion, e.g., $\leq 20\%$) at each scan in the peak. This criterion ensures that the spectra are invariant across the peak. Second, the Q-value must be ≥ 90. The Q-value is an integer between 1 and 100 that measures the deviation between the expected and observed ion ratios for each ion across the peak. The closer the Q-value is to 100, the higher the certainty that sample and library spectra match one another. Third, the Q-ratio must be $\leq 20\%$ of the relative abundance. The Q-ratio is the peak area ratio of the extracted *i*-th and base ions. All of these criteria form a single acceptance condition. Only those scans that meet the above-mentioned criteria are selected for observation by the analyst, with the quantitative ion signal extracted from the peak and used to calculate A_X and A_{IS}. Given the multiple modulated peaks per compound, the

deconvolution algorithms searched for up to twenty individual peaks per fragmentation pattern (or compound). For parent PAH, retention times were used to guide the search algorithms. For alkylated compounds, identification was based solely on spectral deconvolution.

5.3 Results and Discussion

This study reports the first quantitative analysis of parent and alkyl PAH and PASH in coal tar by GC×GC/qMS. When compared to FID or TOF, significant operational tradeoffs are required since qMS cannot approach the data collection rates of these detectors. Although SIM/1-ion detection has the potential of providing many more data points (peak-scans) than full-scan methods, we showed using too few ions leads to significant overestimation of alkylated PAH and PASH[73] in complex matrixes such as coal tar and crude oil and that accurate identification of target compounds requires at least three ions, whose relative abundances are within 20% of the known spectra, for at least four consecutive scans across the chromatographic peak.[47] Past research has shown that the spectrometer must produce at least seven scans per peak to obtain constant peak areas for quantitative analysis and that ion skewing, which hinders compound identification, was prevalent when six or fewer quadrupole peak scans were obtained; for example, five peak scans produced a 32% variation in the mass ratios.[164] Given the limitations of quadrupole technology, the stated goal of providing high quality quantitative data for these compounds in complex matrixes, and recognizing we could deconvolve comingled interfering ions from target spectra, we approached the method development problem as follows.

First, we addressed the need to achieve a minimum of three modulations per 1st dimension peak while avoiding peak wrap-around. Toward this end, some have employed slow temperature programs or lengthened columns to widen peaks. Instead, we used the same temperature program and column length as is typical for GC analysis, but with a much thicker first column stationary phase. Then, GC operating conditions and modulation periods were adjusted (Table 5-1) to optimize first column separation space and achieve three modulations per first dimension peak, even for the least-retained PAH, naphthalene. The most-retained compound, benzo(*g,h,i*)perylene, did not exhibit 2nd dimension wrap-around under these conditions. The thicker-film column lowered the probability that highly impacted samples would overload the stationary phases and as a result, high concentration soil extracts were analyzed as prepared. In contrast, GC/MS analysis of the same samples on columns with 0.25 or 0.32 μm film thicknesses required dilution or split injection.

Second, we adjusted the chromatographic conditions to ensure 2nd dimension peaks were as narrow as possible but with base-widths that yielded at least four consecutive scans/peak, which is the standard mass spectral peak identification criterion. Table 5-2 lists the relative abundances and the relative error calculated by Equation 5-3 for each scan across a modulated acenaphthene peak at one-half of the LOQ. While scans 21749 to 21752 easily meet the RE criterion, ≤ 7, the relative error in scans 21748, 21753, and 21754, due to mass ratio skewing,

Table 5-2. Ion abundances and calculated relative error for each scan across one modulated acenaphthene peak at one-half of the limit of quantitation (LOQ)

Ion (*m/z*)	Expected Abundance	Scan Number (Time, min)						
		21748 (26.978)	21749 (26.979)	21750 (26.980)	21751 (26.981)	21752 (26.982)	21753 (26.983)	21754 (26.984)
		Relative Abundance						
Base (153)	100	100	100	100	100	100	100	100
Qualifier 1 (154)	88	120	94	95	93	92	115	96
Qualifier 2 (152)	45	50	50	48	48	52	61	Ion Missing
Qualifier 3 (151)	17	18	18	17	17	19	21	Ion Missing
Relative Error		**19**	**4**	**3**	**2**	**3**	**18**	**Failed Criteria**

Note: Equation 5-3 used to calculate relative error at each scan except 21754, which is missing confirming ions 151 and 152.

missing ions, or interfering ions, exceed this criterion and are discarded; neither marked as acenaphthene nor included in peak area calculations. To further assess qMS performance under GC×GC conditions, based on the criteria described in the experimental section, we calculated the ion ratio relative standard deviation (RSD) for the 16 PAH at both the midpoint of the calibration curve and the LOQ. The RSD was, on average, 7%. We also examined peak area precision and found that at one-half the LOQ, the qMS produced four consecutive scans that met the identification criteria and peak area RSD of < 15%. In contrast, concentrations at the LOQ for each PAH produced at least six scans per peak, and for all concentrations in the linear portion of the calibration curve, the peak area RSD was 5%, which is excellent.

Tables 5-3 and 5-4 list the DBT and PAH calibration ranges, regression analyses, LOQ, LOD, and matrix spike results. Under the conditions employed, 2^{nd} dimension peaks of structural isomers such as phenanthrene and anthracene, benzo(*a*)anthracene and chrysene, and benzo(*b* and *k*)fluoranthene overlap. As a result, 1^{st} dimension peak separations become large groupings of modulated peaks whose spectra are indistinguishable. For those compounds, the reported data is the average of the signals for each isomer pair.

For GC×GC/MS, the calibration curve produced average response factors, relative standard deviations, and correlation coefficients (r^2) in agreement with those

obtained by GC/MS. Moreover, measurement precision was < 20%. This data was produced from four calibration curves over a 12-month period, highlighting the robustness of the data. It is understood that operation of the qMS in full-scan mode limits measurement sensitivity compared to SIM/1-ion and 2-ion methods, but it ensures accurate identification of target compounds. Nonetheless, the combination of a thicker 1st dimension stationary phase and higher signals due to peak modulation improved measurement sensitivity by 30-fold compared to GC/MS.

To evaluate whether LOQ concentrations were detectable in complex matrixes, an Athabasca tar sand, which is predominately aliphatics, resins, and asphaltenes, was spiked with known concentrations of PAH at one-half LOQ. This concentration approximates the LOD obtained from the statistical analysis of nine replicate samples. The respective matrix spiked concentrations were detectable using both GC×GC/MS and GC/MS, proving the deconvolution software can accurately identify and quantify target compounds independent of the matrix. This result is not possible using conventional data analysis software when additive ion currents from coeluting target and matrix compounds lead to distorted ion ratios.[74,153,165]

Table 5-3. GC×GC/MS calibration and regression analysis

Compound	[1]Range (ng/mL)	[2]$\overline{RF}$ (%RSD)	Slope ± SD	Intercept ± SD	r^2	[3]LOD (ng/g)	[4]Spike (ng/g)
Naphthalene	10-3000	1.04 (11.3)	1.03±0.08	0.00_3±0.00_2	0.99	5.7	6
Acenaphthylene	10-3000	1.19 (12.2)	1.25±0.15	0.02±0.02	0.99	10.7	12
Acenaphthene	10-3000	1.09 (16.2)	0.99±0.11	0.02±0.02	0.99	5.7	6
Fluorene	10-3000	0.65 (14.9)	0.71±0.05	0.02±0.02	1.00	7.5	6
Dibenzothiophene	25-6000	0.68 (14.8)	0.71±0.09	0.02±0.02	1.00	19.3	24
Phenanthrene/Anthracene	10-3000	0.93 (10.1)	0.79±0.16	0.03±0.04	1.00	7.3	6
Fluoranthene	10-3000	0.88 (15.4)	0.97±0.18	0.02±0.02	0.99	5.5	6
Pyrene	10-3000	0.95 (12.0)	1.08±0.19	0.02±0.03	1.00	6.3	6
Benzo(a)anthracene/Chrysene	10-3000	1.10 (13.5)	0.98±0.07	0.02±0.01	0.99	22.3	24
Benzo(b/k)fluoranthene	25-6000	0.73 (12.6)	1.13±0.10	0.05±0.04	0.99	13.5	12
Benzo(a)pyrene	10-3000	0.74 (8.0)	0.88±0.13	0.01±0.01	0.99	17.7	24
Indeno(1,2,3-c,d)pyrene	50-6000	0.76 (14.3)	0.70±0.02	0.01±0.01	1.00	34.2	24
Dibenz(a,h)anthracene	50-6000	0.53 (12.3)	0.40±0.20	0.00_1±0.00	1.00	28.0	24
Benzo(g,h,i)perylene	50-6000	0.76 (19.4)	0.61±0.06	0.01±0.01	1.00	35.8	24

[1] The low end of the concentration range is the LOQ.

[2] The response factor was calculated at eight or more concentrations over the concentration range and then averaged. The $\overline{RF}$ was calculated from four different calibration curves produced over a 12 month period.

[3] LOD was calculated from the student's *t*-test at ~ 1/2 the LOQ.

[4] Actual amount of PAH spiked into Athabasca tar sand extract.

Table 5-4. GC/MS calibration and regression analysis

Compound	[1]Range (ng/mL)	[2]RF (%RSD)	Slope	Intercept	r^2	[3]LOD (ng/g)	[4]Spike (ng/g)
Naphthalene	200-25000	0.89 (10)	0.80	0.00_9	1.00	56.7	50
Acenaphthylene	400-12500	1.18 (19)	1.52	0.06	0.99	69.8	50
Acenaphthene	200-25000	0.86 (16)	0.95	0.00_4	1.00	24.3	25
Fluorene	800-25000	0.92 (20)	1.19	0.09	0.99	171.0	100
Dibenzothiophene	200-25000	0.77 (4)	0.82	0.01	1.00	91	100
Phenanthrene	200-25000	0.88 (7)	0.92	0.02	0.99	26.5	25
Anthracene	200-25000	0.60 (20)	0.84	0.05	0.99	78.0	50
Fluoranthene	800-25000	0.80 (19)	1.02	0.08	0.99	92.5	100
Pyrene	400-25000	0.88 (16)	1.08	0.05	1.00	105.4	100
Benzo(a)anthracene	200-25000	0.75 (9)	0.83	0.01	1.00	88.7	100
Chrysene	200-25000	0.75 (7)	0.83	0.02	0.99	86.4	100
Benzo(b)fluoranthene	400-25000	0.70 (17)	0.81	0.01	0.99	185.0	200
Benzo(k)fluoranthene	400-25000	0.74 (12)	0.83	0.02	0.99	125.9	100
Benzo(a)pyrene	200-25000	0.75 (15)	0.91	0.04	0.99	102.0	100
Indeno(1,2,3-c,d)pyrene	800-25000	0.76 (13)	0.86	0.06	0.99	149.1	100
Dibenz(a,h)anthracene	800-25000	0.66 (18)	0.72	0.00_3	0.99	161.6	100
Benzo(g,h,i)perylene	400-25000	0.79 (18)	0.97	0.04	0.99	117.1	100

[1] The low end of the concentration range is the LOQ.
[2] The response factor was calculated at eight or more concentrations over the calibration range and then averaged.
[3] LOD was calculated from the student's *t*-test at ~ 1/2 the LOQ.
[4] Actual amount of PAH spiked into Athabasca tar sand extract.

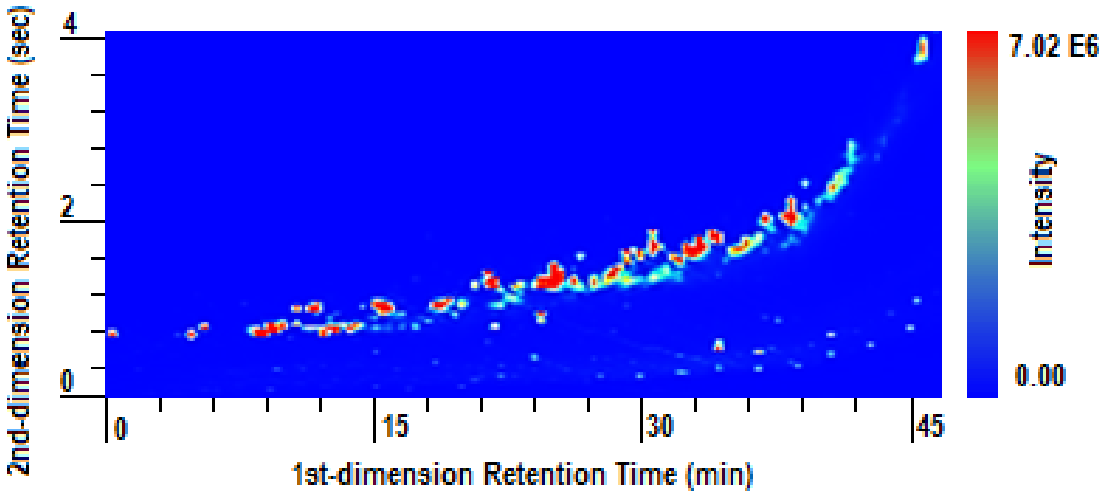

Figure 5-1. GC×GC/MS chromatogram of a weathered coal tar sediment

Figure 5-1 shows the GC×GC/MS chromatogram of coal tar-contaminated sediment from the Hudson River. This sample, representative of coal tar exposed to the environment for decades, is highly weathered and has lost some alkylated PAH and PASH due to evaporation, dissolution and microbial degradation. The TIC chromatogram is shown in Figure 5-2 (top). The bottom figure is the deconvolved RIC chromatogram of the parent and alkyl PAH and PASH. The deconvolution software automatically integrates the peak areas and for those homologues where multiple fragmentation patterns are needed to capture all isomers, it integrates and sums peaks by pattern.

Figure 5-3 is an expanded view of the C_4-phenanthrene GC×GC/MS and GC/MS ion traces for the same sample. The dialog box shows the ions, their relative abundances for one fragmentation pattern, and corresponding ion trace color. The dialog box also shows the acceptance criteria that must be met as well as the number of potential peaks. The top chromatogram displays 10 modulated

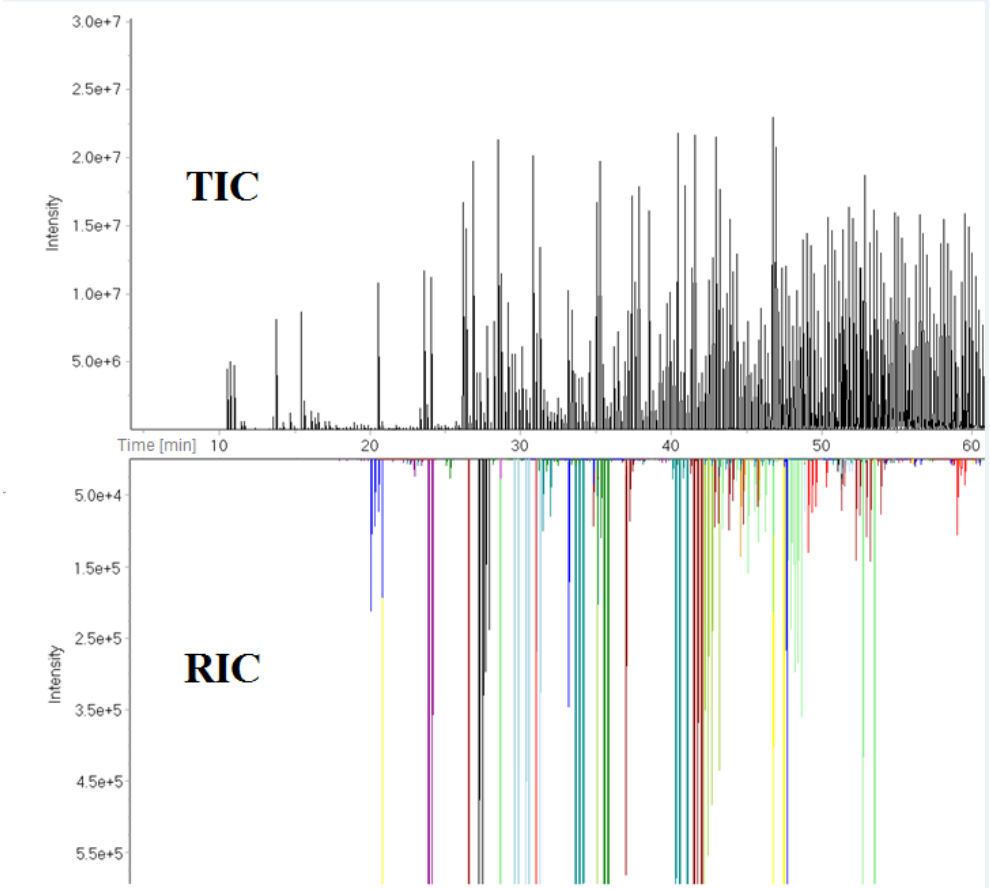

Figure 5-2. Total and reconstructed ion current (TIC/RIC) chromatograms of the coal tar soil sample shown in Figure 5-1

GC×GC/MS peaks, whereas the bottom chromatogram shows two GC/MS peaks for this pattern. The deconvolved ion signal at each peak scan is shown in the figure. When the ion signals meet the compound identity criterion for a given scan, the normalized ion currents are depicted in the form of a histogram for ease of visualization. A magnified view is shown for both GC×GC/MS and GC/MS data. After the ion signals are normalized, only those signals that appear at the same height (± 20%) at a given scan and meet the scan-to-scan acceptance criteria are shown in the histogram. Scans that fail the acceptance criteria are neither integrated nor shown in the histogram, see example above.

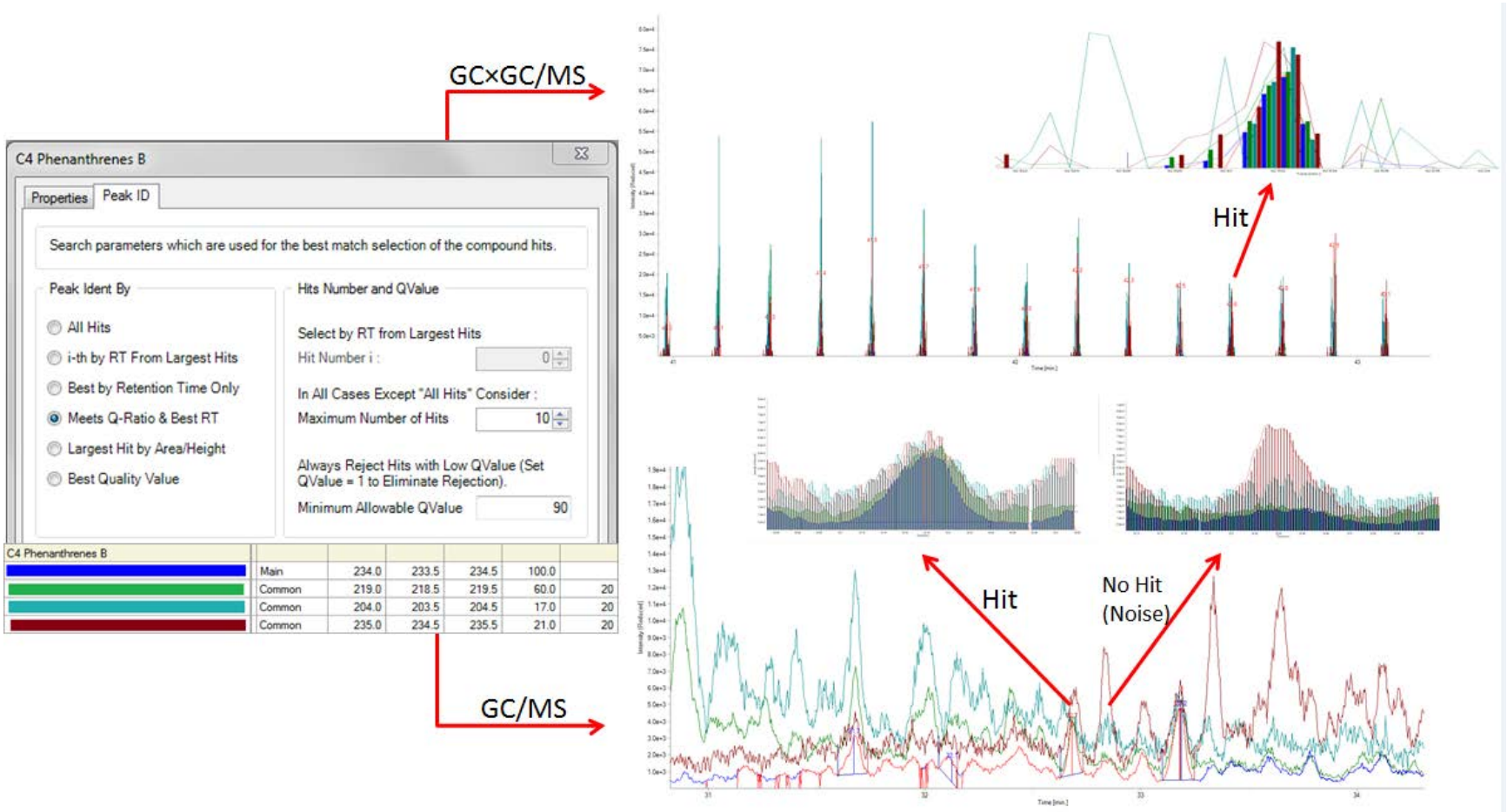

Figure 5-3. Illustrative example of spectral deconvolution of GC/MS and GC×GC/MS data of the coal tar soil shown in Figures 5-1 and 5-2

All GC×GC/MS peaks shown in the figure meet the compound acceptance criteria. In contrast, only the two outside GC/MS peaks meet the acceptance criteria for the fragmentation pattern shown in the dialog box. The two middle peaks do not – only two of the three ions comaximize – making clear these peaks are not C_4-phenanthrenes.

PAH and PASH concentrations in the sediment sample shown in Figure 5-1 were measured by both GC×GC/MS and GC/MS to assess data quality differences. The U.S. Environmental Protection Agency benchmark for accuracy is contingent on the site-specific action levels (AL) required to clean hazardous waste sites.[166,167] If we assume the site is adjacent to residential properties, the concentrations in the sample must meet the RPD shown in Table 5-5.[79] Parent PAH concentrations are well within EPA criteria for accuracy, and although homologue-specific action levels are not reported, results are in excellent agreement and meet the same criteria as parent PAH. Some homologues exceed the low concentration benchmark, presumably due to sensitivity differences, while others are only detected by GC×GC/MS.

Since GC×GC/MS offers improved separation space and the corresponding ability to separate target compounds from matrix interferences, we examined whether homologue identification employing too few ions still produced overestimated concentrations as reported in our previous studies. The same data file was

Table 5-5. PAH and PASH concentrations in a coal tar contaminated soil analyzed by GC×GC/MS and GC/MS using the MFPPH data analysis method

Compound/Homologue	GC×GC/MS (µg/g)	GC/MS (µg/g)	% RPD	2.5×AL (µg/g) and [1](RPD)
Naphthalene	0.7	0.7	0	5 (100)
C_1 Naphthalenes	8.0	10	-20	
C_2 Naphthalenes	15	19	-21	
C_3 Naphthalenes	11	11	0	
C_4 Naphthalenes	4.4	2.1	110	
Fluorene	25	23	9	35 (100)
C_1 Fluorenes	24	21	14	
C_2 Fluorenes	13	9.7	34	
C_3 Fluorenes	2.9	0.8	263	
C_4 Fluorenes	1.6	ND	N/A	
Phenanthrene/Anthracene	93	84	11	355 (100)
C_1 Phenanthrenes	78	87	-10	
C_2 Phenanthrenes	20	24	-17	
C_3 Phenanthrenes	5.5	6.8	-19	
C_4 Phenanthrenes	1.3	0.5	160	
Benzo(a)anthracene/Chrysene	29	34	-15	0.25 (60)
C_1 Chrysenes	27	37	-27	
C_2 Chrysenes	3.0	3.3	-9	
C_3 Chrysenes	0.8	ND	N/A	
C_4 Chrysenes	ND	ND	N/A	
Pyrene/Fluoranthene	73	72	1	262.5 (100)
C_1 Pyrenes	61	76	-20	
C_2 Pyrenes	17	22	-23	
C_3 Pyrenes	4.2	1.9	121	
C_4 Pyrenes	1.1	ND	N/A	
C_1 2-Ring PASH	2.0	2.3	-13	
C_2 2-Ring PASH	3.6	4.3	-16	
C_3 2-Ring PASH	4.3	4.7	-9	
C_4 2-Ring PASH	1.4	1.3	8	
Dibenzothiophene	22	20	10	
C_1 3-Ring PASH	30	29	3	
C_2 3-Ring PASH	22	19	16	
C_3 3-Ring PASH	9.7	7.3	33	
C_4 3-Ring PASH	1.9	0.6	217	
C_1 4-Ring Fused PASH	17	14	21	
C_2 4-Ring Fused PASH	7.3	6.6	11	
C_3 4-Ring Fused PASH	0.7	ND	N/A	
C_4 4-Ring Fused PASH	0.6	0.8	-25	
C_1 4-Ring Condensed PASH	7.3	6.1	20	
C_2 4-Ring Condensed PASH	3.5	3.2	9	
C_3 4-Ring Condensed PASH	6.7	6.0	12	

[1]The relative percent difference (RPD) must be ≤ 60% or ≤ 100% when sample concentrations are greater than or less than 2.5-times the site-specific AL, respectively

analyzed by extracting the molecular ion signal (SIE) and MFPPH ions of each homologue. Table 5-6 lists the concentration differences. SIE significantly overestimated 10 of 20 alkylated PAH and 10 of 15 PASH homologues compared to MFPPH. The high positive bias ranged from thirty to thousands of percent and is consistent with our previous findings.[47] These results further substantiate our contention that identification, and thus quantitation, is subject to matrix bias when too few ions are used to differentiate homologue signals from matrix signals.

Our findings demonstrate quadrupole mass spectrometers can produce sufficient invariant scans to obtain high quality GC×GC data as measured by precision, accuracy, and sensitivity, with spectral deconvolution of MFPPH ions the key to obtaining selective compound detection in complex samples. This is especially important since many of the alkylated PAH and PASH elute within the same retention windows.[47] In addition to the 3-D image normally obtained by GC×GC, the deconvolved RIC traces increase analyst confidence that 3D peaks are correctly assigned. Based on the findings above, we believe spectral deconvolution of GC×GC/qMS data can help to solve the vexing challenges inherent in complex mixture analysis.

Table 5-6. PAH and PASH concentrations resulting from the same GC×GC/MS data fileanalyzed by MFPPH and SIE

Compound/Homologue	MFPPH (µg/g)	SIE (µg/g)	Overestimation (%)
C_1 Naphthalenes	8.0	8.0	0
C_2 Naphthalenes	15	15	0
C_3 Naphthalenes	11	11	0
C_4 Naphthalenes	4.4	4.4	0
C_1 Fluorenes	24	40	67
C_2 Fluorenes	13	24	85
C_3 Fluorenes	2.9	14	383
C_4 Fluorenes	1.6	9.6	500
C_1 Phenanthrenes	78	82	5
C_2 Phenanthrenes	20	22	10
C_3 Phenanthrenes	5.5	7.4	35
C_4 Phenanthrenes	1.3	4.6	254
C_1 Chrysenes	27	27	0
C_2 Chrysenes	3.0	3.5	17
C_3 Chrysenes	0.8	0.9	13
C_4 Chrysenes	ND	ND	N/A
C_1 Pyrenes	61	87	43
C_2 Pyrenes	17	24	41
C_3 Pyrenes	4.2	16	281
C_4 Pyrenes	1.1	2.8	155
C_1 2-Ring PASH	2.0	2.0	0
C_2 2-Ring PASH	3.6	4.7	31
C_3 2-Ring PASH	4.3	5.8	35
C_4 2-Ring PASH	1.4	3.4	143
C_1 3-Ring PASH	30	30	0
C_2 3-Ring PASH	22	23	5
C_3 3-Ring PASH	9.7	26	168
C_4 3-Ring PASH	1.9	3.1	63
C_1 4-Ring Fused PASH	17	20	18
C_2 4-Ring Fused PASH	7.3	10	37
C_3 4-Ring Fused PASH	0.7	20	2757
C_4 4-Ring Fused PASH	0.6	1.0	67
C_1 4-Ring Condensed	7.3	12	64
C_2 4-Ring Condensed	3.5	7.9	126
C_3 4-Ring Condensed	6.7	6.7	0

$$\%Overestimation = \frac{SIE - MFPPH}{MFPPH}$$

Chapter 6 GC×GC, Physical Property Modeling, and the Automated Production of Component Maps to Assess the Weathering of Pollutants

6.1 Introduction

Understanding how local environments impact weathering, including physical (evaporation, adsorption, dissolution, and emulsification), biological (microbial degradation), and chemical (photo- and oxidative degradation) processes, is critical to determining whether the local ecosystem is capable of remediation, *i.e.*, the natural attenuation of pollution effects. Because site-specific weathering processes can dramatically change the chemical composition of fossil fuel mixtures, even at the isomer level,[168] it is important to assess these changes as a function of each component's physical and chemical properties.[169] Once known, one can use this information to determine if natural attenuation is sufficient to reduce pollutant impact on the environment or if active remediation is required. To make this determination, the compositional effects of dissolution, organic phase partitioning, and evaporation must be known; each of which one can examine by studying the aqueous solubility (S_W), octanol-water partition coefficient (K_{OW}), and vapor pressure (V_P) of sample components, respectively.[170,171]

The measurement of aqueous solubility and octanol-water partition coefficient of hydrophobic fossil fuel components such as benzene, polycyclic aromatic hydrocarbons and sulfur heterocycles and their substituted homologues is time-

consuming, challenging, and susceptible to error.[172] For these reasons, gas chromatographic retention indices are often used to estimate these properties.[173,174] GC provides the means to not only estimate these properties, but also to assess the extent to which natural attenuation has occurred, all without the need to identify each sample component or directly measure their properties. Both 1-dimensional GC and 2-dimensional GC×GC can be used to estimate S_W, K_{OW}, and V_P via linear or logarithmic free energy relationships. GC×GC is often used in weathering studies because it provides a visual depiction of the differences between fresh and weathered sample chromatograms, and orthogonal column pairings provide the means to generate LFER to estimate these properties simultaneously.[171] Arey and coworkers derived an empirical expression for the isothermal partition coefficient (*K*), then used this information to estimate V_P, S_W, and the air-water and octanol-water partition coefficients from the 1st and 2nd dimension retention indices of diesel fuel.[175,176] Based on the assumption that the partitioning of the solute is primarily controlled by size and polarizability, a two-component LFER, with the 1st dimension retention index (RI_{1D}) conveying information about size and the 2nd dimension polarizability, environmental researchers have used GC×GC to produce contour maps[177,178] and air and water mass transfer models,[179] and estimate phase-transfer properties, phospholipid membrane−water partition coefficients and corresponding narcosis toxicity.[180]

This line of research is not without its challenges – for example, the calculation of meaningful 2nd dimension retention indices, since either the 2nd dimension hold-

up time ($t_{M,2D}$) or the retention of bracketing compounds at different temperatures across the separation space is required. To this end, researchers have examined column bleed[143] and employed continuous injections of an unretained compound[181] to assess $t_{M,2D}$, and created "hypothetical" bracketing compounds[175,176] and isovolatility curves.[182] Isovolatility curves, the result of continuous solute elution over a prolonged period, can provide the means to obtain retention information at different elution temperatures by creating curved elution lines that cut across the 2nd dimension separation space. Another challenge is that only recently have quadrupole mass spectrometers provided the scan speeds sufficient for invariant spectra across narrow 2nd dimension peaks and, in turn, accurate quantitative analysis of components of complex mixtures, such as PAH, PASH and their alkylated homologs in coal tar and crude oil.[75]

Figure 6-1 shows a weathering map that can be used to inform remedial decisions and to delineate site-specific weathering processes.[177] The axes correspond to volatility and solubility and provide important sample information. For example, sites that contain a large number of volatile and highly-soluble compounds will continue to pose risk to the environment, as opposed to highly-weathered sites in which only non-volatile and insoluble components remain. If these compounds are also biologically inaccessible, the pollution no longer poses risk to the environment. This is especially important since local weathering conditions, even at the same site, may attenuate pollution differently.

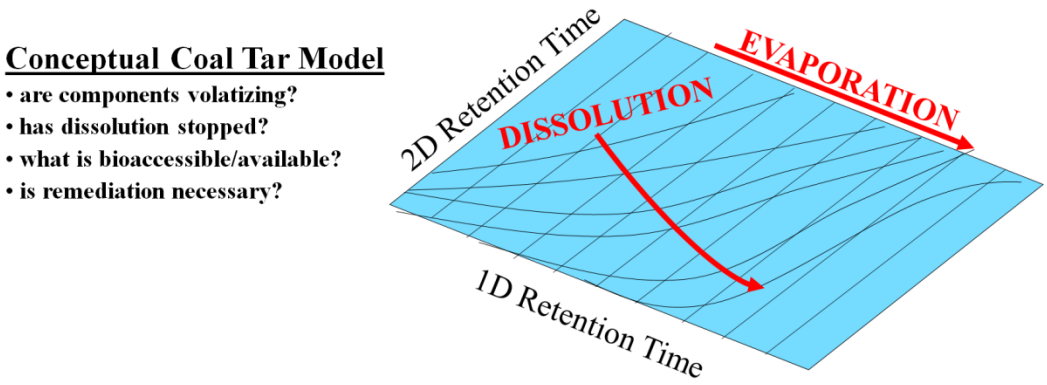

Figure 6-1. Schematic representation of a component map; arrows correspond to weathering processes.

In this study, we report for the first time the use of isovolatility curves to generate retention indices in both GC×GC dimensions at every point in 2D space. In contrast with other studies that employed alkane standards to estimate the properties of aromatic targets, RI are calculated and physical properties are estimated Sample component RI are calculated using 2-, 3-, 4-, and 5-ring PAH as bracketing compounds. Since PAH are mutagenic, carcinogenic, and persistent organic pollutants, they serve as important model compounds for this study. We and others have shown that when target analytes, in this case alkylated PAH and PASH, are bracketed by structurally-similar compounds, accurate measurement of their separation is obtained under linear temperature-programmed conditions.[183,184,185,186] This, in turn, leads to more robust linear free energy relationships and more accurate physical property estimates. This property estimation process has been encoded in a new software program, allowing for automated determination of physical properties from one analysis, with minimal model training and parameter input. Since coal tar is predominantly aromatic,[187] it

serves as an ideal model mixture to test this hypothesis, especially considering our experience with analysis of C_1- to C_4-alkylated PAH and PASH homologues.

6.2 Experimental

Standards and Reagents: Airgas (Salem, NH, USA) supplied the ultra-high purity helium and nitrogen used in this study. Chromatography-grade toluene and dichloromethane were purchased from Sigma-Aldrich (St. Louis, MO, USA). The 16 EPA priority pollutant PAH, dibenzothiophene, and internal standards 1,4-dichlorobenzene-d_4, naphthalene-d_8, phenanthrene-d_{10}, chrysene-d_{12}, and perylene-d_{12} were obtained from Restek (Bellefonte, PA, USA). Supelco (Bellefonte, PA, USA) supplied the base/neutral surrogate spike mix (2-fluorobiphenyl, nitrobenzene-d_5, p-terphenyl-d_{14}) as well as a number of neat standards: anthracene, benzo(*b*)thiophene, fluorene, fluoranthene, hexylbenzene, pyrene, 1-phenyloctane, 1-methylnaphthalene, 2-methylnaphthalene, and 1,7-dimethylnaphthalene. Also purchased were neat standards of *n*-decylbenzene and 2,6-dimethylnaphthalene from Ultra Scientific (North Kingstown, RI, USA) and Crescent Chemical (Islandia, NY, USA), respectively.

Samples and Sample Preparation Procedure: Pure coal tar and impacted soils were obtained from a utility in Illinois and extracted using the modified EPA method 3550C[188,189] described in previous chapters: 15 g of sample was spiked with surrogate mix and sonicated for 10 minutes in 8 mL of 50% (v/v) toluene/dichloromethane (Branson Ultrasonics, Danbury, CT), and the procedure was repeated eight-times to obtain maximum extraction efficiency. Activated

copper and anhydrous sodium sulfate were used to eliminate elemental sulfur and water from the extracts, which were concentrated under a stream of nitrogen prior to the addition of 10 μg/mL of internal standards.

Instrumentation: GC×GC/MS analyses were performed using an Agilent Technologies (Santa Clara, CA, USA) 6890/5975C GC/MS with Gerstel (Mülheim an der Ruhr, Germany) MPS2 autosampler and CIS6 injector. Since most sample components in coal tar are aromatic members of homologous families, instrumental conditions were chosen to maximize utilization of 2D separation space and to increase data granularity. Following the example of Arey and coworkers,[175,176] two different GC×GC/MS methods were employed to evaluate if the accuracy of physical property estimates was method-dependent. These included differences in column manufacturer and size, split ratio, temperature program, flow rate, and modulation time; instrumental parameters for both GC×GC/MS methods are found in Table 6-1. Columns were connected using Restek press-fit connectors or VICI Valco (Houston, TX, USA) low mass external union connectors. The GC×GC cryogenic and thermal modulation hardware was provided by Zoex Corporation (Houston, TX, USA). GC Image (Lincoln, NE, USA) supplied the software to create the three-dimensional chromatograms. Unknown sample components were identified using Ion Analytics (Andover, MA, USA) spectral deconvolution software. 2D retention indices were confirmed by analyzing standards under isothermal conditions; *i.e.*, we compared our GC×GC RI_{2D} to 1D GC/MS RI results for the same compounds

Table 6-1. GC×GC method parameters for property estimation and component map generation

	Method A	**Method B**
GC Parameters		
Injection Mode	20:1 split	splitless
Injection Volume (μL)	1	1
Injection Temperature or PTV Program	-20°C, 12°C/min to 320°C, hold for 5 min	-20°C, 12°C/min to 320°C, hold for 5 min
Flow	1.2 mL/min, constant flow	1.0 mL/min, constant flow
Carrier Gas	Helium	
Transfer Line Temperature	300°C	
Column 1	30 m x 0.25 mm x 0.25 μm Rxi-5SilMS (Restek)	30 m x 0.25 mm x 1.0 μm DB-5 UI (Agilent)
Column 2	1.0 m x 0.25 mm x 0.25 μm Rxi-17SilMS (Restek)	1.5 m x 0.18 mm x 0.36 μm Rxi-17SilMS (Restek)
Modulation Time (s)	12	8
Hot Jet Temperature (°C)	310	
Cryogen Flow (L/min)	15	
Temperature Program	60°C for 1 min, 4.5°C/min to 320°C, hold for 5 min, -20°C/min to 300°C, hold for 5 min	60°C for 1 min, 6.5°C/min to 320°C, hold for 5 min
Run Time (min)	65.77	76.77
MS Parameters		
Solvent Delay (min)	10	17
Mass Range (*m/z)*	50-300	50-350
Scan Rate (scans/s)	23.7	19.8
Quadrupole Temperature (°C)	150	150
Ion Source Temp (°C)	230	230

on the same column. These 1-dimensional GC/MS analyses were performed using a Shimadzu (Columbia, MD, USA) GC2010/QP2010+ instrument on a 30 m × 0.25 mm × 0.25 μm RXI-17MS column provided by Restek. These runs were performed at temperatures between 100 and 300°C at 25°C increments. Methane was used to measure t_M.

Software Programming and Functionality: The automated physical property program was constructed using the R and Octave software environments within MATLAB (Mathworks, Natick, MA, USA). The software's functionality, as described below, is illustrated in Figures 6-2A–6-2C. The program was trained through input of the S_W, V_P, and K_{OW} values and retention times obtained from the bracketing compound isovolatility curves, see Figure 6-2A. As fitting the correct curve to the 2D chromatogram is essential for obtaining accurate retention indices, the MATLAB curve fitting toolbox was utilized to test a number of possible models. During the training step of each regression, the curve toolbox's "fit" function was used to fit a curve based on a specific model (linear, quadratic, power, etc.), with the *x* and *y* values obtained from the 1D and 2D retention times of the isovolatility curve bracketing compounds. The resulting curve was stored and the goodness of fit recorded. This process is repeated for all curve types, and the best fit is selected for further use.

In order to use these isovolatility curves for retention index calculation and physical property estimation, a second spreadsheet was used to input the 1st and 2nd dimension retention times and literature physical property values of training compounds that spanned the retention space and physical property estimation limits of the sample, see Figure 6-2B. This sheet also contained the retention times of the user-defined target compounds.

Using this data, the program compares the RT from the training compounds to those of the isovolatility curves to determine which bracketing standards to use for each training compound. Next, it calculates the 1D and 2D retention indices for each training compound and regresses the known physical properties against the RI values. The literature vapor pressures, octanol-water partition coefficients, and aqueous solubilities of these training compounds are used to construct free energy relationships that output V_P, K_{OW}, and S_W estimates for each point in the 2D chromatogram based solely upon retention indices, see Figure 6-2C. These estimates are used to "map" the entire chromatogram. Partition lines for both vapor pressure and aqueous solubility are evaluated in half-minute intervals across the 2D chromatogram to delineate sections of similar properties. The two resulting surfaces are plotted as a contour map on top of the 2D chromatogram, with the contour lines corresponding to physical property log integer values. The model then outputs V_P, K_{OW}, and S_W estimates for each target compound. Any compound in the sample can be evaluated using this approach. If the physical property literature values of compounds in the sample are known, the model-generated estimates are compared to previously-measured values. In this study, however, there was limited opportunity for these comparisons, given the paucity

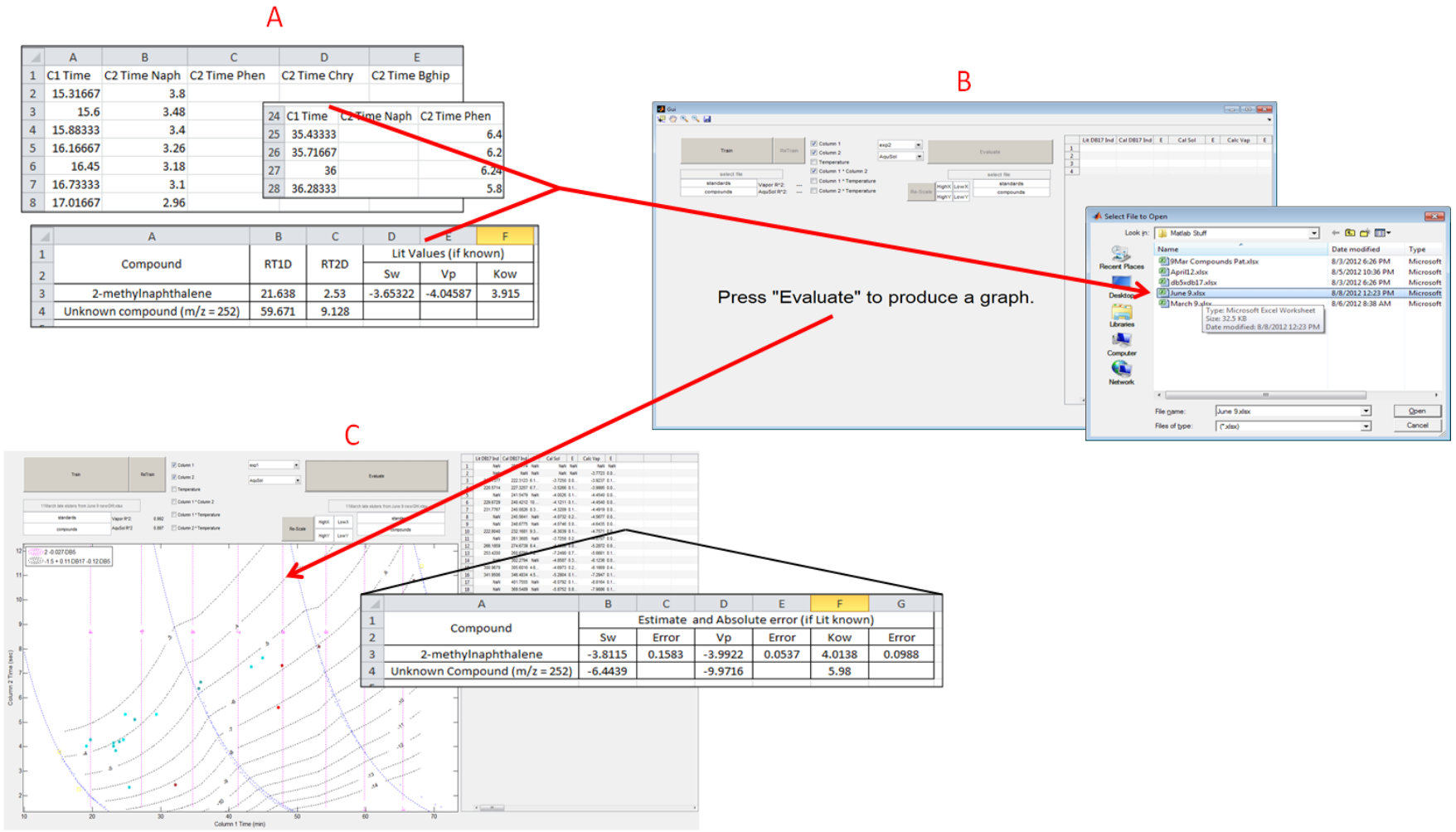

	A	B	C	D	E
1	C1 Time	C2 Time Naph	C2 Time Phen	C2 Time Chry	C2 Time Bghip
2	15.31667	3.8			
3	15.6	3.48			
4	15.88333	3.4			
5	16.16667	3.26			
6	16.45	3.18			
7	16.73333	3.1			
8	17.01667	2.96			

	C1 Time	C2 Time Naph	C2 Time Phen
25	35.43333		6.4
26	35.71667		6.2
27	36		6.24
28	36.28333		5.8

	A	B	C	D	E	F
1	Compound	RT1D	RT2D	Lit Values (if known)		
2				Sw	Vp	Kow
3	2-methylnaphthalene	21.638	2.53	-3.65322	-4.04587	3.915
4	Unknown compound (m/z = 252)	59.671	9.128			

	A	B	C	D	E	F	G
1	Compound	Estimate and Absolute error (if Lit known)					
2		Sw	Error	Vp	Error	Kow	Error
3	2-methylnaphthalene	-3.8115	0.1583	-3.9922	0.0537	4.0138	0.0988
4	Unknown Compound (m/z = 252)	-6.4439		-9.9716		5.98	

Figure 6-2. Input and output software process used to produce component maps and property estimates. (A) Retention times and literature physical property values used to train the model, (B) graphic user interface used to input file from (A) and select modeling parameters, and (C) output of property estimates, visualization map, and error analysis.

of K_{OW} and S_W literature for coal tar components beyond the 16 PAH listed by EPA as target compounds.[132,190,191,192,193] In cases where literature values are available, the program generates an error analysis (model versus literature value estimate) for each LFER. This error analysis is displayed in the output spreadsheet and each compound is plotted on the component map with a user-defined color that corresponds to the magnitude of the error. Importantly, only a single GC×GC analysis is required to produce the contour map and the corresponding property estimates.

6.3 Theory

As outlined by Curvers and expressed in Equation 6-1, retention, *r*, as a function of temperature, *T*, is controlled by two factors: 1) thermodynamics, as described by the bracketed terms; and 2) fluid dynamics, as described by the $t_0(T)$ term:

$$r(T) = \int_{T_0}^{T_R} \frac{dT}{t_0(T)\left[1+\frac{\exp(\Delta S/R)}{\theta}\exp\left(\frac{\Delta H}{RT}\right)\right]} \quad (6\text{-}1)$$

where:

$$t_0(T) = \left(\frac{(P^3-1)}{P^4-2P^2+1}\right)\cdot\left(\frac{128\cdot L^2}{3\cdot p_o\cdot d_c^2}\right)\cdot\left(\eta(T)\right) \quad (6\text{-}2)$$

and θ is the column phase ratio, P is the column pressure ratio (in/out), p_o is the column outlet pressure, L is the column length, d_c is the column inner diameter, and $\eta(T)$ is the dynamic carrier gas velocity.[194] If a mass spectrometer is used, the first term of Equation 6-2 simplifies to an inverse linear function by assuming $P = p_{in}$ such that $P_i^4 - 2P_i^2 + 1 \approx P_i^4$ and $P^3 - 1 \approx P^3$. The middle term in Equation 6-2 is

a combination of constants, and, as noted by Ettre, the $\eta(T)$ term is a linear function within the typical GC temperature range.[195] Therefore, by approximation, Equation 6-2 is a ratio of linear functions, and Equation 6-1, in turn, the integral of an inverse linear function. When P is constant throughout a run, which is common in isothermal separations, the integral of the fluid dynamic term from T_0 to T_R (e.g., the fluid hold up time change versus temperature) is a constant; this mathematical prediction is borne out in practice as t_M is unchanged with constant p_{in} and temperature. Retention, in this case, is entirely dependent on the thermodynamics of the analyte itself. In contrast, when column temperature and/or inlet pressure varies throughout the separation, the integrated fluid dynamic term is a non-linear function. As such, and as is the case in temperature-programmed, constant flow GC, retention is intimately tied to both thermodynamics and fluid dynamics, the latter of which is experimentally condition-dependent. These effects are readily observed in temperature-programmed GC analyses, as the elution order of critical pairs can be reversed with changes to system flow and temperature programming parameters.[196]

Despite this fundamental relationship between fluid dynamic parameters and retention behavior, in practice, the use of retention indices allows for the repeatable measurement of retention behavior. This is observed in inter- and intra-laboratory retention index comparisons, wherein indices typically vary by only a few percent. For example, White's retention index study of 400 compounds led to linear temperature program RI standard deviations of no more

than 0.5 Kováts units,[197] and a comparison of three studies[183,184,185] that reported the RI of PAH (including some examined in this study) under different instrumental conditions led to an average RPD of 0.5%. This small error is partially attributable to unavoidable inconsistencies between chromatographic systems (cold and hot spots, variability in dead volumes and stationary phase crosslinking, etc.) and slight differences in absolute mass on column. Although changing fluid dynamic factors can reverse elution orders, the corresponding retention indices do not change enough to prevent a good regression of elution behavior versus physical property estimation, especially with respect to the considerable error associated with traditional measurements of the physical property.[172] In order for fluid dynamic effects to significantly affect the retention behavior of compounds such that changes in the retention index preclude regression of physical properties, dramatic (and unrealistic) instrumental conditions would be necessary.

RI have been show to correlate with the S_W, V_P, and K_{OW} of a given compound, and LFER have been used to estimate these properties for families of compounds based on their RI.[175,198,199,200,201,202,203,204] These free-energy relationships typically follow the linear or logarithmic forms shown below:

$$X = a_1 Y_1 + a_2 Y_2 + \cdots + a_n Y_n + c \tag{6-3}$$

$$X = a_1 \log Y_1 + a_2 \log Y_2 + \cdots + a_n \log Y_n + c \tag{6-4}$$

where X is the physical property to be determined for a compound, Y_n is either the retention index or a previously- known or determined physical property of that compound, and a_n are fitted constants.[205]

In addition to the fluid dynamic factors discussed above, retention is dependent on multiple thermodynamic factors, including the partial molar enthalpy of solution, partial molar entropy of solution, and partial molar isobaric heat capacity.[183] Predictably, the relationship between temperature and the thermodynamic variable of interest changes dramatically based on the chemistry of the molecule.[206,207] Assumptions are often made about the temperature dependence, or equivalency, of each of these parameters for both the compound of interest and reference compound.[208,209,210,211,212] Care must be taken to minimize the error brought about by these assumptions through the selection of appropriate reference compounds that undergo the same intermolecular reactions as the compounds of interest in the stationary phase (*i.e.*, mechanistically they must be the same).[213] When comparing a family of compounds, such as alkylated PAH, the underlying thermodynamic parameters change with size and structure such that the relative separation remains unchanged despite differences in chromatographic conditions (temperature, heating rate, phase ratio, etc.). However, when reference and analyte compounds behave differently, measurable effects in retention indices and, in turn, physical property modeling are found. To date, however, researchers who have estimated physical properties often use alkanes as reference compounds

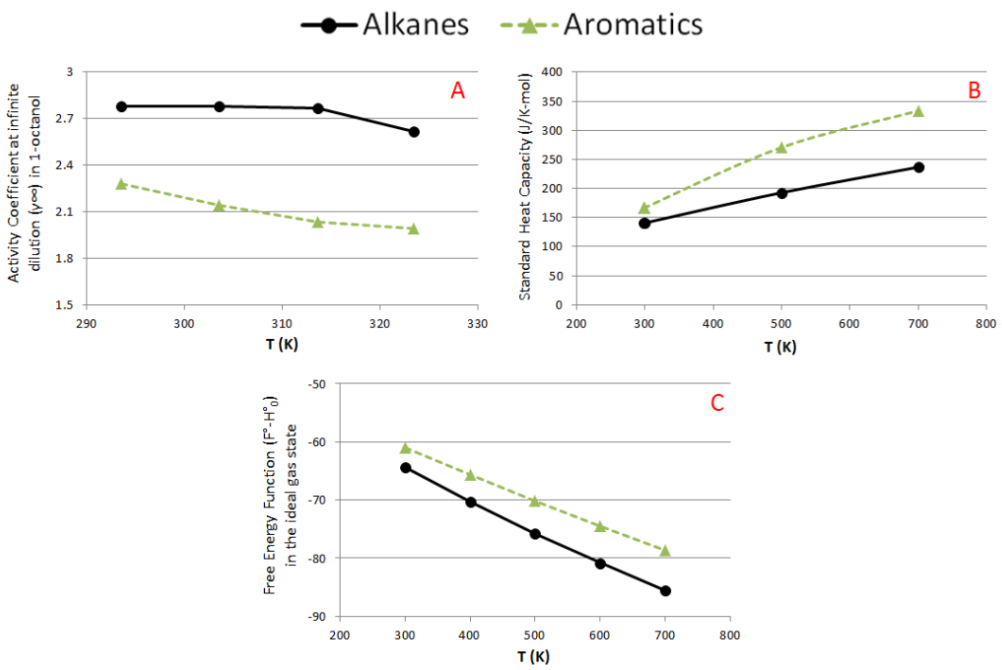

Figure 6-3. Comparison of thermodynamic parameters of two homologous compound families, alkanes and aromatics.

for analyses of polycyclic aromatic hydrocarbons, even though alkanes exhibit different intermolecular behavior than PAH on the same stationary phase.[214] Figure 6-3 compares relevant thermodynamic parameters as a function of temperature for selected compounds in two homologous series – PAH and alkanes.[215,216,217,218] As seen in the figure, differences are found between the two homologous series, both in the parameters themselves as well as the slopes of the functions. The activity coefficient at infinite dilution (Figure 6-3A) can be related to retention behavior by recasting the capacity factor, *k*, as follows:

$$k = \frac{t_r - t_m}{t_m} = \frac{TRn_s}{\gamma_{is}^{\infty} p_i^0 V_M} \qquad (6\text{-}5)$$

Where R is the gas constant, T the temperature, n_s the total number of moles in the stationary phase, $\gamma^{\infty}{}_{i,s}$ the activity coefficient at infinite dilution, p_i^0 the vapor

pressure of the pure solute, and V_M the volume of the stationary phase. It is clear that, as Beens *et al.* state: "there are only two compound-dependent factors that affect retention. These are the vapour pressure of the pure solute, p_i^0, which is an exponential function of the temperature and the activity coefficient of the solute in the stationary phase."[219] Therefore, when the solute and reference compound activity coefficients do not scale with temperature in a uniform manner (see Figure 6-3A), any accuracy in LFER regressions is empirical; useful under only a single set of instrumental conditions. In contrast, LFER-based vapor pressure estimation amongst a homologous series, *i.e.* where $\gamma^{\infty}_{i,s}$ and $\gamma^{\infty}_{i,x}$ scale uniformly with temperature, results in differences of only ~4%, which is in line with the measurement error common in chromatographic measurements. In other words, producing LFER by regressing homologous compounds against one another leads to measurement error on the same order of magnitude as the chromatographic measurements these estimates are based on. As the activity coefficient at infinite dilution is governed by partition thermodynamics, it is intimately related to the aforementioned thermodynamic parameters heat capacity (Figure 6-3B) and free energy (Figure 6-3C). As seen in the figures, these functions are linear across the GC temperature range for the homologous series, but the slopes of the functions are not equivalent, which precludes the use of alkane retention to estimate the physical properties of aromatics with good accuracy, and vice versa. The thermodynamic factors are explainable on a molecular basis. For example, PAH have a much higher affinity for H-bonding and Van der Waals (VdW) interactions than alkanes.[213]

Chemical and structural differences between analytes and standards can dramatically effect retention indices, and in turn, the LFER derived thereof. In this way, the assumptions outlined above provide an obvious limitation – that is, it is only applicable for homologous series of compounds in the same family. On the other hand, since the thermodynamic similarities of the PAH brackets lead to improvements in RI reproducibility for aromatic compounds in general when compared to alkane-based methods, the same brackets should lead to reliable estimates of all aromatic components found in complex samples such as coal tar.

6.4 Results and Discussion

GC×GC offers a distinct advantage in the chromatographic estimation of the physical properties of analytes in complex samples, since orthogonal column pairings provide simultaneous estimation of multiple properties for hundreds of components in a single run, within time scales similar to those of one-dimensional analyses. This is particularly helpful in environmental forensics, as many of the processes that comprise weathering are related to the physical properties of the constituents of the mixture. For example, the specific physical properties examined in this study – aqueous solubility, vapor pressure, and octanol-water partition coefficient – can be utilized to study water washing, evaporation, and organic phase partitioning, respectively. Our goal is to correlate each of these properties with GC retention, and the key to producing a robust correlation is the accurate and precise generation of retention indices.

1st Dimension Retention Index: As illustrated in Figure 6-4, the 1st dimension linear temperature-programmed retention index ($LTPRI_{1D}$) is calculated using Equation 6-6:[183]

$$LTPRI_{1D} = LTPRI_B + \left[\left(\frac{RT_x - RT_B}{RT_{(B+1)} - RT_B}\right) \times 100\right] \quad (6\text{-}6)$$

where *RT* refers to the 1st dimension retention times of target compound *X* and bracketing compounds *B* and *(B+1)*, e.g., in the case of Figure 6-4, naphthalene and phenanthrene, respectively, and $LTPRI_B$ is the retention index of the earlier-eluting bracket compound. The bracketing compound retention indices are: naphthalene (200), phenanthrene (300), chrysene (400), and benzo[*g,h,i*]perylene (500). As discussed in section 6.3, although the 1st dimension separation is temperature-programmed and therefore dependent on fluid and thermodynamics, the corresponding indices are still capable of providing precise retention indices and good correlations to thermodynamic data under controlled conditions.[220] Despite two vastly different experimental conditions (differing column lengths, stationary phase film thicknesses, carrier gas flow rates, and temperature programs), we obtained 1st dimension retention index precision of ±0.4%, which is excellent. This result is consistent with past studies [68,183,184,185] and is an improvement in precision compared to previous GC×GC property estimation studies that employed alkane-bracketed LTPRI[175,176] or retention times.[180]

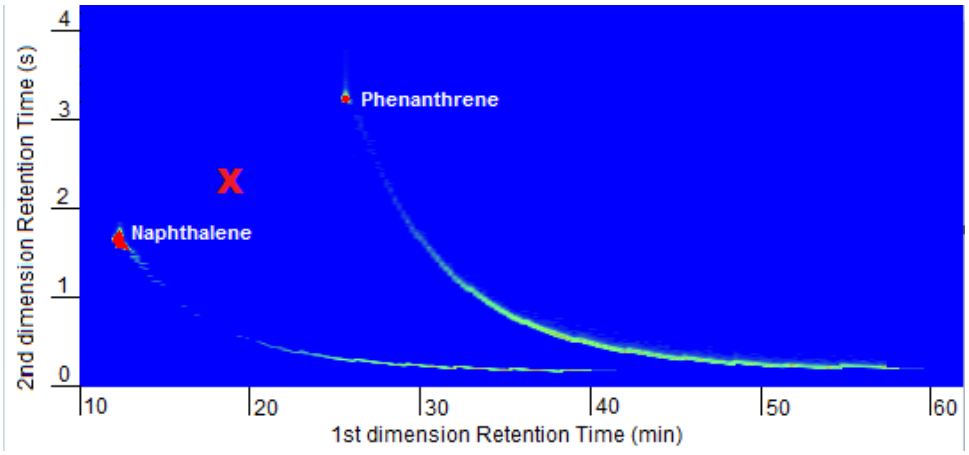

Figure 6-4. Naphthalene and phenanthrene isovolatility curves used to calculate 2nd dimension retention index. While the 1st dimension retention index of point X can be calculated based on RT1D, isovolatility curves (and extrapolation of the phenanthrene isovolatility curve) are required for calculation of the 2nd dimension retention index.

2nd Dimension Retention Index: In contrast to the temperature-programmed 1st column separation, each 2nd dimension separation is effectively isothermal, thus:[221]

$$RI_{2D} = RI_B + \left[\left(\frac{\log(RT_x/RT_B)}{\log(RT_{(B+1)}/RT_B)}\right) \times 100\right] \quad (6\text{-}7)$$

Since isothermal retention indices are directly related to ln *K* (the equilibrium constant for the solute partitioning between two phases), which, in turn, is related to Gibbs free energy, the use of a homologous series and associated indices is not necessary. In this way, any retention index system (or capacity factor *k*) can be used to produce valid thermodynamic data, with the caveat that one must: a) correct for temperature since each ln *K* corresponds to its own 2nd dimension modulation temperature and b) determine $t_{M,2D}$, which is not constant throughout the separation. Beyond these challenges, there has also been historical difficulty

in generating a "meaningful" 2nd dimension retention index in GC×GC analyses, as outlined in the review by von Müehlen and Marriott.[143] Briefly, depending on the homologous series chosen, *e.g.* alkanes, alcohols, amines or FAMEs (a comprehensive list of RI schema can be found in Castello *et al.* 1999),[222] target compounds may not elute within the retention window of the brackets. For example, in Figure 6-4, compound *X* does not elute in the 2nd dimension retention window of naphthalene and phenanthrene (*i.e.*, if not for the isovolatility curves, neither bracket compound would elute at the same 1st dimension time as compound *X*), so their 2nd dimension retention times cannot be compared. While one can analyze the target compound and the brackets using isothermal GC on the same stationary phase as the second column, or continuously introduce the bracket compounds by means of extra plumbing, we developed a simpler method to accurately measure RI_{2D}, in which compound *X* can be compared to *B* and *B+1* at the same elution temperature.

Our method of addressing this issue came from the realization that we could take advantage of the GC×GC modulation process by having the cold jet (a cryotrap of sorts) serve as a secondary inlet. The modulator employed in our system passes a stream of cryogenic gas across a capillary column loop, as shown in Figure 6-5. Periodically, a secondary stream of hot gas with much higher flow rate is pulsed across the same portion of the GC column for a relatively short time. During typical operation, compounds frozen by the cryogen are desorbed when the hot gas passes over the column. However, overloading the modulator prevents the

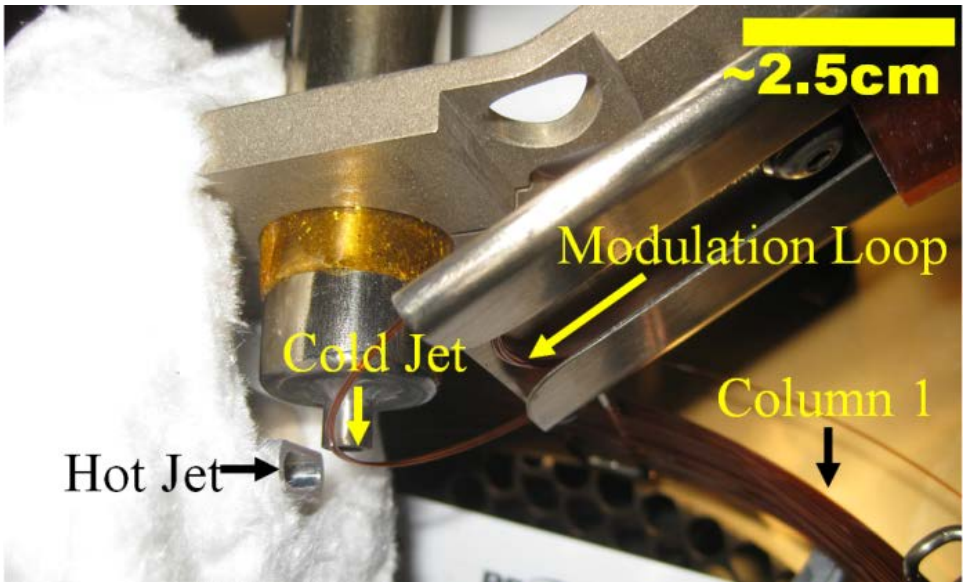

Figure 6-5. GC×GC cryogenic modulator.

solute from desorbing during a single hot gas pulse, leading to residual material frozen in the loop through the next modulation cycle. In effect, this allows some of the analyte that has already eluted through the first column to be "delayed" upon introduction to the second column. The resulting chromatogram is similar to the ones produced using the method employed by Bieri and Marriott,[223] except that no additional plumbing is required. The process essentially generates dozens, if not hundreds, of constant temperature chromatograms for that compound within one GC×GC run. The end result is a 2D chromatogram marked by easily-defined isovolatility bracket curves, see Figure 6-4, which shows distinct chromatographic peak tails with asymptotically decreasing second dimension retention times. This is to be expected, since the analyte experiences a continual increase in modulation temperature during each injection onto the second column, and, as such, the resulting 2nd retention time decreases with each subsequent pulse.

In those cases in which the elution line did not extend far enough in a particular dimension to provide "coverage" for a particular compound (see phenanthrene in Figure 6-4), we used MATLAB's curve fitting functions to extrapolate the isovolatility line across the 2D retention space. The best fit for isovolatility curves was found in an exponential function of the form:

$$RT_{2D} = A \times e^{-b \times RT_{1D}} \tag{6-8}$$

To determine the minimum number of points for an acceptable fit, we varied the number of 1D and 2D bracket compound retention times and used Equation 6-8 to estimate the 2nd dimension retention times for each point on the isovolatility curve. For all bracketing standards, *b* was approximately 0.1, meaning the fitted curves were of similar shape. With as few as five consecutive points along the isovolatility curve, the exponential functions we generated predicted a given compound's RT_{2D} at any RT_{1D} within 5% (0.5 s). As the isovolatility curves are not themselves exact exponential functions, this level of accuracy is excellent. Nonetheless, given the importance of obtaining accurate RT_{2D}, an isovolatility curve of 20 points or more is recommended, as this produces 2nd dimension RT accuracy > 99%.

Based on these results, we examined the accuracy of the 2nd dimension retention indices by comparing the calculated RI_{2D} from the isovolatility curves against isothermally measured indices, see Table 6-2. Excellent agreement was obtained;

the calculated and measured indices were within 1.5 units, or 0.6%, of one another. These findings confirm the validity of our approach for calculating 1st and 2nd dimension retention indices and are comparable to those of the temperature-corrected ln *K* approach, which requires burdensome thermodynamic calculations and training measurements for each unique experimental condition.[175,176] The advantage gained by these retention tails is twofold: in addition to knowing precisely when a compound elutes on the second column at a number of 1D elution temperatures, the highly reproducible tail also permits the estimation of when a compound would have eluted on the second column if it had eluted earlier than it otherwise did. In other words, we can estimate the 2nd dimension retention time of any compound both before and after its 1st dimension elution time. With the ability to determine RI_{1D} and RI_{2D} for the entire separation space, we can now estimate the physical properties of every compound in the sample.

Table 6-2. Retention indices for PAH and alkyl PAH on a DB-17 column as calculated from isothermal GC/MS data and GC×GC 2nd dimension isovolatility curves.

Compound	GC/MS Isothermal RI	GC×GC Calculated RI	% Error
1-methylnaphthalene	220.70	219.85	0.4
2,6-dimethylnaphthalene	231.19	231.18	0.0
2-ethylnaphthalene	229.06	231.36	1.0
2-methylnaphthalene	216.36	216.01	0.2
Acenaphthylene	246.86	246.24	0.3
Anthracene	300.98	303.22	0.7
Fluoranthene	341.72	343.71	0.6
Fluorene	265.86	265.49	0.1
n-C_{10} benzene	253.01	251.13	0.7
n-C_8 benzene	222.14	224.49	1.1
Pyrene	351.46	354.54	0.9

Estimation of Physical Properties: A compound's vapor pressure defines the volatility of a compound, which affects its transport and partitioning in environmental matrices. It can be used to determine a compound's presence in the atmosphere, aqueous media, soil, and soil-bound organics. A partition process dependent only on VdW interactions can be adequately predicted for a group of compounds using only a single-parameter LFER[213] and, as such, vapor pressure values for each component in coal tar was determined using the following single-parameter LFER:

$$V_P = a\, RI_{1D} + c \qquad (6\text{-}9)$$

LFER regression statistics are found in Table 6-3. The excellent correlation between vapor pressure and nonpolar column RI is consistent with models developed by others,[175,176,180] but in this study we obtained a lower standard error of ~10%. Vapor pressure estimates based on our model were accurate to within 1.8% of literature values, on average, see Table 6-4, and are more accurate than those produced by 1D RI-based boiling point estimates.[224] We also estimated vapor pressure using only 2nd dimension retention indices, as retention on the DB-17 column is also partially governed by VdW interactions, and found results similar to those from the 1st column indices, see Table 6-3. The agreement of these results despite the differing phenyl content of these two columns and corresponding changes in molecular interactions suggests that any methylphenyl-

Table 6-3. Linear free energy relationships (LFER) used to estimate physical properties and their corresponding statistics.

Solute Property	GC×GC Method	LFER coefficient $aRI_{1D} + bRI_{2D} + c$			Standard Error	r^2
		a	***b***	***c***		
V_P	A	-0.027		1.9	0.10	0.99
	B	-0.026		1.8	0.11	0.98
	A (Column 2)		-0.0067	-2.9	0.02	0.99
	B (Column 2)		-0.0025	-3.6	0.10	0.98
K_{OW}	A	0.10	-0.09	1.0	0.17	0.98
	B	0.08	-0.07	1.1	0.19	0.95
S_W	A	-0.12	0.11	-0.54	0.24	0.95
	B	-0.09	0.08	-0.28	0.18	0.95

based column can be used to estimate the vapor pressure of aromatic solutes. In the same vein, a column with no phenyl content will likely provide superior results for a homologous series of alkanes.

When examining analyte partitioning that is dependent on multiple types of intermolecular interactions, one would assume that a polyparameter LFER would provide improved results, with each parameter corresponding to a type of intermolecular interaction. In contrast, others have discovered for compound classes whose H-bond interactions are proportional to their van der Waals interactions, a single-parameter LFER will provide results comparable to a two-parameter LFER.[213] Although proportional VdW and H-bonding interactions are characteristic of PAH,[213] we found that polyparameter LFER were markedly superior to the single-parameter LFER for K_{OW} and S_W; *e.g.*, the single-parameter

standard error was on average 3- to 6-times higher than that of the corresponding two-parameter LFER. Therefore, only the polyparameter results are presented.

The remaining two physical chemical properties examined in this study, aqueous solubility and octanol-water partition coefficient, also play important roles in examining the behavior of chemicals in the environment. These properties can be used to determine bioaccumulation factors and partition coefficients with organic carbon, and a reliable assessment of fate in the environment requires accurate values for both properties.[225] In each case, two-parameter LFER was employed:

$$\log S_W \; or \log K_{OW} = aRI_{1D} + bRI_{2D} + c \qquad (6\text{-}10)$$

where *a*, *b*, and *c* are dependent on the property estimated. LFER regression statistics are found in Table 6-3. Results were excellent for S_W and K_{OW}, producing comparable correlation coefficients but smaller standard errors when compared to other studies.[175,176,180] Aqueous solubilities and the octanol-water partition coefficients were within 4.2% and 2.3% of literature values, see Table 6-4. In all, the average error for the three estimated parameters across all compounds was 3.0% for two different GC×GC operating conditions. The model used to obtain these estimates is based on log-linear free energy relationships, which correspond to more accurate estimates than the log-log relationships reported in other work.

Table 6-4. Literature and estimated PAH and alkyl PAH physical properties.

Compound	log V_P (atm)			log S_W (mol-L^{-1})			log K_{OW}		
	Literature	**Calculated**	**% Error**	**Literature**	**Calculated**	**% Error**	**Literature**	**Calculated**	**% Error**
1,3-dimethylnaphthalene	-4.515	-4.574	1.3	-4.291	-4.297	0.1	4.420	4.414	0.1
1,4-dimethylnaphthalene	-4.550	-4.650	2.2	-4.136	-4.326	4.6	4.373	4.441	1.6
1-ethylnaphtalene	-4.479	-4.461	0.4	-4.169	-4.183	0.3	4.397	4.314	1.9
1-methylnaphthalene	-4.055	-4.009	1.1	-3.717	-3.486	6.2	3.870	3.708	4.2
2,6-dimethylnaphthalene	-4.473	-4.499	0.6	-4.167	-4.476	7.4	4.333	4.562	5.3
2-ethylnaphthalene	-4.381	-4.461	1.8	-4.291	-4.284	0.2	4.380	4.399	0.4
2-methylnaphthalene	-4.046	-3.933	2.8	-3.653	-3.564	2.4	3.915	3.771	3.7
Acenaphthene	-4.939	-4.876	1.3	-3.966	-4.034	1.7	3.920	4.202	7.2
Benzo[*a*]fluorene	-7.865	-7.980	1.5	-5.048	-5.371	6.4	5.373	5.444	1.3
Benzo[*a*]pyrene	-9.677	-10.013	3.5	-6.338	-6.089	3.9	6.040	5.872	2.8
Benzo[*b*]fluoranthene	-10.391	-9.972	4.0	-6.599	-6.353	3.7	6.000	5.980	0.3
Dibenz[*a*,*h*]anthracene	-11.606	-11.277	2.8	-7.690	-7.308	5.0	6.750	6.647	1.5
Fluoranthene	-7.179	-7.290	1.5	-5.177	-4.840	6.5	5.195	4.970	4.3
Fluorene	-5.303	-5.291	0.2	-4.157	-4.319	3.9	4.180	4.458	6.6
n-C_{10} benzene	-5.774	-5.668	1.8	-7.958	-7.613	4.3	7.350	7.256	1.3
n-C_8 benzene	-4.828	-4.763	1.3	-6.459	-6.414	0.7	6.300	6.210	1.4
Pyrene	-7.232	-7.549	4.4	-5.187	-4.832	6.8	4.994	4.973	0.4

Component Maps: The component maps in this study are similar to those introduced by Arey and coworkers for diesel fuel.[178,179] Given the K_{OW} and S_W estimates discussed above, the resulting map offers a more accurate delineation than those previously reported. To create the map, the LFER outlined in Equations 6-9 and 6-10 were used to overlay physical property estimates onto corresponding retention times, extrapolated from RI, which can be used to estimate the properties of any compound that elutes within the bounded retention space. In the S_W and K_{OW} component maps shown in Figure 6-6A and 6-6B, the blue lines trace the isovolatility curves, while the red and black contour lines designate the areas of the chromatogram that correspond to a specific value of one of the three physical properties estimated in this study. Each dot on the chromatogram represents a compound identified in the coal tar sample whose physical properties have been estimated based solely on retention indices, using the LFER found in the top-left corner of the map. If the absolute error of each estimated property is less than 0.5 (see Table 6-4 for units), the dot is colored teal. This is the case for each compound found in the figure. Had any property estimate's error been between 0.5 and 1, the corresponding compound's dot would be colored red. In each case, the dot color (teal or red) darkens as the threshold is approached.

In the figure, the black lines correspond to vapor pressure, and as this LFER is based solely on RI_{1D}, the lines are vertical, relating only to the 1st dimension retention time. For example, 1,3-dimethylnaphthalene, which is labeled in the S_W

component map, Figure 6-6A, falls approximately halfway between the black lines labeled -4 and -5, and has an estimated log vapor pressure of -4.57 atm. This compares well with the literature value of -4.52 atm. Since S_W estimates are based upon retention values from both chromatographic dimensions (see Equation 6-10), the corresponding lines curve across the chromatogram. As with the previous example, any compound that lies on the red line labeled -7 has an estimated S_W value of - log 7 mol-L^{-1}. For 1,3-dimethylnaphthalene, we see that it lies in the area almost exactly one-third of the way between the red lines labeled -4 and -5, corresponding to an estimated log S_W of -4.30 mol-L^{-1}, which differs from the literature value by 0.1%. In the bottom chromatogram, Figure 6-6B, benzo[*a*]fluorene is located between red lines 5 and 6, with an estimated log K_{OW} of 5.44. This value differs from the literature value by 0.07 (1.3%). Given 1st and 2nd dimension retention times, V_P, S_W, and K_{OW} can be readily estimated for every compound found in the 2D chromatogram.

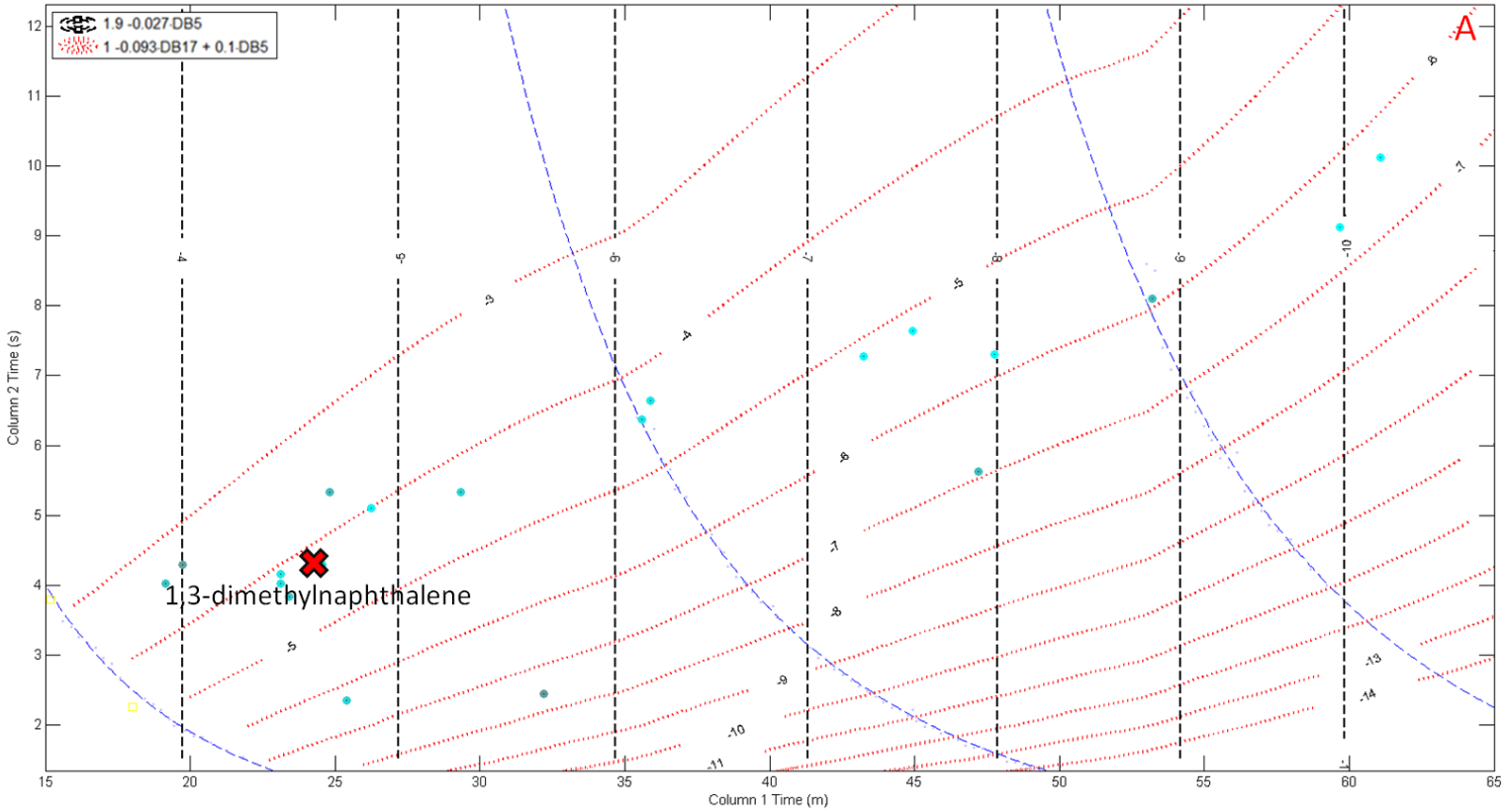
1.9 -0.027·DB5
1 -0.093·DB17 + 0.1·DB5
A
1,3-dimethylnaphthalene
Column 2 Time (s)
Column 1 Time (m)

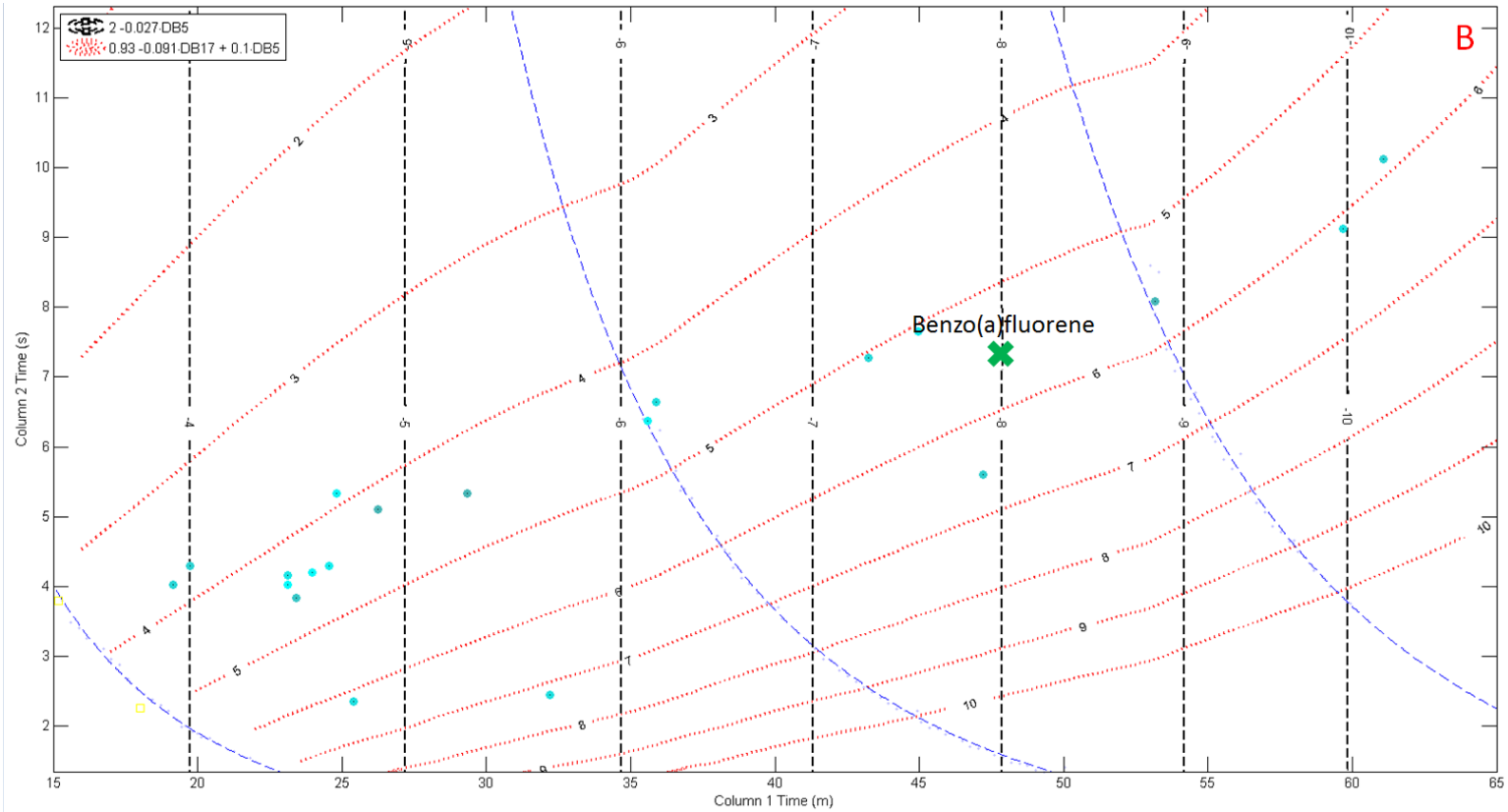

Figure 6-6. Aqueous solubility (A) and octanol-water partition coefficient (B) contour maps derived from the analysis of a coal tar-impacted soil sample. Black (vertical) lines correspond to vapor pressure, red (contour) lines to either S_W (A) or K_{OW} (B). All compound dots are colored teal because the absolute error of each estimated physical property is < 0.5.

Figure 6-7 shows the contour lines overlaid onto the 2D chromatogram of an environmentally-exposed soil and illustrates how this component map can be used to assess physical weathering in a more informed manner. Note that the maps created in this study only allow for the investigation of physical processes and not biological and chemical processes. Visually, we can still see that the sample has only minimally weathered, since many of the aliphatics and a number of the C_1- and C_2-alkylated naphthalenes are present, but the additional value of the component map is that it allows assignment of volatility and solubility values to sample components. It is clear from the map that a wide range of organics, whose respective log V_P and log S_W are between -4 and -10 atm and -3 and -7 mol-L^{-1}, have not been lost to the environment. An examination of these compounds suggests not only that the sample will continue to weather, but also by which physical weathering process, *i.e.*, dissolution and/or evaporation. For example, both carbazole and the C_4-alkylated biphenyls, identified in the figure by A and B, lie on the same volatility line, but their aqueous solubilities differ by two orders of magnitude. The biphenyls are far more likely to be affected by water-washing than carbazole. If the same site is analyzed later and C_4-biphenyl is present but carbazole is not, it could be inferred that the sample and, thus, the site, was water-washed to a greater extent than volatilized. Similarly, the biphenyls and benzo[*a*]pyrene (B and C) lie on the same S_W contour line, but have widely differing volatilities. The former is far more likely to be affected by evaporation than the latter. Assessments such as these can be made for any point in the chromatogram, whether the compound has been identified or not, over the

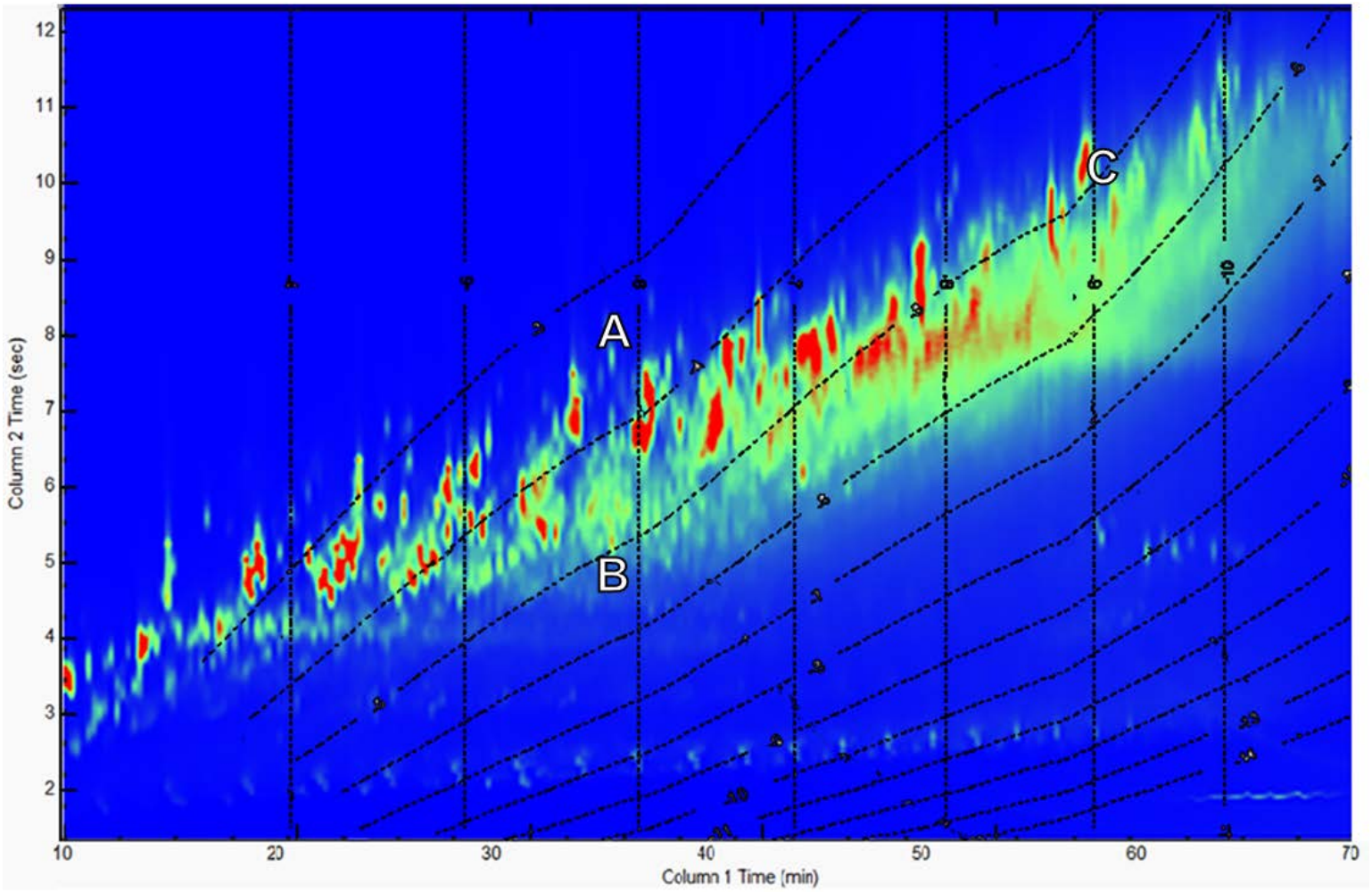

Figure 6-7. Vapor pressure (vertical) and aqueous solubility (contour) lines from Figure 5 overlaid onto a GC×GC chromatogram of the same sample; compounds that lie on the same line possess the same physical properties.

lifetime of the site, from contamination to final remediation. Specific to this site, it is clear that volatile and soluble compounds remain and further release of pollutants is likely.

The outcome of this research supports hazardous waste site investigation and cleanup projects. In addition to providing quantitative measurements of pollutant concentrations, GC×GC/MS data in conjunction with our model discerns the mechanism and progression of how a site weathers due to dissolution, organic phase partitioning, and evaporation caused by the local environment. Our improved method for obtaining retention information, if combined with LFER-based approaches to estimating phospholipid−water partition coefficients and, in turn, bioaccumulation,[180] should provide insight into how contaminants weather due to biological processes. In addition, correlating weathering processes with Abraham solvation parameters[226] and other molecular descriptors should further inform forensic investigations, such as longitudinal assessments of how weathering patterns change over time. Moreover, this approach can be used by researchers in a wide range of disciplines, including toxicology (bioaccumulation and toxicity studies) and restoration (ecological and urban planning studies).

Chapter 7 **Conclusions and Future Directions**

An analytical chemist responsible for the investigation of a site that has been contaminated with coal tar or another fossil fuel-based pollutant faces a number of challenges. Success is dependent on the accurate quantitation of target analytes and delineation of pollutant zones, yet interferences from both the sample matrix and target analytes themselves can easily hinder this undertaking. Underestimation of contamination or failure to identify a "hot spot" can lead to severe consequences to the environment and human health, while each additional day dedicated to site assessment and pollution remediation can cost site owners thousands of dollars. In effect, the scientist is a hostage of the trade-offs necessitated by the three vertices of the so-called analytical triangle: speed, accuracy, and cost.

Whether focused on improvements in field analytics, chromatographic technology, or data analysis, the studies that compose this dissertation were performed in support of these beleaguered individuals – ways to improve speed and accuracy, and by doing so, facilitate site remediation. Each study was performed with an eye on the analytical figures of merit – accuracy, precision, sensitivity, selectivity, and limits of detection and quantitation. Improvement of these figures of merit lessens both the burden on analytical chemists and the corresponding indecision and assessment risk.

A logical next step in this line of research is the combination of all five studies into a comprehensive field analytical method. While bringing cryogen to a site may be cumbersome, it would serve a dual purpose – both in TEDSS cryotrapping and GC×GC modulation. Screening measurements can be made as described in Chapter 1, and upon contact with a pollutant zone of interest, rather than perform the specified GC/MS analysis, the user would analyze the sample via GC×GC/MS with an IL column in the 2nd dimension. While this sacrifices speed, it would not need to be performed regularly; only at the analyst's discretion. Data analysis would be based on MFPPH and the spectral deconvolution described in Chapters 2 and 5, and the results providing not only accurate quantitation of sample components, but also utilized in conjunction with the modeling methodology described in Chapter 6 to discern the mechanism and progression of site weathering. The end result would be a field-based analytical technique that would lead to improvements in nearly all of the aforementioned analytical figures of merit – increased separation and more accurate quantitation of target compounds and rapid assessment of the state of weathering. In addition, by incorporating alkane, hopane/sterane, and fatty acid bracketing standards into this approach, we could begin to delineate physical weathering from the less predictable effects of biodegradation and chemical oxidation.

Beyond this, my graduate career was also marked by a number of projects that, for various reasons, did not find their way into this dissertation. The use of the TEDSS system to detect household mold is one such promising line of research.

In short, the TEDSS umbilical cord can be snaked behind walls and through ducts and collect those MVOC (microbial VOC) released by fungal species. While the low concentrations of MVOC found in ambient air push the limits of the instrument, the speciation of various fungal genera proves a greater challenge. MVOC vary by general, growth medium, and life cycle stage, but a review of the literature reveals that many of these compounds are produced by a majority of genera – the compounds unique enough to produce MVOC "fingerprints" of value have yet to be identified. While it is clear that these compounds exist, as canines have been trained to detect hazardous mold, the first step in this line of research is to determine the identity of these compounds and if they are produced at a level that can be consistently detected by GC/MS – in effect, creation of comprehensive database of MVOC. With this in hand, the so-called "hunt" can begin in earnest.

Another project that is ripe for continuation is a quantitative examination of water washing. Continuous 5-year exposure of coal tar and crude oil to a circulating water bath, with sampling of the water and substance in question every day, then week, then month, would elucidate weathering on a compound-by-compound level. If these samples were analyzed by GC×GC/MS, the weathering maps could be used to improve upon mass transfer models and truly add value to a heretofore purely semiquantitative approach.

References

[1] Moorthy, B. *Issues in Toxicology* **2008,** 3, 97-135.
[2] Patri, M. *Annals of Neurosciences* **2009,** 16, (1), 22-30.
[3] Sinsheimer, J. E.; Hooberman, B. H.; Das, S. K.; Savla, P. M.; Ashe, A. J. *Environmental and Molecular Mutagenesis* **1992,** 19, (3), 259-264.
[4] Toyooka, T.; Ibuki, Y. *Environmental Toxicology and Pharmacology* **2007,** 23, (2), 256-263.
[5] Mahadevan, B.; Courter, L. A.; Baird, W. M. In *New Developments in Mutation Research*; Valon, C. L., Ed.; Nova Science Publishers, Inc.: Hauppauge, N. Y., 2007, p 19-40.
[6] Swartz, C. D.; King, L. C.; Nesnow, S.; Umbach, D. M.; Kumar, S.; DeMarini, D. M. *Mutation Research/Fundamental and Molecular Mechanisms of Mutagenesis* **2009,** 661, (1-2), 47-56.
[7] Pelroy, R. A.; Stewart, D. L.; Tominaga, Y.; Iwao, M.; Castle, R. N.; Lee, M. L. *Mutation Research/Genetic Toxicology* **1983,** 117, (1-2), 31-40.
[8] Jacob, J. *Polycyclic Aromatic Compounds* **2008,** 28, (4-5), 242-272.
[9] Irigaray, P.; Belpomme, D. *Carcinogenesis* **2010,** 31, (2), 135-148.
[10] Croisy, A.; Mispelter, J.; Lhoste, J. M.; Zajdela, F.; Jacquignon, P. *Journal of Heterocyclic Chemistry* **1984,** 21, (2), 353-359.
[11] Warshawsky, D. *Journal of Environmental Science and Health, Part C: Environmental Carcinogenesis and Ecotoxicology Reviews* **1992,** 10, (1), 1 - 71.
[12] Kropp, K. G.; Fedorak, P. M. *Canadian Journal of Microbiology* **1998,** 44, (7), 605-622.
[13] Pereira Netto, A. D.; Cunha, I. F.; Krauss, T. M. *Bulletin of Environmental Contamination and Toxicology* **2004,** 73, (6), 1072-1077.
[14] Meador, J. P.; Stein, J. E.; Reichert, W. L.; Varanasi, U. In *Reviews of Environmental Contamination and Toxicology* 1995; Vol. 143, p 79-165.
[15] Hyötyläinen, T.; Oikari, A. *Chemosphere* **2004,** 57, (2), 159-164.
[16] Ogata, M.; Miyake, Y. *Water Research* **1979,** 13, (12), 1179-1185.
[17] Ogata, M.; Miyake, Y. *Acta Medica Okayama* **1978,** 32, (6), 419-425.
[18] Eastmond, D. A.; Booth, G. M.; Lee, M. L. *Archives of Environmental Contamination and Toxicology* **1984,** 13, (1), 105-111.
[19] Hawthorne, S. B.; Miller, D. J.; Kreitinger, J. P. *Environmental Toxicology and Chemistry* **2006**, *25*, 287-296.
[20] Tobiszewski, M.; Namieśnik J. *Environmental Pollution* **2012,** 162, 110-119.
[21] Daling, P. S.; Faksness, L.-G.; Hansen, A. B.; Stout, S. A. *Environmental Forensics* **2002**, *3*, 263 - 278.
[22] *Procedures for the derivation of ESBs for the protection of benthic organisms: PAH mixtures, EPA/600/R-02/01* (United States Environmental Protection Agency Office of Research and Development, Washington, DC, 2003).
[23] *Methods for the derivation of site-specific equilibrium partitioning sediment guidelines (ESGs) for the protection of benthic organisms: non-ionic organics, EPA/822/R/02/042* (US Environmental Protection Agency Office of Science and Technology, Washington, DC, 2004).
[24] Mahler, B. J.; Metre, P. C. V.; Crane, J. L.; Watts, A. W.; Scoggins, M.; Williams, E. S. *Environ. Sci. Technol.* **2012**, 46, 3039-3045.
[25] Hatheway, A. W. *Remediation of Former Manufactured Gas Plants and Other Coal-Tar Sites*; CRC Press: Boca Raton, FL, 2011.
[26] Yim, U. H.; Kim, M.; Ha, S. Y.; Kim, S.; Shim, W. J. *Environmental Science & Technology* **2012,** 46, 6431-6437.
[27] Wardlaw, G. D.; Nelson, R. K.; Reddy, C. M.; Valentine, D. L. *Organic Geochemistry* **2011,** 42, 630-639.
[28] National Research Council of the National Academies, *Oil in the sea III: Inputs, fates, and effects* (The National Academies Press, Washington, DC, 2003).
[29] Kennicutt II, M. C. *Oil and Chemical Pollution* **1988**, *4*, 89-112.
[30] *Cleaning up the Nation's Waste Sites: Markets and Technology Trends, EPA 542-R-04-015*, United States Environmental Protection Agency: Washington D.C., 2004.
[31] Robbat, A., Jr.; Smarason, S.; Gankin, Y. V., *Field Analytical Chemistry and Technology* **1998**, 2 (5), 253-265.

[32] *Using dynamic field activities for on-site decision making: a guide for project managers, office of solid waste and emergency response, OSWER No. 9200.1-40 EPA/540/R-03/002,* United States Environmental Protection Agency: Washington D.C., 2003.
[33] Robbat, A., Jr.; Kenny, J. E.; Smarason, S.; Pepper, J. W.; Wright, A. O. *Remediation* **1998**, 9, 95–111.
[34] Kram, M.L.; Keller, A. A.; Massick, S. M.; Laverman, Complex, L.E. *Soil & Sediment Contamination* **2004**, *13*, 103–118.
[35] Rossabi, J.; Riha, B. D.; Haas, J.; Eddy-Dilek, C. A.; Lustig, A.; Carrabba, M.; Hyde, K.; Belo, J. *Vadose Zone Science and Technology Solutions* **2000**, *1*, 431–444.
[36] Garcia-Gomez, R. S.; Pandiyan, T.; Aguilar-Iris, V. E.; Luna-Pabello, V.; Duran de Bazua, C. *Water, Air, and Soil Pollution* **2004**, *158*, 137–151.
[37] Griffin, T. W.; Watson, K. W. *Ground Water Monitoring and Remediation* **2002**, Spring, 48–59.
[38] McAndrews, B.; Heinze, K.; DiGuiseppe, W. *Soil and Sediment Contamination* **2003**, *12* (6), 799–813.
[39] Considine, T.; Robbat, A., Jr. *Environ. Sci. Technol.* **2008**, *42*, 1213-1220.
[40] Robbat Jr., A.; Smarason, S.; Gankin, Y. V. *Field Analytical Chemistry & Technology* **1999**, *3*, 55-66.
[41] Robbat Jr., A.; Gorshteyn, A. *Field Analytical Chemistry & Technology* **2000**, *4*, 85-92.
[42] Robbat Jr., A. *Field Analytical Chemistry & Technology* **2001**, *5*, 60-68.
[43] Breault, R. F.; Durant, J. L.; Robbat Jr., A. *Report 2005-5191: Sediment Quality of Lakes, Rivers, and Estuaries in the Mystic River Basin, Eastern Massachusetts, 2001–03*; US Geological Survey Information Services: Reston, VA, 2005, p 110.
[44] *Test Methods for Evaluating Solid Waste, SW-846;* United States Environmental Protection Agency: Washington D.C., 1986.
[45] Short, J.W.; Jackson, T.L.; Larsen, M.L.; Wade, T.L. In *Proceedings of the Exxon Valdez Oil Spill Symposium*, edited by Rice, S.D.; Spies, R.B.; Wolfe, D.A.; Wright, B.A.; American Fisheries Society: Bethesda, MD, 1996.
[46] Wang, Z.; Fingas, M.; Page, D. S. *Journal of Chromatography A* **1999**, 843, 369-411.
[47] Antle, P.M.; Zeigler, C.D.; Wilton, N.M.; Robbat Jr., A. *International Journal of Environmental Analytical Chemistry* **2013**, 94 (4), 332-347.
[48] Anderson, J.L.; Armstrong, D.W.; Wei, G.T. *Analytical Chemistry* **2006**, 78, 2892-2902.
[49] Anderson, J.L.; Armstrong, D.W. *Analytical Chemistry* **2005**, 77, 6453-6462.
[50] Qi, M.; Armstrong, D.W. *Analytical and Bioanalytical Chemistry* 388 (2007): 889-899.
[51] Breitbach, Z.S.; Armstrong, D.W. *Analytical and Bioanalytical Chemistry* 390 (2008): 1605-1617.
[52] Davis, J. M.; Giddings, J. C. *Analytical Chemistry* **1983**, *55*, 418-424.
[53] Giddings, J. C. *Journal of Chromatography A* **1995**, *703*, 3-15.
[54] Bertsch, W. *Journal of High Resolution Chromatography* **1999**, *22*, 647-665.
[55] Giddings, J. C. *Journal of Chromatography A* **1995**, *703*, 3-15.
[56] Beens, J. Chromedia: 2009.
[57] Blumberg, L.; Klee, M. S. *Journal of Chromatography A* **2010**, *1217*, 99-103.
[58] MacNamara, K.; Leardi, R.; Hoffman, A. *LCGC North America* **2004**, *22*, 166-186.
[59] Gorecki, T.; Harynuk, J. J.; Panic, O. *Journal of Separation Science* **2004,** 27, 359-379.
[60] Seeley, J. V. *Journal of Chromatography A* **2012**, 1255, 24-37.
[61] De-Geus, H.; de Boer, J.; Brinkman, U. *TrAC – Trends in Analytical Chemistry* **1996,** 15, 168-178.
[62] Bertsch, W. *Journal of High Resolution Chromatography* **2000,** 23, 167-181.
[63] de la Mata, A. P.; Harynuk, J. J. *Analytical Chemistry* **2012**, 84, 6646-6653.
[64] Beens, J.; Boelens, H.; Tijssen, R.; Blomberg, J. *Journal of High Resolution Chromatography* **1998,** 21, 47-54.
[65] Gankin, Y. V.; Gorshteyn, A.; Smarason, S.; Robbat, A., Jr. Analytical Chemistry 1998, 70, 1655-1663.

[66] Douglas, G.S.; Emsbo-Mattingly, S.D.; Stout, S.A.; Uhler, A.D.; McCarthy, K. J. in *Introduction to Environmental Forensics*, edited by Murphy, B.L.; Morrison R. D.; Elsevier Academic Press: Burlington, MA, 2007.
[67] *National Coastal Condition Assessment: Laboratory Methods Manual, EPA/841/R-09/002*. United States Environmental Protection Agency: Washington D.C., 2010.
[68] Zeigler, C. D.; Schantz, M. M.; Wise, S.; Robbat, A. J. *Polycyclic Aromatic Compounds* **2011**, 32 (2), 154-176.
[69] Zeigler, C.D.; MacNamara, K.; Wang, Z.; Robbat Jr, A. *Journal of Chromatography A* **2008**, *1205*, 109-116.
[70] Zeigler, C.D.; Robbat Jr, A. *Environmental Science & Technology* **2012**, *46*, 3935-3942.
[71] Schade, T.; Andersson, J. T. *Journal of Chromatography A* **2006**, *1117*, 206-213.
[72] Baldwin, L. J.; Tedjamulia, M. L.; Stuart, J. G.; Castle, R. N.; Lee, M. L. *Journal of Heterocyclic Chemistry* **1984**, *21*, 1775-1779.
[73] Zeigler, C.D.; Wilton, N.D.; Robbat Jr., A. *Analytical Chemistry* **2012**, *84*, 2245-2252.
[74] Robbat, A., Jr.; Smarason, S.; Gankin, Y. V. *Field Analytical Chemistry & Technology* **1999**, *3*, 55-66.
[75] Antle, P. M.; Zeigler, C. D.; Gankin, Y.; Robbat, A. *Analytical Chemistry* **2013**, *85*, 10369–10376.
[76] Robbat Jr., A.; Smarason, S.; Gankin, Y. V. *Field Analytical Chemistry & Technology* **1998**, 2, 253-265.
[77] Robbat Jr., A.; Gorshteyn, A. *Field Analytical Chemistry & Technology* **2000**, *4*, 85-92.
[78] Robbat Jr., A. *Field Analytical Chemistry & Technology* **2001**, 5, 60-68.
[79] Robbat Jr, A.; Considine, T.; Antle, P. M. *Chemosphere* **2010**, *80*, 1370-1376.
[80] Gorshteyn, A.; Smarason, S.; Robbat Jr, A. *Environmental Science & Technology* **1999**, *33*, 2474-2480.
[81] Robbat, A. J. *Environmental Testing and Analysis* **2000**, *9*, 15-19, 33.
[82] W. Youngblood and M. Blumer, *Geochimica Cosmochimica Acta* **1975**, 39, 1303.
[83] Douglas, G. S.; Bence, A. E.; Prince, R. C.; McMillen, S. J.; Butler, E. L. *Environmental Science & Technology* **1996**, 30, 2332-2339
[84] *Standard Test Method for Determination of Parent and Alkyl Polycyclic Aromatics in Sediment Pore Water Using Solid-Phase Microextraction and Gas Chromatography/Mass Spectrometry in Selected Ion Monitoring Mode, D7363 – 11*, ASTM International: West Conshohocken, PA, 2011.
[85] *Sampling and Analytical Methods of the National Status and Trends Program, NOAA Technical Memorandum NOS ORCA 130*,National Oceanic and Atmospheric Administration: Silver Spring, MD, 1998.
[86] Hegazi, A. H.; T. Andersson, J. In *Oil Spill Environmental Forensics*; Academic Press: Burlington, 2007, p 147-168.
[87] Havenga, W. J.; Rohwer, E. R. *Polycyclic Aromatic Compounds* **2002**, *22*, 327-338.
[88] Sauer, T. C.; Michel, J.; Hayes, M. O.; Aurand, D. V. *Environment International* **1998**, *24*, 43-60.
[89] Wang, Z.; Fingas, M.; Blenkinsopp, S.; Sergy, G.; Landriault, M.; Sigouin, L.; Foght, J.; Semple, K.; Westlake, D. W. S. *Journal of Chromatography A* **1998**, *809*, 89-107.
[90] Wang, Z.; Fingas, M.; Sigouin, L. *Journal of Chromatography A* **2001**, *909*, 155-169.
[91] Boehm, P. D.; Douglas, G. S.; Burns, W. A.; Mankiewicz, P. J.; Page, D. S.; Bence, A. E. *Marine pollution bulletin* **1997**, *34*, 599-613.
[92] Page, D.S.; Boehm, P.D.; Douglas, G.S.; Bence, A.E. in *Exxon Valdez Oil Spill: Fate and Effects in Alaska Waters*, Wells, P.G.; Butler, J.N.; Hughes, J.S., eds. ASTM International, Philadelphia, PA, 1995.
[93] Wang, Z.; Fingas, M. *Journal of Chromatography A* **1997**, *774*, 51-78.
[94] Stout, S.A., Wang, Z. in *Oil Spill Environmental Forensics: Fingerprinting and Source Identification*, edited by Wang, Z and Stout, S.A. Academic Press: Burlington, MA, 2007.
[95] Wang, Z.; Fingas, M.; Li, K. *Journal of Chromatographic Science* **1997** 32 (9), 367.
[96] Wang, Z.; Fingas, M.; Sergy, G. *Environmental Science & Technology* **1995**, *29*, 2622-2631.

[97] Sauer, T.C.; Boehm, P.D. *MSRC Technical Report Series 95-032: Hydrocarbon chemistry analytical methods for oil spill assessments*. Marine Spill Response Corporation, Washington, DC, 1995.
[98] Fernandez-Varela, R.; Andrade, J.M.; Muniategui, S.; Prada, D. *Journal of Chromatography A* 1217 (52), 8279.
[99] Bobinger, S.; Andersson, J. T., *Environmental Science and Technology* **2009,** *43* (21), 8119-8125.
[100] Fathalla, E. M.; Andersson, J. T., *Environmental Toxicology and Chemistry* **2011,** *30* (9), 2004-2012.
[101] Andersson, J.; Hegazi, A.; Roberz, B., *Analytical and Bioanalytical Chemistry* **2006,** *386* (4), 891-905.
[102] Hegazi, A.H., Andersson, J.T., in Oil Spill Environmental Forensics, Academic Press, Burlington, 2007, pp. 147-168.
[103] Moustafa, N. E.; Andersson, J. T., *Fuel Processing Technology* **2011,** *92* (3), 547-555.
[104] Liang, F.; Lu, M.; Birch, M. E.; Keener, T. C.; Liu, Z., *Journal of Chromatography A* **2006,** *1114* (1), 145-153.
[105] Andersson, J. T.; Weis, U., *Journal of Chromatography A* **1994,** *659* (1), 151-161.
[106] Andersson, J. T., *Journal of Chromatography A* **1986,** *354*, 83-98.
[107] Andersson, J. T.; Schmid, B., *Journal of Chromatography, A* **1995,** *693*, 325-338.
[108] Mössner, S. G.; Lopez de Alda, M. J.; Sander, L. C.; Lee, M. L.; Wise, S. A., *Journal of Chromatography A* **1999,** *841* (2), 207-228.
[109] Machado, M. E.; Fontanive, F. C.; de Oliveira, J. V.; Caramao, E. B.; Zini, C. A., *Analytical and Bioanalytical Chemistry* **2011,** *401* (8), 2433-2444.
[110] Machado, M. E.; Bregles, L. P.; de Menezes, E. W.; Caramao, E. B.; Benvenutti, E. V.; Zini, C. A., *Journal of Chromatography A* **2013,** *1274*, 165-172.
[111] Nolte, T.; Posch, T. N.; Huhn, C.; Andersson, J. T., *Energy & Fuels* **2013,** *27* (1), 97-107.
[112] Panda, S. K.; Schrader, W.; al-Hajji, A.; Andersson, J. T., *Energy & Fuels* **2007,** *21* (2), 1071-1077.
[113] Herod, A. A.; Bartle, K. D.; Kandiyoti, R., *Energy & Fuels* **2007,** *21* (4), 2176-2203.
[114] Machado, M. E.; de Menezes, E. W.; Bregles, L. P.; Caramao, E. B.; Benvenutti, E. V.; Zini, C. A., *Journal of Separation Science* **2013,** *36* (9-10), 1636-1643.
[115] Anderson, J. L.; Armstrong, D. W.; Wei, G. T., *Analytical Chemistry* **2006,** *78* (9), 2892-2902.
[116] Anderson, J. L.; Armstrong, D. W., *Analytical Chemistry* **2005,** *77* (19), 6453-6462.
[117] Qi, M.; Armstrong, D. W., *Analytical and Bioanalytical Chemistry* **2007,** *388* (4), 889-899.
[118] Breitbach, Z. S.; Armstrong, D. W., *Analytical and Bioanalytical Chemistry* **2008,** *390* (6), 1605-1617.
[119] Ragonese, C.; Sciarrone, D.; Tranchida, P. Q.; Dugo, P.; Mondello, L., *Journal of Chromatography A* **2012,** *1255*, 130-144.
[120] Reyes-Contreras, C.; Dominguez, C.; Bayona, J. M., *Journal of Chromatography A* **2012,** *1261*, 164-170.
[121] de Boer, J.; Blok, D.; Ballesteros-Gomez, A., *Journal of Chromatography A* **2014,** *1348*, 158-63.
[122] Chen, X. F.; Huang, X. Y.; Wang, G. H.; Zhang, J.; Di, D. L., *Asian Journal of Chemistry* **2014,** *26* (8), 2271-2276.
[123] Hantao, L. W.; Najafi, A.; Zhang, C.; Augusto, P.; Anderson, J. L., *Analytical Chemistry* **2014,** *86* (8), 3717-3721.
[124] Mahe, L.; Dutriez, T.; Courtiade, M.; Thiebaut, D.; Dulot, H.; Bertoncini, F., *Journal of Chromatography A* **2011,** *1218* (3), 534-544.
[125] Seeley, J. V.; Seeley, S. K.; Libby, E. K.; Breitbach, Z. S.; Armstrong, D. W., *Analytical and Bioanalytical Chemistry* **2008,** *390* (1), 323-332.
[126] Weber, B. M.; Harynuk, J. J., *Journal of Chromatography A* **2013,** *1271*, 170-175.
[127] Weber, B. M.; Harynuk, J. J., *Journal of Separation Science* **2014,** *37* (12), 1460-1466.
[128] Zeng, A. X.; Chin, S. T.; Nolvachai, Y.; Kulsing, C.; Sidisky, L. M.; Marriott, P. J., *Analytica Chimica Acta* **2013,** *803*, 166-173.

[129] Delmonte, P.; Kia, A. R. F.; Kramer, J. K. G.; Mossoba, M. M.; Sidisky, L.; Rader, J. I., *Journal of Chromatography A* **2011,** *1218* (3), 545-554.
[130] Destaillats, F.; Guitard, M.; Cruz-Hernandez, C., *Journal of Chromatography A* **2011,** *1218* (52), 9384-9389.
[131] Schade, T.; Andersson, J. T., *Journal of Chromatography A* **2006,** *1117* (2), 206-213.
[132] Lai, W.; Song, C., *Fuel* **1995,** *74* (10), 1436-1451.
[133] Abraham, M. H., *Chemical Society Reviews* **1993,** *22* (2), 73-83.
[134] Anderson, J. L.; Ding, J.; Welton, T.; Armstrong, D. W., *Journal of the American Chemical Society* **2002,** *124* (47), 14247-14254.
[135] Robbat, A.; Corso, N. P.; Doherty, P. J.; Marshall, D., *Analytical Chemistry* **1986,** *58* (9), 2072-2077.
[136] Baldwin, L.J.; Tedjamulia, M.L.; Stuart, J.G.; Castle, R.N.; Lee, M.L. *Journal of Heterocyclic Chemistry* **1984**, 21, 1775-1779.
[137] Harvey, R.G. *Polycyclic Aromatic Hydrocarbons: Chemistry and Carcinogenicity*. Cambridge, UK: Cambridge University Press, 1991.
[138] International Union of Pure and Applied Chemistry. *Nomenclature of Organic Chemistry* (2nd ed., Vol. 1). London, UK: Butterworth-Heinemann, 1996.
[139] Klemm, L. H. *Heterocycles* **1990,** 30, 1219-29.
[140] Huang, K.; Han, X.; Zhang, X.; Armstrong, D.W. *Analytical and Bioanalytical Chemistry* **2007**, 389, 2265-2275.
[141] Lee, M.L.; Vassilaros, D.L.; White, C.M.; Novotny, M. *Analytical Chemistry* **1979**, 51, 768-773.
[142] Vassilaros, D. L.; Kong, R. C.; Later, D. W.; Lee, M. L. *Journal of Chromatography* **1982**, *252*, 1-20.
[143] von Muehlen, C.; Marriott, P.J. *Analytical and Bioanalytical Chemistry* 2011, 401, 2351-2360.
[144] Sabirov, D. S. *Computational and Theoretical Chemistry* **2014**, DOI: 10.1016/j.comptc.2014.01.001
[145] Anderson, J. L.; Ding, R.; Ellern, A.; Armstrong, D.W. *Journal of the American Chemical Society* **2004,** 127, 593-604.
[146] Wang, Z.; Fingas, M., *Environmental Science & Technology* **1995,** *29* (11), 2842-2849
[147] Hegazi, A. H.; Andersson, J. T.; Abu-Elgheit, M. A.; El-Gayar, M. S., *Chemosphere* **2004,** *55* (7), 1053-1065.
[148] Andersson, J. "Separation Methods in the Analysis of Polycyclic Aromatic Sulfur Heterocycles" In *Handbook of Analytical Separations, Vol 3: Environmental Analysis*, edited by W. Kleiböhmer, 75-98. London: Elsevier Science B.V., 2001.
[149] Gorecki, T.; Harynuk, J. J.; Panic, O. *Journal of Separation Science* **2004,** 27, 359-379.
[150] De-Geus, H.; de Boer, J.; Brinkman, U., *TrAC – Trends in Analyical Chemistry* **1996,** 15, 168-178.
[151] Davis, J. M. *Analytical Chemistry* **1991,** 63, 2141-2152.
[152] Blumberg, L. M.; David, F.; Klee, M. S.; Sandra, P. *Journal of Chromatography A* **2008,** 1188, 2-16.
[153] Robbat Jr, A.; Kowalsick, A.; Howell, J. *Journal of Chromatography A* **2011**, 1218, 5531-5541.
[154] Blumberg, L.; Klee, M. S. *Journal of Chromatography A* **2010,** 1217, 99-103.
[155] Schoenmakers, P.J.; Marriott P.J.; Beens, J. *LCGC Europe* **2003,** 16, 335–339.
[156] Harynuk, J. J.; Kwong, A. H.; Marriott, P. J. *Journal of Chromatography A* **2008,** 1200 (1), 17-27.
[157] Davis, J. M.; Stoll, D. R.; Carr, P. W. *Analytical Chemistry* **2008,** 80, 461-473
[158] Mohler, R. E.; Tu, B. P.; Dombek, K. M.; Hoggard, J. C.; Young, E. T.; Synovec, R. E. *Journal of Chromatography A* **2008,** 1186, 401-411.
[159] Zeng, Z.-D.; Chin, S.-T.; Hugel, H. M.; Marriott, P. J. *Journal of Chromatography A* **2011,** 1218, 2301-2310.
[160] de Rijk, T. C.; Mol, H. G. J.; Punt, A.; van der Kamp, H.; van der Lee, M.; van der Weg, G. *J. AOAC International* **2011,** 94, 1722-1740.

[161] Vasilieva, V.; Scherr, K. E.; Edelmann, E.; Hasinger, M.; Loibner, A. P. *Journal of Biotechnology* **2012,** 157, 460-466.
[162] McGregor, L. A.; Gauchotte-Lindsay, C.; Daeid, N. N.; Thomas, R.; Daly, P.; Kalin, R. M. *Journal of Chromatography A* **2011,** 1218, 4755-4763.
[163] Gauchotte-Lindsay, C.; Richards, P.; McGregor, L. A.; Thomas, R.; Kalin, R. M. *Journal of Chromatography A* **2012,** 1253, 154-163.
[164] Adahchour, M.; Brandt, M.; Baier, H.-U.; Vreuls, R. J. J.; Batenburg, A. M.; Brinkman, U. A. T. *Journal of Chromatography A* **2005**, 1067, 245-254.
[165] Robbat, Jr., A.; Hoffmann, A.; MacNamara, K.; Huang, Y. *J. AOAC International* **2008**, 91, 1467-1477.
[166] *Region 1 EPA-NE data validation functional guidelines for evaluating environmental analyses*, Part II, Section VOA/SV – IX. US Environmental Protection Agency, Office of Science and Technology: Washington, DC, 1996.
[167] OSWER No. 9355.4-24, *Supplemental guidance for developing soil screening levels for superfund sites: Appendix A.* US Environmental Protection Agency, Office of Science and Technology: Washington, DC, 2002.
[168] Kennicutt II, M.C. *Oil and Chemical Pollution* 1988, 4, 89-112.
[169] Douglas, G. S.; Bence, A. E.; Prince, R. C.; McMillen, S. J.; Butler, E. L.; *Environmental Science & Technology* 1996, 30, 2332-2339.
[170] Sherblom, P. M. ; Gschwend P. M.; Eganhouse, R. P. *Journal of Chemical Engineering Data*, 1992, 37, 394-399.
[171] Nelson, R. K.; Kile, B. M.; Plata, D.; Sylva, S. P.; Li, X.; Reddy, C. M.; Gaines, R. B.; Frysinger, G. S.; Reichenbach, S.E. *Environmental Forensics* 2006, 7, 33-44.
[172] Ruzicka, K.; Koutek, B.; Fulem, M.; Hoskovec, M. *Journal of Chemical and Engineering Data* **2012**, *57*, 1349-1368.
[173] Tse, G.; H. Orbey, H.; Sandler, S.I. *Environmental Science & Technology*. 1992, 26, 2017-2022.
[174] Mackay, D.; Boethling, R.S. *Handbook of Property Estimation Methods for Chemicals*, CRC Press, Boca Raton, FL, 2000.
[175] Arey, J. S.; Nelson, R. K.; Xu L.; Reddy, C. M. *Analytical Chemistry* 2005, 77, 7172-7182.
[176] Arey, J. S.; Nelson, R. K.; Xu L.; Reddy, C. M. *Analytical Chemistry* 2007, 79, 4736-4736.
[177] Frysinger, G. S.; Gaines, R. B.; Reddy, C.M. *Environmental Forensics*, 2002, 3, 27-34.
[178] Arey, J. S.; Nelson, R. K.; Reddy. C.M. *Environmental Science & Technology* 2007, 41, 5738-5746.
[179] Arey, J. S.; Nelson, R. K.; Plata, D.L.; Reddy, C.M. *Environmental Science & Technology* 2007, 41, 5747-5755.
[180] Tcaciuc, A. P.; Nelson, R. K.; Reddy, C. M.; Gschwend, P. M. *Environmental Science & Technology* **2012**, *46*, 3449-34
[181] Klee, M. S.; Blumberg, L. M. *Journal of Chromatography A* **2010**, *1217*, 1830-1837.
[182] Western, R.J.; Marriott, P.J. *Journal of Separation Science* 2002, 25, 831-838.
[183] Rostad, C. E.; Pereira, W. E. *Journal of High Resolution Chromatography* **1986**, *9*, 328-334.
[184] M. L. Lee, D. L. Vassilaros, C. M. White and M. Novotny, *Analytical Chemistry* 1979, 51, 768-773.
[185] D. L. Vassilaros, R. C. Kong, D. W. Later and M. L. Lee, *Journal of Chromatography* 1982, 252, 1-20.
[186] Gonzalez, F. R.; Nardillo, A. M. *Journal of Chromatography A* **1999**, *842*, 29-49.
[187] *Fuels and Lubricants Handbook: Technology, Properties, Performance, and Testing*; Totten, G. E.; Westbrook, S. R.; Shah, R. J., Eds.; ASTM International: West Conshohocken, PA, 2003; Vol. 1.
[188] United States Environmental Protection Agency, SW-846 Method 3550C: Ultrasonic Extraction, Washington, D.C., 1996.
[189] Bartle, K. D.; Lee, M. L.; Wise, S. A., Chemical Society Reviews **1981**, 10 (1), 113-158.
[190] Lei, Y. D.; Chankalal, R.; Chan, A.; Wania, F. *Journal of Chemical & Engineering Data* **2002**, *47*, 801-806.

[191] Haftka, J. J. H.; Parsons, J. R.; Govers, H. A. J. *Journal of Chromatography A* **2006**, *1135*, 91-100.
[192] Pearlman, R. S.; Yalkowsky, S. H.; Banerjee, S. *Journal of Physical Chemistry Reference Data* **1984**, *13*, 555-562.
[193] Mackay, D.; Shiu, W.Y.; Ma, K.C. *Illustrated Handbook of Physical-Chemical Properties and Environemental Fate for Organic Chemicals : Polynuclear Aromatic Hydrocarbons, Polychlorinated Dioxins, and Dibenzofurans*, Lewis Publishers, Chelsea, MI, 1992.
[194] Curvers, J.; Rijks, J.; Cramers, C.; Knauss, K.; Larson, P. *Journal of High Resolution Chromatography* **1985**, *8*, 607-610.
[195] Ettre, L.S. *Chromatographia* 1984, 18, 243.
[196] Pell, R.J.; Gearhart, H.L. *Journal of High Resolution Chromatography Communications* 1987, 10, 388.
[197] White, C. M.; Hackett, J.; Anderson, R. R.; Kail, S.; Spock, P. S. *Journal of High Resolution Chromatography* **1992**, *15*, 105-120.
[198] Letcher, T. M.; Naicker, P. K. *Journal of Chromatography A* **2004**, *1037*, 107-114.
[199] Hamilton, D.J. *Journal of Chromatography A* 1980, 195, 75-83.
[200] Hackenberg, R.; Schutz, A.; Ballschmiter, K. *Environmental Science & Technology* **2003**, *37*, 2274-2279.
[201] Donovan, S.F. *Journal of Chromatography A* 1996, 749, 123-129.
[202] Schwarzenbach, R.P.; Gschwend, P.M.; Imboden, D.M. *Environmental Organic Chemistry* John Wiley & Sons, New York, NY, 1993.
[203] Hoskovec, M.; Grygarova, D.; Cvacka, J.; Streinz, L.; Zima, J.; Verevkin, S. P.; Koutek, B. *Journal of Chromatography A* **2005**, *1083*, 161-172.
[204] Hawker, D. W.; Connell, D. W. *Environmental Science & Technology* **1988**, *22*, 382-387.
[205] Miller, M. M.; Ghodbane, S.; Wasik, S. P.; Tewari, Y. B.; Martire, D. E. *Journal of Chemical and Engineering Data* **1984**, *29*, 184-190.
[206] Shiu, W.Y.; Ma, K.C. *Journal of Physical Chemistry Reference Data* 2000, 29, 41-130.
[207] Shiu, W.Y.; Ma, K.C. Ma, *Journal of Physical Chemistry Reference Data* 2000, 29, 387-462.
[208] Gonzalez, F.R. *Journal of Chromatography A* 2004, 1037, 233-253.
[209] Castells, R. C.; Arancibia, E. L.; Miguel Nardillo, A. *Journal of Chromatography A* **1990**, *504*, 45-53.
[210] Aldaeus, F.; Thewalim, Y.; Colmsjö, A. *Analytical and Bioanalytical Chemistry* **2007**, *389*, 941-950.
[211] Goss, K.; Schwarzenbach, R. P. *Environmental Science & Technology* **1999**, *33*, 3390-3393.
[212] Koutek, B.; Cvacka, J.; Streinz, L.; Vrkocova, P.; Doubsky, J.; Simonova, H.; Feltl, L.; Svoboda, V. *Journal of Chromatography A* **2001**, *923*, 137-152.
[213] Goss, K.; Schwarzenbach, R. P. *Environmental Science & Technology* **2001**, *35*, 1-9.
[214] Spieksma, W.; Luijk, R.; Govers, H. A. J. *Journal of Chromatography A* **1994**, *672*, 141-148.
[215] Gruber, D.; Langenheim, D.; Gmehling, J.; Moollan, W. *Journal of Chemical and Engineering Data* **1997**, *42*, 882-885.
[216] Alberty, R. A.; Reif, A. K.*Journal of Physical Chemistry Reference Data* 1988, 17, 241-253.
[217] Alberty, R. A.; Gehrig, C. A. *JJournal of Physical Chemistry Reference Data* 1984, 13, 1173-1197.
[218]Rossini, F.D. *Selected values of physical and thermodynamic properties of hydrocarbons and related compounds, comprising the tables of the American Petroleum Institute Research Project 44 extant as of December 31, 1952*, American Petroleum Institute, Carnegie Press, Pittsburgh, PA, 1953.
[219] Beens, J.; Tijssen, R.; Blomberg, J. *Journal of High Resolution Chromatography* **1998**, *21*, 63-64.
[220] Engkvist, O.; Borowski, P.; Bemgard, A.; Karlstrom, G.; Lindh, R.; Colmsjo, A. *Journal of Chemical Information and Computer Sciences* **1996**, *36*, 1153-1161.
[221] van Den Dool, H.; Dec. Kratz, P. *Journal of Chromatography A* **1963**, *11*, 463-471.
[222] Castello, G. *Journal of Chromatography A* **1999**, *842*, 51-64.
[223] Bieri, S.; Marriott, P. J. *Analytical Chemistry* **2008**, *80*, 760-768.
[224] Eckel, W. P.; Kind, T. *Analytica Chimica Acta* **2003**, *494*, 235-243.

[225] Miller, M. M.; Wasik, S. P.; Huang, G. L.; Shiu, W. Y.; Mackay, D. *Environmental Science & Technology* **1985**, *19*, 522-529.
[226] Abraham, M. H., *Journal of Chromatography* **1993,** *644* (1), 95-139.